SAPIENZA
UNIVERSITÀ DI ROMA

TESI DI DOTTORATO IN COTUTELA
THÈSE DE DOCTORAT EN COTUTELLE

Effect of Micro-Particle Addition on Frictional Energy Dissipation and Strength of Concrete: Experiments and Modelling

presentata a - présentée devant

Sapienza Universitá di Roma
l'Institut National des Sciences Appliquées de Lyon

per ottenere il titolo di - pour obtenir le grade de

DOTTORE DI RICERCA - DOCTEUR

Dottorato di ricerca in - École doctorale:

Meccanica Teorica e Applicata
Mécanique, Énergétique, Génie Civil, Acoustique

Spécialité:

MÉCANIQUE - GÉNIE MÉCANIQUE - GÉNIE CIVIL

da - par

Daria SCERRATO

Tesi discussa il 7 novembre 2014 davanti alla Commissione giudicatrice
Thése soutenue le 7 Novembre 2014 devant la Commission d'examen

Commissione - Jury

Philippe BOISSE	Professeur (INSA de Lyon) Examinateur
Francesco DELL'ISOLA	Professeur (Università Sapienza di Roma) Directeur de thèse
Norman E. DOWLING	Professeur (Virginia Tech) Rapporteur
Ali LIMAM	Professeur (INSA de Lyon) Directeur de thèse
Angela MADEO	Maître de Conférence (INSA de Lyon) - LGCIE Co-encadrante
Giuseppe PICCARDO	Professeur (Università di Genova) Rapporteur
Luca PLACIDI	Maître de Conférence (Univ. Telematica UniNettuno) Examinateur

Abstract

In this thesis, a two-degrees-of-freedom, non-linear model is introduced aiming to describe internal friction phenomena which have been observed in some modified concrete specimens undergoing slow dynamic compression loads and having various amplitudes but never inducing large strains. The motivation for the theoretical effort presented here arose because of the experimental evidence described in some papers in which dissipation loops for concrete-type materials are shown to have peculiar characteristics. Since viscoelastic models –linear or non-linear– do not seem suitable to describe either qualitatively or quantitatively the measured dissipation loops, it is proposed to introduce a micro-mechanism of Coulomb-type internal dissipation associated to the relative motion of the faces of the micro-cracks present in the material. In addition, numerical simulations, showing that the proposed model is suitable to describe some of the available experimental evidences, is presented. These numerical simulations motivate further developments of the considered model and supply a tool for the design of subsequent experimental campaigns.

Furthermore, the effect of micro-particle additives such as calcium carbonate on internal dissipation of concrete was experimentally investigated. The damping performance of concrete can be improved by adding to the mixture different kinds of micro-particles with suitable size which fill the pores of the matrix and change the contact interaction between internal surfaces of voids. It was determined that the energy dissipation of the concrete increases with the increasing content of micro particles at least when the concrete matrix is "soft" enough to allow microscopic motions. On the other hand, the increasing percentage of micro-particles addition can affect the mechanical strength of the material. Thus, there is a reasonable compromise in incorporating these micro-particles to obtain higher damping without weakening the mechanical properties. Several concrete mixes were prepared by mixing cement powder with different percentages of micro-fillers. A concrete mix without addition of micro-particles was molded as a reference material for the sake of comparison. All these specimens were tested under cyclic loading in order to evaluate energy dissipation starting from the area of a dissipation loop detected in the diagram relative to a representative cycle. The experimental determination of the dissipated energy shows a significant increase in the damping capability of the cement-based materials with micro-filler compared to the standard concrete. The experimental results presented seem to indicate that the proposed model is suitable to describe the mechanical behavior of modified and unmodified concrete, provided that the introduced parameters are suitably tuned in order to best fit the available experimental data.

Keywords: Modified concrete - Continua with microstructure - Frictional sliding - Energy dissipation under cyclic load

Effet de l'addition de micro-particules sur la dissipation d'énergie et la résistance mécanique du béton: essais et modélisation

Si un béton classique est constitué d'éléments de granulométrie décroissante, en commençant par les granulats, le spectre granulométrique se poursuit avec la poudre de ciment puis parfois avec un matériau de granulométrie encore plus fine comme une fumée de silice (récupérée par exemple au niveau des filtres électrostatiques dans l'industrie de l'acier). L'obtention d'un spectre granulométrique continu et étendu vers les faibles granulométries permet d'améliorer la compacité, donc les performances mécaniques. L'idée de base de cette thèse a été d'utiliser comme éléments de granulométrie fine des fillers à base de calcaire. Ces fillers ont des granulométries très fines qui leur permettent de remplir les micro-fissure généralement présentes à l'intérieur du béton. La surface rugueuse des grains de ces fillers permet de modifier le coefficient de frottement entre les lèvres de chaque fissure. Le résultat souhaité est celui de produire un béton qui dissipe par frottement plus d'énergie par rapport à un béton standard. Un béton de ce type pourrait avoir des applications importantes dans l'ingénierie civile, surtout pour ce qui concerne l'absorption des vibrations dans la ville et les constructions en régions séismiques. Les théories des milieux continus généralisés permettent de tenir compte de l'effet de la microstructure des matériaux sur leur comportement macroscopique et, en particulier, de décrire la dissipation d'énergie dans le béton sujet à des chargements cycliques. Un modèle continu généralisé avec une variable cinématique supplémentaire a été développé dans le cadre de cette thèse qui permet de décrire le glissement relatif des lèvres des fissures dans le béton à l'échelle microscopique. La relation entre ces micro-mouvements au niveau des lèvres de fissures et la dissipation d'énergie observée à l'échelle macroscopique a ensuite été étudiée. Les équations en forme forte qui dérivent de cette modélisation continue sont obtenues à l'aide d'un principe variationnel de Hamilton-Rayleigh dans lequel on a intégré la nature dynamique du problème ainsi que la possibilité de décrire des phénomènes de dissipation au niveau microscopique. Le modèle obtenu permet de décrire les cycles d'hystérésis typiques du béton sujet à des chargement cycliques et ses paramètres ont été calés sur des essais menés au LGCIE de l'INSA de Lyon. Des études paramétriques concernant les paramètres reliés à la microstructure du matériau ont permis d'identifier l'effet que l'addition des micro-fillers a sur le comportement mécanique global du béton lorsque il est sujet à des chargement dynamiques.

Mots-Clés: Béton modifié - Milieux continus avec microstructure - Frottement à l'échelle microscopique - Dissipation d'énergie sous chargement cyclique

Acknowledgments

I would like to thank Prof. Norman Dowling for having supported me in understanding the behavior of the experimental apparatus, for his help in setting up the experimental tests needed and for his fatherly advice in writing some parts of my thesis.

I also thank Prof. Limam for allowing me to perform the experimental tests needed and for having supplied all the measurement instruments.

I would like to show my deepest gratitude to Prof. Francesco dell'Isola for his scientific support, for helping me in the development of the mathematical model and for his precious teachings.

I thank Dr Angela Madeo for her support in my research work and for her hospitality in Lyon.

I also would like to thank Prof. Philippe Boise for accepting to be a member of the examining committee.

I would like to acknowledge Prof. Piccardo for accepting to review my thesis.

I should thank Dr. Luca Placidi for accepting to be the alternate member of the committee.

A dutiful acknowledgement to Dr. Alessandro Della Corte for his useful comments and advices.

Lastly, a special thank to Dr. Ivan Giorgio for his fundamental help in all steps of the development of this work and for his great patience, precious in the moments when the results were difficult to obtain.

Thank you.

Contents

List of Figures

List of Tables

Chapter I

Introduction

I.1 Background and Motivations

The common materials used in the various fields of industrial and civil engineering, reaching the limit of their mechanical and technological characteristics, require new developments in order to fit the growing demand for performance. The properties of engineering materials can be optimized by combining different constituents in order to improve the performance of the new material compared to the individual components.

Many of these improved materials reveal a rather complex behavior with respect to the conventional ones used in engineering. This is a consequence of their advanced structure/composition.

In particular, we want to focus our attention on concrete, developing a model suitable to describe the correlations between the microscopic and macroscopic properties of this material. This will permit obtaining the needed information that allows improving mechanical and functional performance.

Concrete is a material which has drastically changed the construction techniques of the twentieth century. This material, together with the metal bars of reinforcement, allowed the construction of reinforced concrete structures, whose performances are by far superior than those of all structures built previously.

Reinforced concrete structures are more convenient than purely metallic structures if one considers the quality/cost ratio. Moreover, when suitably designed, such structures are less subject to deterioration phenomena (such as oxidation in the metallic structures) and aging.

For these reasons, it is commonly believed that no further developments are possible for this technology, which is considered fully mastered and substantially optimized. This may indeed not be the case: It is possible to design new materials

with mechanical properties similar to concrete, and even more effective, by adding to the cement powder some particles of other inert material to obtain a new composite system.

Here it is useful to define concrete and the principal concrete-making components. The following definitions are adapted from ASTM C 125 (Standard Definition of Terms Relating to Concrete and Concrete Aggregates), and ACI Committee 116 (A Glossary of Terms in the Field of Cement and Concrete Technology): Concrete is a composite material that consists essentially of a binding medium within which are embedded particles or fragments of aggregate. In hydraulic-cement concrete, the binder is formed from a mixture of hydraulic cement and water (Mehta, Paulo, Monteiro [2005]). Cements used in construction can be characterized as being either hydraulic or non-hydraulic. Hydraulic cements (e.g., Portland cement) harden because of hydration, a chemical reaction between the anhydrous cement powder and water. Thus, they can harden underwater or when constantly exposed to wet weather. The chemical reaction results in hydrates that are not very water-soluble and so are quite durable in water. Non-hydraulic cements do not harden underwater; for example, slaked limes harden by reaction with atmospheric carbon dioxide.

Aggregate is the granular material, such as sand, gravel, crushed stone, crushed blast-furnace slag, or construction and demolition waste, that is used with a cementing medium to produce either concrete or mortar. The term coarse aggregate refers to aggregate particles larger than 4.75 mm (No. 4 sieve), and the term fine aggregate refers to aggregate particles smaller than 4.75 mm but larger than 75 μm (No. 200 sieve). Gravel is the coarse aggregate resulting from natural disintegration by weathering of rock. The term sand is commonly used for fine aggregate resulting from either natural weathering or crushing of stone. Crushed stone is the product resulting from industrial crushing of rocks, boulders, or large cobblestones. Iron blast-furnace slag, a by-product of the iron industry, is the material obtained by crushing blast-furnace slag that solidified by slow cooling under atmospheric conditions. Aggregate from construction and demolition waste refers to the product obtained from recycling of concrete, brick, or stone rubble.

Cement is a finely pulverized, dry material that by itself is not a binder but develops the binding property as a result of hydration (i.e., from chemical reactions between cement minerals and water). A cement is called hydraulic when the hydration products are stable in an aqueous environment.

Based on unit weight, concrete can be classified into three broad categories. Concrete containing natural sand and gravel or crushed-rock aggregates, generally weighing about 2400 kg/m^3, is called *normal-weight concrete*, and it is the most commonly used concrete for structural purposes. For applications where a higher

strength-to-weight ratio is desired, it is possible to reduce the unit weight of concrete by using natural or pyro-processed aggregates with lower bulk density. The term *light-weight concrete* is used for concrete that weighs less than about 1800 kg/m^3. *Heavy-weight concrete*, used for radiation shielding, is a concrete produced from high-density aggregates and generally weighs more than 3200 kg/m^3. It is useful to divide concrete into three general categories based on compressive strength:

- Low-strength concrete: less than 20 MPa;
- Moderate-strength concrete: 20 to 40 MPa;
- High-strength concrete: more than 40 MPa.

Moderate-strength concrete, also referred to as ordinary or normal concrete, is used for most structural work. High-strength concrete is used for special applications. It is not possible here to list all concrete types. There are numerous modified concretes which are appropriately named, for example, fiber- reinforced concrete, expansive-cement concrete, and latex-modified concrete.

The selection of an engineering material for a particular application has to take into account its ability to withstand the applied force. Depending on how the stress is acting on the material, the stresses are further distinguished from each other, for example, compression, tension, flexure, shear, and torsion. The stress-strain relationships in materials are generally expressed in terms of strength, elastic modulus, ductility, and toughness.

Strength is a measure of the amount of stress required to fail a material. The working stress theory for concrete design considers this material as mostly suitable for bearing compressive load; this is because only the compressive strength of the material is generally specified. Since the strength of concrete is a function of the cement hydration process, which is relatively slow, traditionally the specifications and tests for concrete strength are based on specimens cured under standard temperature-humidity conditions for a period of 28 days. Typically, the tensile and flexural strengths of concrete are of the order of 10 and 15 percent, respectively, of the compressive strength. The reason for such a large difference between the tensile and compressive strength is attributed to the heterogeneous and complex microstructure of concrete. The *modulus of elasticity* is defined as the ratio between the stress and the reversible strain. In homogeneous materials, the elastic modulus is is unaffected by microstructural changes. This is not true of the heterogeneous multiphase materials like concrete. The elastic modulus of concrete in compression varies from 14×10^3 MPa to 40×10^3 MPa.

The significance of the elastic limit in structural design lies in the fact that it represents the maximum allowable stress before the material undergoes permanent

deformation. Therefore, the engineer must know the elastic modulus of the material because it influences the rigidity of a design.According to ACI Building Code 318, with a concrete mass density between 1500 and 2500 kg/m^3, the modulus of elasticity can be determined from

$$E_c = \rho^{1.5} \times 0.043 \ f_c^{\frac{1}{2}}$$

where E_c is the static modulus of elasticity (MPa), ρ is the mass density (kg/m^3) and f_c is 28-day compressive strength of standard cylinders (MPa).

Poisson's ratio is not generally needed for most concrete design computations; however, it is needed for structural analysis of tunnels, arch dams, and other statically indeterminate structures.

With concrete the values of Poisson's ratio generally vary between 0.15 and 0.20. There appears to be no consistent relationship between Poisson's ratio and concrete characteristics such as water-cement ratio, curing age, and aggregate gradation. However, Poisson's ratio is generally lower in high-strength concrete, and higher for saturated concrete and for dynamically loaded concrete.

The amount of inelastic strain that can occur before failure is a measure of the *ductility* of the material. The energy required to break the material is represented by the area under the stress-strain curve. The term *toughness* is used as a measure of this energy. The contrast between toughness and strength should be noted; the former is a measure of energy, whereas the latter is a measure of the stress required to fracture the material. Thus, two materials may have identical strength but different values of toughness. In general, however, when the strength of a material increases, the ductility and the toughness decrease; also, very high-strength materials usually fail in a brittle manner (i.e., without undergoing any significant plastic strain).

Concrete is a composite material; however, many of its characteristics do not follow the laws of mixtures. For instance, under compressive loading both the aggregate and the hydrated cement paste, if separately tested, would fail elastically, whereas concrete itself shows inelastic behavior before fracture. Also, the strength of concrete is usually much lower than the individual strength of the two components. Such anomalies in the behavior of concrete can be explained on the basis of its microstructure, especially the important role of the interfacial transition zone between coarse aggregate and cement paste.

For concrete the relationship between stress and strain is dependent of the loading time. If a concrete specimen is held for a long period under a constant stress, for instance 50% of the ultimate strength of the material, it will exhibit plastic strain. The phenomenon of gradual increase in strain with time under a sustained stress is called *creep*. When creep in concrete is restrained, it manifests itself as

a progressive decrease of stress with time. The stress relief associated with creep has important implications for the behavior of plain, reinforced, and prestressed concrete structures.

Professional judgment in the selection of construction materials should take into consideration not only the strength, dimensional stability, and elastic properties of the material but also its durability, which has serious implications for the life-cycle cost of a structure. *Durability* is defined as the service life of a material under given environmental conditions.

In general, there is a relationship between strength and durability when low strength is associated with high porosity and high permeability. Permeable concretes are, of course, less durable. The permeability of concrete depends not only on mix proportions, compaction, and curing, but also on microcracks caused by the ambient temperature and humidity cycles.

Concrete can be modeled as a porous medium composed of a solid matrix with pores, that typically are characterized by two different sizes, namely about $10^{-3}\mu$m and 1 to 100 μm.

Different theories to model porous material have been developed in the literature. One of the early theories is the Effective Moduli Approach. The general philosophy in this context is to extend the use of homogeneous classical elasticity to inhomogeneous materials by replacing the elastic constants of the classical homogeneous theory by suitable effective elastic constants or moduli. The idea of equivalent homogeneity for an inhomogeneous material such as a porous elastic solid is that the scale of the inhomogeneity is assumed to be several orders of magnitude smaller than the characteristic dimension of the problem of interest and, therefore, there exists an intermediate dimension over which the inhomogeneous properties can be averaged. Depending on the length scale of the intermediate dimension, the elastic constants for the real inhomogeneous material can be replaced by the effective elastic moduli of the 'equivalently homogeneous' model material. The effective bulk and shear moduli can be calculated by a self-consistent method due to Frohlich, Sack [1946]. The calculation uses the notion of an equivalent homogeneous continuum. The bulk modulus k is determined by applying a hydrostatic pressure, and the shear modulus μ by applying a simple homogeneous shear stress. Each pore is surrounded by a spherical shell of real material, and the reaction of the rest of the material is estimated by replacing it by equivalent homogeneous material. An important example of the effective moduli calculations are the formulas due to Mackenzie [1950].

In these formulas it suffices to equate the stored elastic energy to the work done by the externally applied pressure in order to derive the effective compressibility. This calculation, however, follows the lines of ordinary elasticity theory, and both

the effective compressibility and the effective shear modulus are derived without any particular hypothesis on the size of pores. For this reason it was assumed that the real material contained isolated spherical holes, randomly distributed throughout the volume, and that the real material was homogeneous and isotropic. It was also assumed that the volume of all the holes was small compared with the total volume, and that, this volume contained a large number of holes. The effective moduli approach is powerful because it can be used to predict effective material properties from the properties of the single constituents.

Another approach used for the study of porous materials is the theory of Elastic Material with voids developed by Cowin, Nunziato [1983]. This theory is focused on characterizing the overall bulk behavior of porous solids in which the skeletal or matrix material is elastic and the interstices are voids which contain nothing of mechanical or energetic significance. To account properly for the compaction or extension of the voids, they assign to the material the mathematical structure of a distributed body. The body is assumed to occupy a bounded, regular region $\mathcal{B}$ of Euclidean 3D-Space in its reference configuration. The concept of a distributed body also asserts that for every pair (X, t) in $\mathcal{B}$ the apparent mass density $\rho = \hat{\rho}(X, t)$ has the decomposition

$$\rho = \gamma\nu \tag{I.1}$$

where $\gamma = \hat{\gamma}(X, t)$ is the density of the matrix material, also called true density, and $\nu = \hat{\nu}(X, t)$, $0 < \nu \leq 1$, is the volume distribution function. Indeed, this distribution function is the volume fraction of solid material found at the point X at time t and hence is a measure of the volume change of the bulk material which results from void compaction (i.e., void volume reduction) or distention. The fields displacement and ν clearly describe the overall kinematical behavior of the material.

In contrast with the Cowin approach the Theory of Poroelasticity deals with the deformation of a porous elastic solid containing a viscous fluid and was proposed by Biot in several pioneering papers (Biot [1941, 1956, 1962,a]). He considers the tensor stress as composed of two parts: one which is caused by the hydrostatic pressure of the fluid filling the pores, and the other caused by the average stress in the skeleton. In this sense the stresses in the medium are said to be carried partly by the fluid and partly by the solid constituent. In order to completely describe the macroscopic condition of the porous medium, an additional variable giving the amount of fluid in the pores is considered, i.e. the increment of fluid mass per unit volume of material called the variation in fluid content m_f.

Despite the difference in constitution, materials such as concrete or some rock types exhibit similar behavior which is mainly due to phenomena of microcracking.

The theoretical study of the degradation of brittle materials due to microcracking is usually addressed in the context of the Damage Mechanics. This is a recent discipline of Solid Mechanics whose promoters are Kachanov [1982] and Rabotonov [1969]. Moreover, some aspects of the behavior of Porous Brittle Materials typically are interpreted according to the Theory of Microcracking. In the study of microcracked materials we can identify two different schools of thought. One of these approaches mainly concerns the evaluation of the effects of interaction between the microcracks (see Kachanov [1994] or Nemat-Nasser, Hori [1993]). The other one leads directly to the micromechanical modeling of damage (see Krajcinovic [1996]).

According to the latter point of view, Pensée, Kondo, Dormieux [2002] describe porous materials which present a brittle behavior, considering pores as microfractures. Indeed, in some cases, pores can be regarded as cavities in which one size is very small compared to the other two dimensions. For example, an elliptical crack can be regarded as an ellipsoidal cavity, the length of one of whose principal axes becomes very small in comparison with the length of the other two principal axes. In particular, the authors are focused on the study of the effect of interaction inside the microcracks. When an external load is applied, the two superimposed faces of a crack come in contact and start sliding on each other, generating a friction force that dissipates some of the energy applied to the material. The energy dissipated by friction represents a loss of energy of the system that cannot be recovered; it is for this reason that hysteretic behavior for concrete material tested under cyclic load can be observed.

If some microparticles are added to the concrete matrix in such a way that they can fill the space between the two faces of each crack, it can be expected that the energy dissipation due to friction phenomena changes according to the physical properties of the microparticles themselves. Thus, a new concrete can be synthesized by adding microparticles, in such a way that they change the frictional sliding behavior of the cracks under an external load. These additives, that will be called ‘fillers’ for their ability of ‘filling’ the voids of the concrete matrix, are of different types, and according to their intrinsic differences, they are expected to affect the energy dissipation in a different way.

Chapter II

Modeling of Microcracked Media

II.1 Models for internal dissipation in solids

The problem of modeling internal dissipation in solids is very old and, for this reason, a huge literature concerning this subject is available. For clear reasons of consistency we limit ourselves to draft some considerations and to cite some among the relevant papers. It is indeed rather difficult to distinguish between the dissipated energy which participates in damage and plastic phenomena (even by producing new micro-cracks or enlarging the existing ones) and the dissipated energy which is associated with friction related to reversible internal relative motions. Interesting investigations which are meant to describe internal dissipation in the presence of the damage progress are presented in Savage, Byerlee, Lockner [1996], Boma, Brocato [2010], Pensée, Kondo, Dormieux [2002], Fantozzi et al. [1982], Fantozzi, Ritchie [1981], Lomniz [1957] where various mechanisms of damage and plasticity are taken into account, even at different length scales. (See also Rinaldi, Lai [2007b], Rinaldi [2013], Rinaldi, Lai [2007a], Rinaldi, Krajcinovic, Mastilovic [2007]). On the other hand, the classical work of Kimball, Lovell [1927], Zener [1940] study the internal mechanisms of dissipation in solids when no relevant damage phenomena occur at the macroscopic level. In the same spirit are the papers Pensée, Kondo, Dormieux [2002], Fantozzi et al. [1982], Fantozzi, Ritchie [1981], Shamy, Denissen [2003], Spears, Feltham [1972], Wegel, Walther [1935], Hernández et al. [2002], Darve, Labanieh [1982], Yu, Kobayashi, Hawkins [1993], Brailsford [1964], where several models for dissipation of energy due to elastic deformation rate and relative motion of different parts of considered bodies are studied and applied in the case of metals or even concrete. Finally, two papers which accept a point of view very similar to ours are Adelaide et al. [2010], Bhattacharjee, Léger [1993] where the internal dissipation mechanisms are clearly distinguished in two different types,

one producing crack generation and growth, and the second being related to reversible relative motion of micro-crack faces. In Adelaide et al. [2010] micro-crack surfaces relative motion is described by means of a tensorial quantity, distinguished from plastic and elastic deformations. In some works (see e.g. Bhattacharjee, Léger [1993]) the analysis is based directly on a finite-dimensional model to be used for numerical simulations; however, internal friction is there regarded as a phenomenon also driven by opening and closing of already existing cracks. Different work exists on the mathematical modeling of reversible damping effects. In linear approaches, often stress-strain relations with integral kernels are used, while for geometrically nonlinear problems, the addition of rate-equations for some internal variables seems to be more useful; see e.g. Neff [2005a, 2003, 2006] for incorporation of grain boundary relaxation effects.

II.2 State of the art and preliminary work

In this section the effect of microcracking on the mechanical behavior of nonlinear quasi-brittle materials is described. This approach is based on the assumption of no interaction between microcracks and includes the effects of interaction between the two faces of each microcrack when they come in contact under the influence of an external load. Understanding and modeling the inelastic behavior of these microcracked materials has received considerable attention during the last twenty years. Continuum Damage Mechanics (CDM), based on the use of internal damage variables, constitutes undoubtedly the most appropriate framework for the analysis of the consequences of microcracking in engineering materials.

When an external load is applied to a microcracked material, the two superimposed faces of each crack start sliding on each other, generating a friction force that dissipates some of the energy provided from the external load itself. It is for this reason that macroscopic dissipation loops of concrete under cyclic loading can be detected. It is worth noting that if the energy dissipation is mostly due to the frictional sliding of the internal microcracks Pensée, Kondo, Dormieux [2002], a purely macroscopic approach is not sufficient to predict the mechanical behavior of a microcracked material (such as concrete). Since it allows us to relate the macroscopic properties to specific microstructural mechanisms, micromechanics may give a deeper insight of the behavior of a microcracked material subjected to a given external load. In other words, micromechanics allows us to explain some macroscopic features, such as dissipation loop under cycling loading, by means of microscopic phenomena, such as frictional sliding of microcracks Pensée, Kondo, Dormieux [2002].

We denote by Ω the Representative Elementary Volume (REV) of a medium

made of an isotropic matrix containing many microcracks, that we call ω. It is assumed that the characteristic size of these microcracks is small compared to the dimension of REV; this occurs for example in materials which present a low level of porosity [1] in their initial state. Due to the flattened shape of microcracks, each of them is characterized by an upper face ω^+ and a lower face ω^-, and by a normal vector of unit length $\mathbf{n}$, oriented towards ω^+ . In the REV it is possible to distinguish different families of microcracks, characterized by the same normal vector $\mathbf{n}$.

For each microcrack the unilateral contact conditions are considered. These are divided, naturally, into the conditions in the normal direction and those in the tangential directions. To describe them we denote by $[|\mathbf{u}|] = \mathbf{u}^{\omega^+} - \mathbf{u}^{\omega^-}$ the jump of displacement $\mathbf{u}$ and its normal and tangential components on ω, given by

$$[|u_n|] = [|\mathbf{u}|] \cdot \mathbf{n}, \qquad [|\mathbf{u}_\tau|] = [|\mathbf{u}|] - [|u_n|] \ \mathbf{n}. \tag{II.1}$$

Similarly, the normal and tangential components of the velocity field $[|\dot{\mathbf{u}}|]$ on the cracks are defined by

$$[|\dot{u}_n|] = [|\dot{\mathbf{u}}|] \cdot \mathbf{n}, \qquad [|\dot{\mathbf{u}}_\tau|] = [|\dot{\mathbf{u}}|] - [|\dot{u}_n|] \ \mathbf{n}. \tag{II.2}$$

Below we refer to the tangential components $[|\mathbf{u}_\tau|]$ and $[|\dot{\mathbf{u}}_\tau|]$ as the *slip* and the *slip rate*, respectively. We also denote by f_n and $\mathbf{f}_\tau$ the normal and tangential components of the stress field σ on the face of the microcracks, i.e.

$$f_n = \sigma\mathbf{n} \cdot \mathbf{n}, \qquad \mathbf{f}_\tau = \sigma\mathbf{n} - f_n \ \mathbf{n}. \tag{II.3}$$

The component $\mathbf{f}_\tau$ represents the friction force on the contact surface.

The contact is modeled by the *Signorini-Coulomb contact condition* and can be stated as follows:

$$\begin{cases} [|u_n|] \geq 0 & (a) \\ f_n \leq 0 & (b) \\ [|u_n|] \, f_n = 0 & (c) \end{cases} \tag{II.4}$$

These conditions can be interpreted as follows: (i) if microcracks are open, inequality $[|u_n|] > 0$ shows that there is no contact and the faces are not subjected to any reaction, since $f_n = 0$; (ii) if microcracks are closed there is a contact, $[|u_n|] = 0$, and a compressive stress is established on the faces $f_n \leq 0$. Otherwise the condition (a) establishes that the faces do not interpenetrate. The Signorini contact condition

[1] The porosity can be expressed as $\varphi = 1 - \frac{V_f}{V}$ where V_f is the effective volume of the solid part and V is the volume of REV

was first introduced in Signorini [1933] and then used in many papers (see e.g. Shillor, Sofonea, Telega [2004] for further details and references).

We turn now to the conditions in the tangential directions, called also frictional conditions or friction laws. The simplest one is the so-called frictionless condition in which the friction force vanishes during the process, i.e.,

$$\mathbf{f}_\tau = \mathbf{0} \text{ on } \omega \times (0,T) \tag{II.5}$$

where $(0,T)$ is the time interval considered.

This is an idealization of the process, since even completely lubricated surfaces generate shear resistance to tangential motion. However, eq. (II.5) is a sufficiently good approximation of the reality in some situations. In the case when the friction force $\mathbf{f}_\tau$ does not vanish on the contact surface, the contact is frictional. Frictional contact is usually modeled with the Coulomb law of dry friction or its variants. According to this law, the magnitude of the tangential traction $\mathbf{f}_\tau$ is bounded by a function, the so-called friction bound, which is the maximal frictional resistance that the surface can generate; also, once slip starts, the frictional resistance opposes the direction of the motion and its magnitude reaches the friction bound. Thus,

$$\|\mathbf{f}_\tau\| \leq g \qquad \text{if } [|\dot{\mathbf{u}}_\tau|] = \mathbf{0} \text{ on } \omega \times (0,T)\,, \tag{II.6}$$

$$\mathbf{f}_\tau = -g\,\frac{[|\dot{\mathbf{u}}_\tau|]}{\sqrt{[|\dot{\mathbf{u}}_\tau|]\cdot[|\dot{\mathbf{u}}_\tau|]}} \qquad \text{if } [|\dot{\mathbf{u}}_\tau|] \neq \mathbf{0} \text{ on } \omega \times (0,T)$$

where g represents the friction bound. Note that the Coulomb law (II.6) is characterized by the existence of *stick-slip zones* on the contact boundary at each time $t \in [0,T]$. Indeed, it follows from (II.6) that if in a point $x \in \omega$ the inequality $\|\mathbf{f}_\tau(x,t)\| < g(x)$ holds, then $[|\dot{\mathbf{u}}_\tau(x,t)|] = 0$ and the material point x is in the so-called stick zone; if $\|\mathbf{f}_\tau(x,t)\| = g(x)$, then the point x is in the so-called slip zone. We conclude that Coulomb's friction law (II.6) models the phenomenon according to which slip may occur only when the magnitude of the friction force reaches a critical value, the friction bound g.

Often, especially in engineering literature, the friction bound g is chosen as

$$g = g(f_n) = \tilde{\mu}\,|f_n| \tag{II.7}$$

where the non-negative $\tilde{\mu}$ is the coefficient of dynamic friction. We observe that the friction coefficient $\tilde{\mu}$ is not an intrinsic thermodynamic property of a material, a body or its surface, since it depends on the contact process and the operating conditions. The issue is considerably complicated by the following facts. Engineering surfaces

are not smooth surfaces but contain asperities and various irregularities. Moreover, very often they contain some or all of the following: moisture, various debris, wear particles, oxide layers, chemicals and materials that are different from those of the parent body. Therefore, it is not surprising that the friction coefficient is found to depend on the surface characteristics, on the surface geometry and structure, on the relative velocity between the contacting surfaces, on the surface temperature, on the wear or rearrangement of the surface, and, therefore, on its history. Until very recently, mathematical models for frictional contact used a constant friction coefficient. In particular it is possible to distinguish two kind of friction, static and dynamic friction. The coefficient of dynamic friction is usually less than the coefficient of static friction for the same materials. In recent publications the dependence of $\tilde{\mu}$ on the process parameters has been incorporated into the models; the coefficient of friction can be chosen as $\tilde{\mu} = \tilde{\mu}\left([|\dot{\mathbf{u}}_\tau|]\right)$.

According to Andrieux, Bamberger, Marigo [1986] the study of REV can be decomposed into two subproblems: the first is a classic problem of linear homogeneous elasticity; the second one takes into account the displacement discontinuity on the faces of the microcracks. The idea is to distinguish in the macroscopic response the effects due to discontinuity of the displacement on the microcracks. Thus, the effective displacement field $\mathbf{u}$ is given by the sum of a term resulting from bulk deformations and a term resulting from the micro-displacement discontinuity. Moreover, given the particular form of microcracks, two fields that characterize the discontinuities can be introduced:

1. a non-negative scalar variable β which describes the opening of the cracks and represents their volume

$$\beta(\mathbf{n}) = \mathcal{N} \int_{\omega^+} [|u_n|]\,(\mathbf{x}) dS \tag{II.8}$$

2. a variable vector γ which is the sliding vector

$$\gamma(\mathbf{n}) = \mathcal{N} \int_{\omega^+} \left([|\mathbf{u}|] - [|u_n|]\ \ \mathbf{n}\right)(\mathbf{x}) dS = \mathcal{N} \int_{\omega^+} [|\mathbf{u}_\tau|]\, dS \tag{II.9}$$

where $\mathcal{N}$ is the density (number per unit volume) of microcracks of the family considered.

As it can be seen from eq. (II.9), the magnitude of the sliding vector $|\gamma|$ is a measure of the relative displacement of the two faces of a certain family of cracks. It is worthy of note that both the scalar opening parameter β and the sliding vector γ depend on the normal $\mathbf{n}$ of the corresponding generic family of coin-shaped cracks, all having the same normal.

Under compressive loading some closed mesocracks may exhibit frictional sliding and produce complex macroscopic behavior. Some authors (Pensée, Kondo, Dormieux [2002]) have developed a model based on CDM that is able to predict how microscopic frictional sliding can affect the macroscopic behavior of the material; this model will be briefly presented in the remainder of this section. When mesocracks are closed ($\beta = 0$), for the application of an external load, their faces can slide in the presence of friction; in this case the macroscopic potential W is written as the sum of two contributions,

$$W = W^{(1)} + W^{(2)} \tag{II.10}$$

where $W^{(1)}$ is the term purely elastic and $W^{(2)}$ represents the contribution due to the discontinuity of the displacement, in detail

$$W^{(1)} = \frac{1}{2} E^{(1)} : \mathbb{C}^s : E^{(1)} \tag{II.11}$$

being $\mathbb{C}^s$ the fourth-order Elasticity tensor of the solid matrix, $E^{(1)}$ the second-order Small Strain tensor, the symbol (:) the double contraction, and

$$W^{(2)} = \frac{H_0}{2d} \left\{ \beta^2 + \left(1 - \frac{\nu^s}{2} \right) \gamma \cdot \gamma \right\} \tag{II.12}$$

where d is the density of a particular family of microcracks defined as the number of cracks per unit volume times the mean radius of the generic microcrack (see Budiansky, O'Connel [1976]), and the coefficient H_0 can be expressed as

$$H_0 = \frac{3Y^s}{16\left(1 - {\nu^s}^2\right)} \tag{II.13}$$

in which Y^s and ν^s are respectively Young's modulus and Poisson's ratio of solid matrix. The eq. (II.12) has been obtained assuming the Small Strain tensor $E^{(2)}$ due to the presence of microcracks as:

$$E^{(2)} = \beta \left(\mathbf{n} \otimes \mathbf{n} \right) + sym \left(\gamma \otimes \mathbf{n} \right) \tag{II.14}$$

Finally, using the decomposition $E = E^{(1)} + E^{(2)}$ for the macroscopic deformation, we can simply write

$$W(E, \beta, \gamma) = \frac{1}{2}(E - E^{(2)}) : \mathbb{C}^s : (E - E^{(2)}) + \frac{H_0}{2d} \left\{ \beta^2 + \left(1 - \frac{\nu^s}{2} \right) \gamma \cdot \gamma \right\} \tag{II.15}$$

Moreover, it can be noted that the eq. (II.15) is applicable easily to the case in which the microcracks are closed, namely $\beta = 0$.

As explained before, the sliding vector γ, as defined in eq. (II.9), represents a measure of the relative displacement between the two faces of a given family of cracks, so that if $\dot{\gamma}$ is the sliding rate. The volume energy dissipated when the material is subjected to cyclic loading of time period T can be written as

$$E_{vol}^{diss} = \int_0^T \mathcal{N} \int_{\omega^+} \tilde{\mu} \ |f_n| \ \ [|\dot{u}_\tau|] \ dS \ dt \tag{II.16}$$

where $\tilde{\mu}$ is the dynamic friction coefficient, since $[|\dot{u}_\tau|] \neq 0$. When one can assume that $\tilde{\mu}$ and $|f_n|$ are constant on all the cracks belonging to the family considered then the expression (II.16) reduces to

$$E_{vol}^{diss} = \tilde{\mu} \int_0^T \ |f_n| \ \ |\dot{\gamma}| \, dt = \tilde{\mu} \int_0^T |f_n| \sqrt{\dot{\gamma} \cdot \dot{\gamma}} dt \tag{II.17}$$

Herein the Coulomb friction model is applied on closed cracks, in which, due to the uniform contact constraints on the faces, the saturation of the friction criterion occurs over the entire crack. Assuming that the variation of the applied external macroscopic load occurs with a rate which is much slower than the rate of induced microdynamics phenomena, then one can accept the so called Instantaneous Micro-Equilibrium Hypothesis: At every instant, inside the REV, the micro-displacement field can be estimated to be equal to the field which is the solution of the linear elastic problem formulated for the REV, in which the external load is represented by the macro-stress field σ, considered as applied to the boundary of the REV. In this framework the sliding vector γ can be expressed as a function of the macrostress tensor σ as (see Pensée, Kondo, Dormieux [2002])

$$\gamma = \frac{2d}{H_0 \left(2 - \nu^s\right)} \left(\delta - \mathbf{n} \otimes \mathbf{n}\right) \cdot \left(\sigma \mathbf{n}\right) \tag{II.18}$$

where δ is Kronecker tensor. Hence, differentiating eq. (II.18) with respect to time, the sliding rate becomes

$$\dot{\gamma} = \frac{2d}{H_0 \left(2 - \nu^s\right)} \left(\delta - \mathbf{n} \otimes \mathbf{n}\right) \cdot \left(\dot{\sigma} \mathbf{n}\right) \tag{II.19}$$

Thus, substituting eqs. (II.19) and (II.3) in eq. (II.17), the volume energy dissipated can be written as

$$E_{vol}^{diss} = \tilde{\mu} \frac{2d}{H_0 \left(2 - \nu^s\right)} \int_0^T |\sigma \mathbf{n} \cdot \mathbf{n}| \sqrt{\left[\left(\delta - \mathbf{n} \otimes \mathbf{n}\right) \cdot \left(\dot{\sigma} \mathbf{n}\right)\right]^2} dt \tag{II.20}$$

In order to measure this energy, an uniaxial state of stress is considered:

$$\sigma = \sigma_{33} \left(\mathbf{e}_3 \otimes \mathbf{e}_3\right) \tag{II.21}$$

where $\{\mathbf{e}_1, \mathbf{e}_2, \mathbf{e}_3\}$ is the vector basis in $\mathbb{R}^3$. By replacing eq. (II.21) in eq. (II.20), and representing the normal vector in terms of components, we obtain the following

$$E_{vol}^{diss}(\mathbf{n}) = \tilde{\mu}\frac{2d}{H_0(2-\nu^s)}\int_0^T \sigma_{33}\ \dot{\sigma}_{33}\ \left(1-n_1^2-n_2^2\right)^{\frac{3}{2}}\sqrt{\left(n_1^2+n_2^2\right)}dt \tag{II.22}$$

in which it is considered the unit-length constraint on $\mathbf{n}$:

$$n_1^2 + n_2^2 + n_3^2 = 1$$

This expression for the energy dissipation over a period T is clearly function of the unit normal $\mathbf{n}$, and hence it depends on the particular family of microcracks considered. More specifically, for a material with a directionally uniform distribution of microcracks, the whole energy dissipated can be estimated by integrating eq. (II.22) over the entire solid angle, obtaining

$$E_{vol}^{diss} = \tilde{\mu}\frac{2d}{H_0(2-\nu^s)} \int_0^T \sigma_{33}\ \dot{\sigma}_{33}\ \left[\int_{-1}^{1} dn_1 \int_{-\sqrt{1-n_1^2}}^{\sqrt{1-n_1^2}} \left(1-n_1^2-n_2^2\right)^{\frac{3}{2}}\sqrt{\left(n_1^2+n_2^2\right)}dn_2\right] dt \tag{II.23}$$

corresponding to an isotropic crack distribution.

We remark that the dissipated energy (II.23) is expressed as function of the stress σ_{33} instead of γ because is easier to measure the stress.

II.3 Continua with microstructure

The standard models usually introduced to study the deformation of cyclically compressed specimens of modified (or not modified) concrete do not seem suitable to describe all of the complex phenomena of internal dissipation which are experimentally observed, especially in the range of small strains. Indeed, (see Madeo [2006], Bowland [2012]) the dissipation loops measured under cyclic loads with relatively small amplitude show very peculiar qualitative features (see fig. II.1):

- the two branches present different (varying) curvatures on the loading and unloading paths;
- the turning points seem to have the form of cusps;

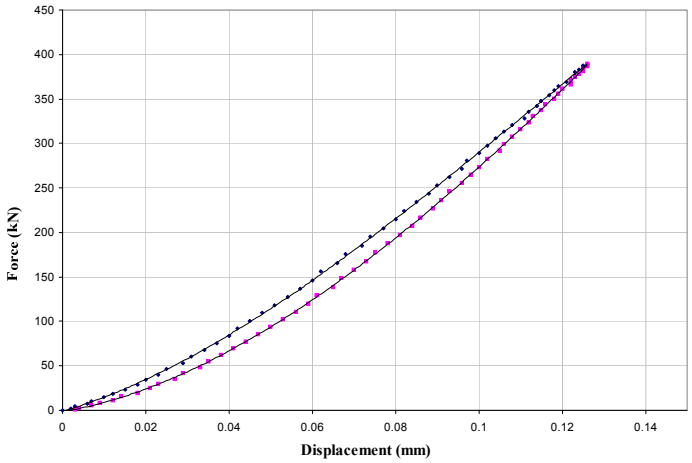

Figure II.1: Example of measured dissipation loop in concrete-based material.

- the distance between the loading/unloading branches varies in a non-linear way with the applied compression loads.

Even when, at a macro-level, the compression loads and deformations are relatively small, these experimental observations suggest that some non-linear elastic mechanisms are occurring at the micro-level, together with a Coulomb dissipation mechanism related to micro-motions, this may explain the observed evidence. The discussion of the rigorous modeling and mathematical issues arising from the observed evidence is delicate and deserves attention. Herein we consider a simple and efficient model that is conceivable to fit the targeted experimental evidence and we study its most relevant features.

In the framework of the above mentioned theory proposed by Pensée, Kondo, Dormieux [2002], we develop a novel model based on the theory of micromorphic media (see Eringen [1999]). In particular, we choose to introduce an extra kinematical field φ, in addition to the standard macroscopic displacement, to describe the relative displacement of superimposed faces of the microscopic cracks, which are known to be present in concrete materials. The introduction of extended kinematics to study materials with microstructure was developed by many authors in the decades 1950-1980. (See e.g. Eringen [1999, 2001], Eringen, Edelen [1972], Eringen, Suhubi [1964a,b], Pietraszkiewicz, Eremeyev [2009], Green, Rivlin [1964c, 1965, 1964b,a], Mindlin [1964, 1965], Mindlin, Eshel [1968], Toupin [1962, 1964]). These authors study deformation, damage and internal friction phenomena occurring in deformable bodies, which, at a suitable micro-level, may show strong inhomogeneities in geometrical and mechanical properties. Models of continua with enriched kinematics are known as micromorphic models and originated with the works of Mindlin

[1964] and Eringen [1999]. Such micromorphic models can also be seen as a way to obtain, as suitable limit cases, other very common generalized continuum theories which are known as second gradient theories (see e.g. Germain [1972, 1973]). These latter theories have the same kinematics as classical Cauchy continuum theories (only displacement field), but the microstructure of the continuum is accounted for by suitable length-scales associated with the assumption that the strain energy density depends on the second gradient of displacement. Various micromorphic and higher-gradient theories have been re-proposed in the last years to study different kinds of physical systems with microstructure. (See e.g. dell'Isola, Seppecher [1995], Ferretti et al. [2013], Forest [2009], Forest, Cordero, Busso [2011], Forest, Sievert [2006], Kotronis et al. [2005], Misra, Chang [1993], Misra, Ching [2013], Misra, Singh [2013], Misra, Yang [2010], Pohd, Bruhns [1993], Yang, Misra [2010, 2012], Yang, Ching, Misra [2011], Auffray, Bouchet, Brechet [2009, 2010]). Recently, a relaxed micromorphic model has been proposed in Ghiba et al. [2013], which accounts for possible micro-heterogeneities with a considerably reduced number of constitutive parameters compared to classical micromorphic models. We can summarize by saying that micromorphic models are able to catch the complexity of the coupling phenomena between micro- and macro-motions. We claim that these micro-macro coupling phenomena actually dominate dissipation in solids constituted by grains bonded with viscoelastic cement. As the internal frictional phenomena which we have in mind obviously can also occur in beams and shells, the concept of additional microstructural or internal variables that we discuss may be adapted to many different cases, such as the continuum models treated in Altenbach, Eremeyev [2009b, 2011], Altenbach, Eremeyev, Lebedev [2011], Altenbach, Eremeyev [2010a, 2009a], Eremeyev, Pietraszkiewicz [2004], Eremeyev [2005], Eremeyev, Altenbach, Morozov [2009], Eremeyev, Pietraszkiewicz [2011], Altenbach et al. [2010], Eremeyev, Freidin, Sharipova [2003], Pietraszkiewicz, Eremeyev [2007], Eremeyev, Freidin, Sharipova [2007] for shells with surface stresses or micro-polar extra kinematical descriptors. The same applies for the models of Altenbach, Eremeyev [2008, 2009a], Altenbach, Eremeyev, Morozov [2012] for continua showing viscoelastic behavior. In future investigations it could be useful to conceive homogenization procedures aimed at deducing the most suitable macroscopic models for describing the phenomena we have in mind and which seem to be associated with the proposed model of continuum with microstructure. (See e.g. Alibert, Seppecher, dell'Isola [2003] for a homogenization process leading to second gradient materials). This would allow setting up a micro-macro identification procedure for the determination of macroscopic constitutive parameters characterizing the mechanical behavior of modified concrete, starting from its microscopic internal structure. Herein we consider a

continuum model with microstructure, *aiming to describe* some of the dissipation phenomena occurring in deformable bodies, which, at a micro-level, are constituted by a compact matrix presenting a uniform and isotropic distribution of penny-shaped micro-cracks. We are aware that this last assumption is rather simplified: Not only are micro-cracks not in general isotropically and homogeneously distributed in the reference configuration, but even if they are so, they will lose these properties in the current configuration. Therefore, one should expect that for a careful and detailed modeling of the phenomena that we have in mind, one should introduce some tensor fields (see e.g. Adelaide et al. [2010]) in order to describe the evolution of the state of micro-cracks inside the Representative Elementary Volume (REV). We start to consider a simple scalar field φ whose evolution describes, in an approximate and averaged way, the total amount of relative displacement of crack faces present in the considered REV. It will be assumed that the number of micro-cracks, and their geometrical and mechanical properties, do not change in the dynamic phenomena considered. In other words, we assume that damage is not progressing. Rather, the dissipative phenomena which we want to describe are related to the relative motion of the two superimposed surfaces of cracks, which slide with respect to each other and come back to their initial position at the end of any loading cycle.

II.4 Methods for reducing the degrees of freedom in considered models

The concrete specimens tested in the experimental work of Madeo [2006], the behavior of which we want to reproduce, are three-dimensional. Therefore, the suitable model to be introduced is a model (possibly non-linear) of a three-dimensional continuum. However, to simplify the model used, one can think of following the method pioneered by Saint-Venant. (For some generalizations of the classical problem named after him and discussion of the central idea of his method, see e.g. Batra, dell'Isola, Ruta [2005], dell'Isola, Batra [1997], dell'Isola, Ruta, Batra [1998], Andreaus, Ruta [1998] and the references therein.) This method permits the reduction of the complexity of the problem of determining the deformation of a specimen, the shape of which is cylindrical in its reference configuration. More particularly, the problem of solving a system of PDEs is reduced to the simpler one of solving a system of ODEs.

We assume that:

- the cylinders considered are deformed only in the Saint-Venant compression (with Poisson effect) mode;

- the frequency of the forcing load is much smaller than the eigen-frequencies of the cylinders;
- the distribution of micro-cracks is uniform, so that one scalar quantity is sufficient to describe the internal micro-motion in the cylinder;
- the imperfections present neither cause nor influence the instabilities in any way, global or local. In particular, they do not change the microstructure evolution. (The literature in the field is immense; the reader is referred e.g. to Luongo [2001], Jamal et al. [2003], and references therein.)

Once having adopted the previous hypotheses, the problem to be solved consists then in

- looking for the evolution equation for the newly introduced kinematical descriptor φ describing micro-displacement with Coulomb dissipation;
- determining the modifications to be introduced in standard evolution equations for the displacement field;
- determining the coupling terms between these equations.

In order to obtain the reduced model, one could conceive of a more or less mathematically rigorous process starting from a Cauchy model at a given *small* length scale for the material inside a REV, in which the boundary conditions at crack faces are chosen to include Coulomb-type friction. We do not address such a delicate analysis in this work, and we will instead formulate a macroscopic model which shows the qualitative behavior which is expected on the basis of appropriate phenomenological considerations. In fact, we present a target theory, to which such a *homogenization* process should reduce. It is clear that the constitutive parameters appearing in the phenomenological theory which we develop can be determined only by means of the comparison of suitable numerical simulations with corresponding experimental evidence. Hence, we perform parametric studies of the proposed model, in order to be able to subsequently tune these parameters to direct the design of a measurements campaign.

The model presented here may have wide applicability. However, it is tailored with a view towards a precise application which is of interest in structural and civil engineering. Actually, our attention is focused, in particular, on the description of mechanical behavior of concrete-like materials with enhanced internal frictional dissipation. This enhancement is obtained by changing the recipe of the concrete mix, by adding suitable inert additives, whose grains have the size needed to fill crack

voids or to improve friction contact of crack faces. (See e.g. Madeo [2006], Pensée, Kondo, Dormieux [2002], Bowland [2012] and references there cited.) The numerical simulations which are presented in this thesis needed to be calibrated carefully, because of the strong nonlinearities they present, and because of the singular nature of ODEs usually associated to Coulomb friction. These points are not addressed in the present investigation. In this aspect, and also for what concerns the modeling difficulties, the model proposed here resembles closely the one studied in dell'Isola, Hutter [1998]). The numerical results obtained show that the proposed model is suitable for describing some of the experimental evidence discussed in Madeo [2006]. The main peculiarities of the proposed model can be summarized as follows:

- nonlinearities appear only in terms of the parameter φ and its time derivative,
- Coulomb dissipation mechanisms play a role only in the evolution equation for φ,
- dissipation cycles in the force-displacement behavior show a variety of qualitative behaviors, depending on the choice of constitutive parameters, which is general enough to encompass the structure which has been observed, as in Madeo [2006] and reproduced in fig. II.1.

II.5 Some considerations about future perspectives and limits of the model presented

To assess their possible use in our applications, the system of ODEs that we consider presents non-trivial mathematical difficulties which need to be studied. This mathematical study is preliminary to the formulation of a suitable variational principle, developed to supply the governing equations of systems which are more general than the one considered here. Moreover, the role of the micro-displacement parameter φ, as conceived in this work, will need to be further specified. More specifically, one may ask if it is possible to regard such a parameter as an internal variable. (This is done in very similar models; see e.g. dell'Isola, Woźniak [1997a,b], dell'Isola, Rosa, Woźniak [1997c, 1998] and references there cited.) Or should it be regarded as a truly micro-structural parameter, as done e.g. in Toupin [1962, 1964], Green, Rivlin [1964b,a], Mindlin [1964], Misra, Singh [2013], Misra, Yang [2010], Sedov [1972], dell'Isola, Batra [1997] and references there cited. The mathematical relevance of such a question is not negligible. Indeed, in the first case the deformation energy is assumed to depend on φ only, while in the second one also a dependence on $\nabla\varphi$ will appear. As a consequence, the evolution equations for φ in the first case will

not involve partial derivatives, but which will be present in the second case. A related problem concerns the highest order of the derivatives of the displacement field, which we will need to introduce in connection with deformation energy, to obtain the desired generalized model. It is indeed known (see e.g. Alibert, Seppecher, dell'Isola [2003] and references there cited) that high contrast in the mechanical properties at the micro-level, which surely is present in the physical system considered here, requires the introduction of higher order continua. (See e.g. dell'Isola, Guarascio, Hutter [2000], dell'Isola, Seppecher [1995], Ferretti et al. [2013], Forest [2009], Forest, Cordero, Busso [2011], Forest, Sievert [2006], Madeo, dell'Isola, Darve [2013], Nadler, Papadopoulos, Steigmann [2006], Sciarra, dell'Isola, Coussy [2007] and references there cited.) In this thesis, we are assuming that the population of cracks present in the specimens considered is constant in number and does not change its mechanical and geometrical properties because of the applied loads. In other words, we assume that the level of damage at the microlevel is not changing during the loading/unloading process. (For similar approaches see e.g. Adelaide et al. [2010], Altenbach, Eremeyev [2008], Andreaus, Baragatti [2009], Bhattacharjee, Léger [1993], Boma, Brocato [2010], Boukria, Limam [2012], Carpinteri, Lacidogna, Pugno [2004], Contrafatto, Cuomo [2002, 2005], Ciancio, Carol, Cuomo [2006, 2007] and references there cited.) Indeed, the experimental evidence presented in Madeo [2006] shows that there is no degradation in the mechanical properties when the intensity of the applied loads is below a precise threshold, provided the duration of loading is limited in time. This means that dissipation occurs at crack surfaces without relevant abrasion. (See e.g. D'Annibale, Luongo [2013] and references there cited.) It also occurs without any plastic phenomenon. (See e.g. Contrafatto, Cuomo [2002, 2005, 2006], Cuomo, Contrafatto [2000], Cuomo, Ventura [1998] and references therein.) Further, there is no formation of new cracks. (See Hillerborg, Modéer, Petersson [1976] and related literature.)

We will not assume in this thesis that there is an explicit dependence of the strain energy density on the space gradient of φ. This means that we are assuming that the micro-motion inside one REV does not depend on the micro-motions inside the contiguous ones. This is equivalent to saying that we do not account for the possibility of describing, at a macroscopic scale, the presence of high gradients of microscopic relative displacements. This hypothesis is quite sensible since no localization phenomena are observed in the mechanical tests performed. The model which is presented here has been tailored to be used for modified concrete. However, one should consider that many possible applications can be imagined for it. Actually, internal friction is a phenomenon which plays a relevant role in different contexts, for instance in the flow in porous media. (See e.g. dell'Isola, Guarascio, Hutter [2000],

dell'Isola, Hutter [1998], Federico, W. Herzog [2008a], dell'Isola, Madeo, Seppecher [2009], Madeo, dell'Isola, Darve [2013], Misra, Chang [1993], Quiligotti, Maugin, dell'Isola [2002, 2003], Sciarra, dell'Isola, Hutter [2001], Sciarra, dell'Isola, Coussy [2007] and references there cited.) In such cases internal friction competes with Darcy or Brinkman dissipation. Another related case is growing tissues, as described using micro-structured continuum models, as in Federico, W. Herzog [2008b], Federico, Gasser [2010], Lekszycki, dell'Isola [2012], Madeo, Lekszycki, dell'Isola [2011], Madeo [2006], where internal friction seems to play a non-negligible role in mechano-sensing phenomena controlling tissue synthesis.

It has to be finally remarked that the modification of concrete by means of suitable inert additives, proposed in Madeo [2006] is founded on some precise theoretical considerations which need to be further developed. (See e.g. Pensée, Kondo, Dormieux [2002].) Actually, the idea is the following: The concrete recipe is modified in order to increase its *dissipation capability* without favoring the onset of plastic deformation or crack formation and growth. In order to develop this idea, an important theoretical effort is required. One has to adapt the methods used in the theory of structural modification. (See e.g. Carcaterra, Akay [2007, 2011, 2006], Culla, Sestieri, Carcaterra [2003] and references there cited.) Other useful methods are those of the design of smart materials and structures. (See e.g. Andreaus, dell'Isola, Porfiri [2004], dell'Isola, Vidoli [1998a,b], Maurini, dell'Isola, Del Vescovo [2004], Maurini, Pouget, dell'Isola [2004, 2006], Porfiri, dell'Isola, Santini [2005], Vidoli, dell'Isola [2001, 2000] and references there cited.) In the first type of theories the concept which is exploited is the following: One adds to the system some coupled subsystems in which the energy preferably flows and in which it remains trapped until it is somehow dissipated. We remark that this effect can be obtained by using only linear phenomena (see Carcaterra, Akay [2007]) and that its analysis is based on the concept of internal or micro-structural evolutionary variables whose evolution equations are suitably designed. This is also the concept on which the second of the aforementioned research streams is based: The coupled systems are designed in order to *internally resonate with the principal system and the damping elements are tailored to optimize energy dissipation.*

In conclusion, the change of the concrete recipe which is envisaged here should forecast the formation of suitable slave microstructures, as follows:

- Their motion is activated by macro-deformation
- Their presence does not modify the mechanical strength of the modified concrete
- Their damping capabilities reduce (or do not alter) the damage progress in

the presence of cyclic load.

One of the main conclusions to which the present work leads is that the modeling tool which seems more suitable in this context is a microstructure field theory coupled with standard methods of optimization and control. More precisely, once having introduced a new scalar kinematical parameter φ, which is intended to measure the overall relative displacement of micro-cracks faces inside a Representative Elementary Volume (REV) of the specimens considered, we postulate, on the basis of reasonable simplifying assumptions, some coupled Ordinary Differential Equations governing both macroscopic strains and micro-deformations of internal micro-cracks. We aim to describe *(i)* linear and non-linear deformation phenomena occurring because of the aforementioned relative displacement, *(ii)* coupling phenomena between macro-motion and micro-motion, and *(iii)* Coulomb dissipation phenomena occurring at crack faces. The model presented assumes no crack growth or crack production, but simply the existence of a reversible (although dissipative) internal micro-motion due to the presence, in the reference configuration, of micro-cracks.

II.6 Modelling

The model for concrete-based materials which we want to introduce is a very particular case of a continuum with microstructure (see e.g. Eringen [2001], Mindlin [1964]). Our final aim is to investigate the mechanism of internal dissipation due to Coulomb friction. Many authors examine the different mechanisms of internal dissipation in brittle materials such as concrete; see e.g. for more details Lomniz [1957], Bhattacharjee, Léger [1993]. In particular, we want to focus our attention on dissipation in materials (such as concrete) which present voids typically characterized by a shape as a coin (coin-shaped cracks), and materials (such as modified concrete e.g. Madeo [2006], Bowland [2012]) containing microscopic components such as micro-filler, used to improve damping performances without compromising mechanical strength. A new additional and independent micro-structural kinematical variable φ is introduced to take into account the interaction between the opposite faces of voids (micro-cracks) when they come in contact and slide one with respect to the other because of the externally applied load. We assume that the deformation energy of the medium considered is characterized by a volumetric strain energy density Ψ which depends on the basic kinematic descriptors, i.e. the classical displacement field $\mathbf{u}$ and the new scalar field φ, which represents the relative

displacement of two superimposed faces of micro-cracks. In particular, we set

$$\Psi\left(E,\varphi\right)=\frac{1}{2}\left[2\mu\,\mathrm{tr}(\mathbf{E}\,\mathbf{E})+\lambda\left(\mathrm{tr}\mathbf{E}\right)^{2}\right]+\frac{1}{2}k_{1}\varphi^{2}+\frac{1}{3}k_{2}\varphi^{3}+\frac{1}{4}k_{3}\varphi^{4}+\alpha\varphi\sqrt{I_{2}^{(d)}}\quad\text{(II.24)}$$

where λ and μ are the Lamé parameters for linearly elastic isotropic materials. Also, $\mathbf{E}=\left(\nabla\mathbf{u}+\nabla\mathbf{u}^{T}\right)/2$ is the linearized Green-Lagrange deformation tensor, and the scalar $I_{2}^{(d)}$ is the second invariant of the deviatoric strain tensor $\mathrm{dev}\,\mathbf{E}=\mathbf{E}-\frac{1}{3}\mathrm{tr}\,\mathbf{E}\,\mathbb{I}$ defined as

$$I_{2}^{(d)}=\frac{1}{2}\,\mathrm{tr}\,\left(\mathrm{dev}\,\mathbf{E}\,\mathrm{dev}\,\mathbf{E}\right).$$

The ansatz (II.24) on the strain energy density will be justified *a posteriori* on the basis of available experimental evidence. On the other hand, the kinetic energy density of the system considered is defined by

$$\mathcal{K}=\frac{1}{2}\,\rho\,\dot{\mathbf{u}}^{2}+\frac{1}{2}\,\rho_{\varphi}\,\dot{\varphi}^{2}\quad\text{(II.25)}$$

where ρ is the mass density of the bulk material and the ρ_{φ} is an effective macroscopic mass density linked to the micro-structural variable φ. It can be checked that, since the micro-strain field φ is assumed to have the dimensions of a length, the units of the parameter ρ_{φ} are the same as the units of the macroscopic bulk mass density ρ. Since the dissipation is not negligible, the governing equations of the medium considered do not have a variational structure, but they possess a quasi-variational structure. In this context we introduce a Rayleigh potential $\mathcal{R}$, which is aimed to describe Coulomb-type friction dissipation, in the form

$$\mathcal{R}=\zeta\,\mathrm{tr}\mathbf{E}\,\left(\frac{\mathrm{Log}(\,\mathrm{Cosh}(\,\eta\,\dot{\varphi}\,)\,)}{\eta}\right),\quad\text{(II.26)}$$

where ζ and η are constitutive constants. We can notice that, in particular, the constant η can be seen as the inverse of a characteristic velocity associated with microscopic motions, while the constant ζ directly accounts for dissipation due to microscopic frictional sliding. Few words need to be spent here; actually, in the literature, the Coulomb friction force is usually modeled by the introduction of the function signum, whose argument is the velocity of the kinematical quantity on which friction forces are acting.

This function, when appearing in differential equations, is a source of strong singularities and numerical or chaotic instabilities, whose regularization and study can be performed using the methods described in the literature. (See e.g. Luongo, Di Egidio [2006], Luongo, Romeo [2009], Michel, Limam, Jullien [2000], Luongo, Zulli, Piccardo [2009] and references therein.) Also, based on physical considerations, we propose to regularize the function signum with a hyperbolic tangent, modulated

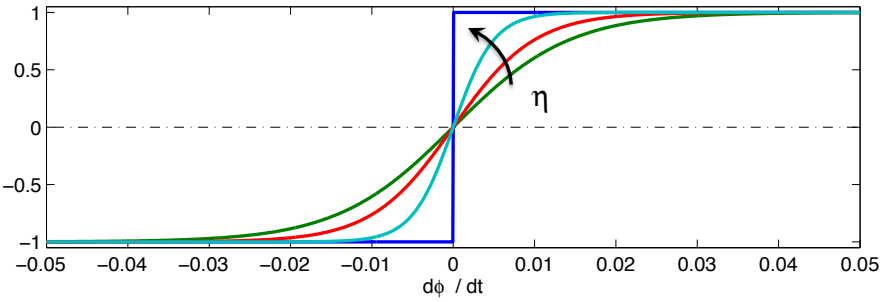

Figure II.2: Friction law with varying the parameter η.

with an amplitude ζ (giving the maximum of friction force which may be exerted) and with a suitably chosen slope given by η, triggering the range of velocity, where friction force is an increasing function of the velocity (see fig. II.2). This is equivalent to state that we assume a Navier-Stokes type of dissipation for low micro-velocities. This physical assumption, although reasonable, needs to be justified with more detailed analyses and can also be related to bifurcation and instability phenomena which may occur in modified concrete (see e.g. Jamal et al. [2003] and references therein).

In conclusion, the virtual work due to internal dissipation can be written as

$$\delta W^{(Diss)}\left(\mathbf{E},\varphi,\dot{\varphi}\right)=\int_0^T\int_V\left(\frac{\partial\mathcal{R}}{\partial\dot{\varphi}}\,\delta\varphi\right)\mathrm{d}V=\int_0^T\int_V\zeta\,\mathrm{tr}\,\mathbf{E}\tanh(\,\eta\,\dot{\varphi}\,)\,\delta\varphi\,\mathrm{d}V,$$

where V is the volume which the specimen occupies in its reference configuration and $[0,T]$ is the time interval during which we observe the motion of the specimen. We can write the governing equations in weak form of the concrete-based material as

$$-\,\delta W^{(Elast)}+\delta W^{(Iner)}=-\delta W^{(Diss)}+\delta W^{(Ext)} \tag{II.27}$$

in which

$$\delta W^{(Elast)}=\int_0^T\int_V\delta\Psi\,\mathrm{d}V,\qquad\qquad \delta W^{(Iner)}=\int_0^T\int_V\delta\mathcal{K}\,\mathrm{d}V,$$

$$\delta W^{(Ext)}=\int_0^T\int_{\partial V}\mathbf{F}^{ext}\cdot\delta\mathbf{u}\,\mathrm{d}S,$$

with the expressions for the strain energy and kinetic energy densities given by eqs. (II.24) and (II.25), respectively, and where $\mathbf{F}^{ext}$ are the surface externally applied forces.

II.6.1 Simplified equations of motion based on Saint-Venant theory for the case of simple compression

We use from here on the fact that the experiments which are targeted in this work are simple compressions of cylindrical concrete specimens, so that we assume that Saint-Venant theory for simple compression can be applied. In this way, we are able to deduce the simplified equations in strong form directly from expression (II.27). To do so, we start recalling that, in the case of axial compression along the x_3 axis of a Saint-Venant cylinder, one has

$$\mathbf{E} = \begin{pmatrix} -\nu\,\varepsilon & 0 & 0 \\ 0 & -\nu\,\varepsilon & 0 \\ 0 & 0 & \varepsilon \end{pmatrix}, \qquad \mathbf{u} = \begin{pmatrix} -\nu\,\varepsilon\,x_1 \\ -\nu\,\varepsilon\,x_2 \\ \varepsilon\,x_3 \end{pmatrix},$$

where we set $\varepsilon = E_{33} = u_{3,3}$, with ν the Poisson coefficient, and x_1, x_2 and x_3 are the Lagrangian coordinates (in a given reference frame with origin on the axis of the cylinder) of the material points constituting the considered specimen. We also explicitly remark that another assumption of the Saint-Venant model is that the field ε does not depend on x_1, x_2, x_3, but only, possibly, on time. We make the same assumption for the micro-displacement field φ. With these simplifying assumptions, it can be checked that, in the particular case considered, integrating by parts in time, considering isochronous motions and arbitrary variations $\delta\varepsilon$ and $\delta\varphi$, the principle of virtual powers (II.27) implies

$$\begin{cases} M\ddot{\varepsilon} + K\varepsilon + \tilde{\alpha}\varphi = f_0 + f_1\sin(\omega t) \\ \\ m_\varphi\ddot{\varphi} + \tilde{k}_1\varphi + \tilde{k}_2\varphi^2 + \tilde{k}_3\varphi^3 + \tilde{\alpha}\varepsilon - \tilde{\zeta}\tanh(\eta\,\dot{\varphi})\,\varepsilon = 0 \end{cases} \tag{II.28}$$

where

$$M = \int_V \rho\left(\nu^2\left(x_1^2 + x_2^2\right) + x_3^2\right)\mathrm{d}V, \quad m_\varphi = \int_V \rho_\varphi\,\mathrm{d}V,$$

$$K = \int_V \left(\lambda + 2\,\mu + 4\,(\lambda+\mu)\,\nu^2 - 4\,\lambda\,\nu\right)\,\mathrm{d}V, \quad \tilde{\alpha} = \int_V \left(\sqrt{3}/3\,(1+\nu)\,\alpha\right)\,\mathrm{d}V,$$

$$\tilde{k}_1 = \int_V k_1\,\mathrm{d}V, \quad \tilde{k}_2 = \int_V k_2\,\mathrm{d}V, \quad \tilde{k}_3 = \int_V k_3\,\mathrm{d}V, \quad \tilde{\zeta} = \int_V \zeta\,(1-2\,\nu)\,\mathrm{d}V.$$

Moreover, the external applied forces have been chosen to be those of a simple dynamic compression, i.e. $\mathbf{F}^{ext} = (0, 0, -F)^T$, with $F = F_0 + F_1\sin(\omega t)$. With this

assumption, it can be checked that the loads appearing in eqs. (II.28) are defined as $f_0 = k\,F_0$ and $f_1 = k\,F_1$ with $k = \int_{\partial V} L\,\mathrm{d}S$ and L the length of the cylinder. Some comments are needed at this point:

- One can easily estimate the equivalent mass M by assuming that the volume mass density of concrete specimens is homogeneous (and known) while the displacement field depends linearly on the reference configuration variables and on elongation.

- We assume that elastic non-linearities are involved only in the evolution equation for the variable φ.

- The function $\tilde{k}_1\varphi + \tilde{k}_2\varphi^2 + \tilde{k}_3\varphi^3$ is assumed to be monotonously increasing.

- The deformation energy clearly needs to be positive definite and, consequently, suitable restrictions on the stiffness parameters must be considered.

- The amplitude of the Coulomb frictional force, for obvious physical reasons, has to be smaller than the lowest amplitude of the applied external load. (See the papers Luongo, Di Egidio [2006], Di Egidio, Luongo, Paolone [2007], Michel, Limam, Jullien [2000], Jamal et al. [2003] and references therein for a discussion of the possible bifurcation phenomena which may occur.)

- Many other possible dissipation regimes can be conceived in order to regularize the discontinuous dependence assumed in a Coulomb-type model for friction. Each of them would represent a different physical phenomenon, which would have different effects on the turning points of dissipation loops (i.e. when $|\dot{\varphi}|$ is suitably small). In this work we assume that viscous Navier-Stokes dissipation effects are dominant when the microstructure velocity $|\dot{\varphi}|$ is suitably small, while they vanish and need to be replaced by Coulomb friction beyond a given micro-velocity level.

The eqs. (II.28) are very similar to those presented in Bastien, Schatzman, Lamarque [2000], Lamarque, Bernardin, Bastien [2005]. The former paper describes rheological models based on simple constitutive elements –springs, dash-pot, Saint-Venant elements– and provides mathematical study, existence and uniqueness results, and an adapted numerical scheme. The latter paper consider a locally Lipschitz continuous term in the deterministic or stochastic frame.

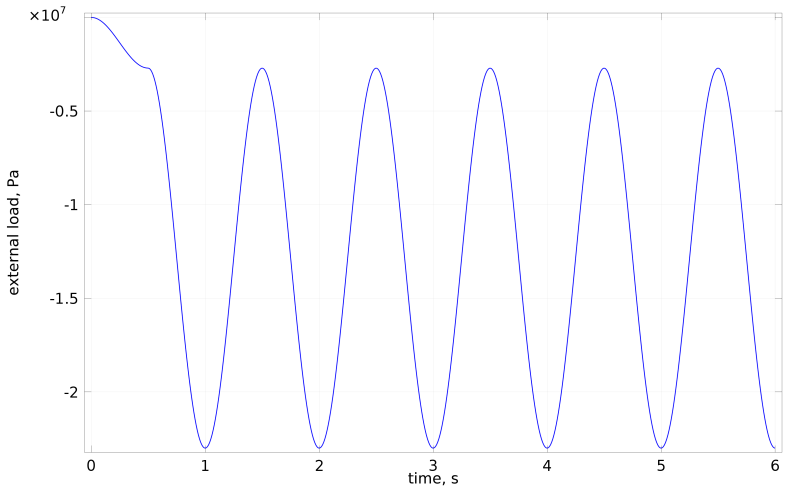

Figure II.3: Cyclic external load.

II.7 Numerical simulations: specimen in pure compression

For numerical simulations, we limit our attention to cylindrical specimens with diameter $\phi = 11.28$ cm and height $h = 22$ cm. All simulations are performed via the automatic code *COMSOL Multiphysics*®. As for boundary conditions, the specimen is constrained at the bottom with a zero displacement in the direction x_3. A cyclic external load per unit area is applied on the top in the direction x_3 and with a frequency of 1 Hz, which is very low compared with the natural frequencies of the testing sample, to avoid troublesome inertial effects. For the same reason, an initial smooth ramp is employed as shown in fig. II.3.

In order to illustrate the performance of the model proposed for the cement-based materials studied in this thesis, we consider several numerical simulations performed by varying the parameters introduced in eq. (II.28). All other parameters which are not varying take the values prescribed in tab. II.1. We show in tab. II.2 the ranges of values for the introduced parameters used to perform numerical parametric studies.

The numerical values shown in tab. II.1 have been determined by means of the following calibration process:

- in the static loading case the measured stress-strain relationship has to be verified;

- the value of the parameter φ has to be compatible with the order of magnitude of known dimensions of typical cracks in concrete;

Table II.1: Reference values of the parameters used in the numerical simulations.

Parameter	Value	Unit
M	7.8×10^{-2}	$\mathrm{kg\,m^2}$
m_φ	7.8×10^{-5}	kg
K	25×10^{9}	N m
$\tilde{\alpha}$	1.9×10^{11}	N
$\tilde{k}_1$	1.86×10^{12}	N/m
$\tilde{k}_2$	9.4×10^{13}	$\mathrm{N/m^2}$
$\tilde{k}_3$	9.2×10^{19}	$\mathrm{N/m^3}$
$\tilde{\zeta}$	1.5×10^{11}	N
η	2×10^{2}	s/m

- equivalent mass coefficients are determined by taking into account the volume mass density of concrete and an estimate of the percentage of total mass of concrete specimens which is moved because of crack faces movement;
- amplitude of Coulomb friction force has to be smaller than the force deforming micro-cracks;
- coupling between micro and macro motion must respect positive definiteness of the deformation energy;

Some parametric studies are performed in the remainder of this thesis on the crucial parameters of the model presented. Unless otherwise specified, the typical ranges of values assigned to the material parameters in the numerical simulations are those listed in tab. II.2.

II.7.1 Effect of the basic parameters of the model presented on the area of dissipation loops

In this subsection we show the effect of any single parameter of the proposed model on the area and shape of the dissipation loops. We start by considering the effect of the Coulomb friction coefficient $\tilde{\zeta}$ on the amplitude of dissipation loops, the area of

Table II.2: Ranges of values of the material parameters to be used in the numerical simulations on concrete.

Parameter	Range of values	Unit
$\tilde{k}_1$	$1.7 \times 10^{12} - 1.93 \times 10^{12}$	N/m
$\tilde{k}_2$	$0 - 8 \times 10^{15}$	N/m^2
$\tilde{k}_3$	$6.5 \times 10^{19} - 9.5 \times 10^{20}$	N/m^3
$\tilde{\alpha}$	$1.7 \times 10^{11} - 2 \times 10^{11}$	N
$\tilde{\zeta}$	$10^{10} - 4 \times 10^{11}$	N

which is seen to increase monotonically with $\tilde{\zeta}$. However, because of the strong non linearity of system considered, the variation of the other relevant parameters also greatly influences the dissipating capability.

Figure II.4 shows the variation of energy dissipation loops in a stress-strain diagram when varying the friction coefficient $\tilde{\zeta}$. It can be directly remarked that the area of the loops is increased when increasing the value of the coefficient $\tilde{\zeta}$. This is completely sensible, since the mechanism which we want to associate with the parameter $\tilde{\zeta}$ is the dissipation at the scale of micro-cracks, which is due to the relative motion of the two superimposed faces of each crack as a consequence of the application of the external dynamic load. This numerical evidence is a step towards the conception of suitable experimental campaigns on concrete modified with micro-fillers enhancing its dissipative properties. Indeed, it is sensible to assume that different micro-fillers with different mechanical and physical characteristics may fill the micro-voids which are present inside the concrete matrix and change the microscopic friction coefficient $\tilde{\zeta}$ with respect to that of unmodified concrete.

Figure II.5 shows the variation of dissipation loops when varying the coefficient $\tilde{\alpha}$, i.e. the coupling parameter between the micro-structural variable φ and the macroscopic strain. It is worth noticing that the effect of increasing micro-macro coupling implies that the dissipation loop is shifted towards the right. Increasing the value of the coupling parameter means that the contribution to macroscopic deformation due to microscopic motion becomes more and more important and greater macroscopic strains can be attained with the same force level. Moreover, we notice that the fact of increasing the coupling parameter $\tilde{\alpha}$ changes the shape of the dissipation loop giving rise to characteristic curvatures of the loading-unloading branches which are observed in available experimental curves (see fig. II.1). We

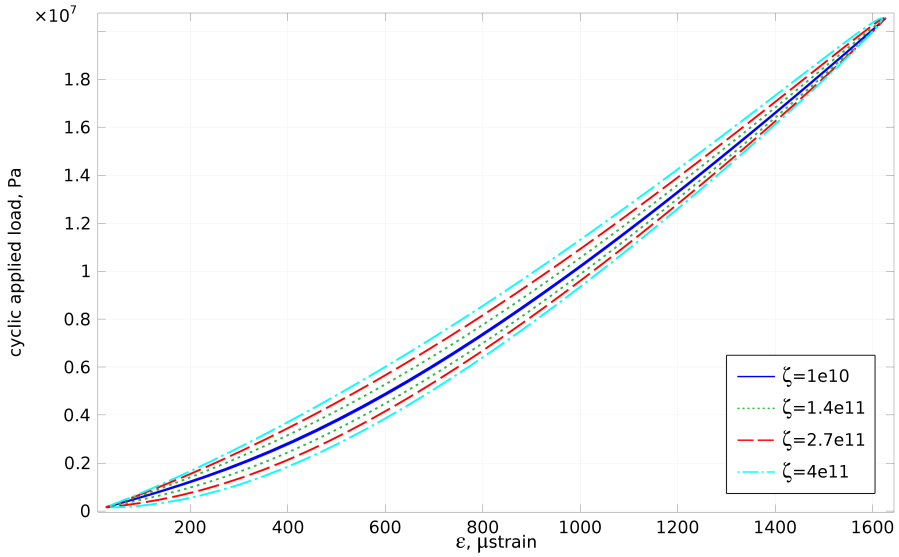

Figure II.4: Influence of the friction coefficient $\tilde{\zeta}$ on the energy dissipation loops for cement-based materials. $\tilde{\zeta} = [1 \times 10^{10},\ 1.4 \times 10^{11},\ 2.7\,10^{11},\ 4 \times 10^{11}]$.

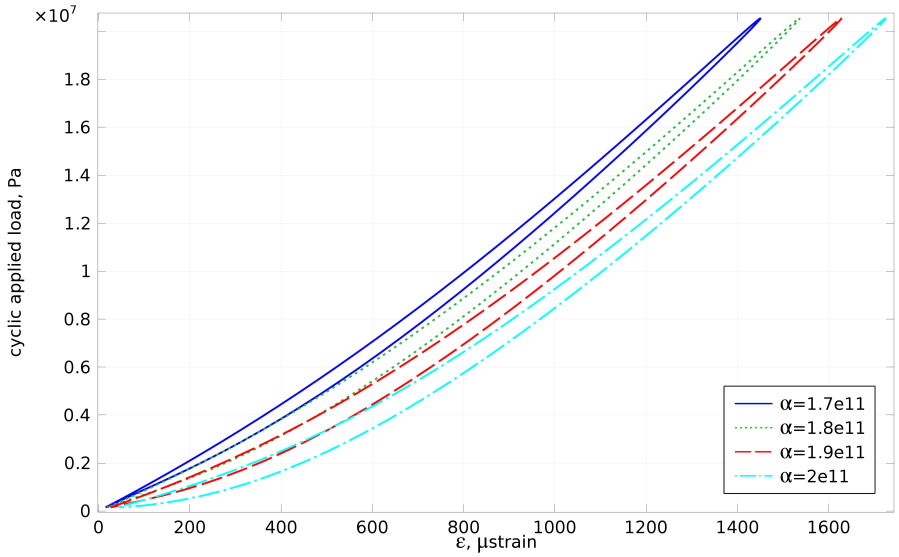

Figure II.5: Influence of the material parameter $\tilde{\alpha}$ on the energy dissipation loops for cement-based materials. $\tilde{\alpha} = [1.7 \times 10^{11},\ 1.8 \times 10^{11},\ 1.9 \times 10^{11},\ 2 \times 10^{11}]$.

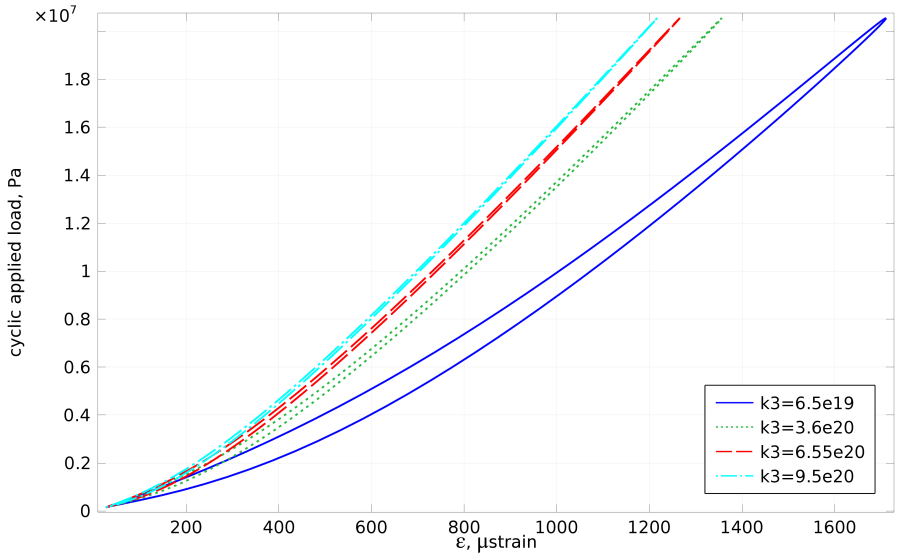

Figure II.6: Influence of the material parameter $\tilde{k}_3$ on dissipation loops for cement-based materials. $\tilde{k}_3 = [6.5 \times 10^{19},\ 3.6 \times 10^{20},\ 6.55 \times 10^{20},\ 9.5 \times 10^{20}]$.

finally remark that with smaller coupling, the obtained loops can be seen to show a slightly smaller area and thus a reduced dissipation.

In fig. II.6 dissipation loops are depicted which show the effect of the material parameter $\tilde{k}_3$. It is possible to remark that, contrarily to what happens with the coupling parameter $\tilde{\alpha}$, high values of $\tilde{k}_3$ increase the whole stiffness of the system and consequently decrease the energy dissipated in each cycle. More precisely, $\tilde{k}_3$ can be interpreted as a microscopic stiffness which makes more difficult the relative motion of crack faces when it takes higher values. For example, $\tilde{k}_3$ may be expected to be higher when considering a concrete matrix prepared with higher mechanical strength concrete. It can be observed (but we do not show explicit pictures here) that if one sets $\tilde{k}_3$ to be zero, then the characteristic sickle shape of the dissipation loop associated with the Coulomb friction phenomena is completely lost and the dissipation loop resembles more an ellipsoid, which is known to be associated with viscous dissipation phenomena. Hence, we can conclude that the constitutive parameter $\tilde{k}_3$, intrinsically associated with the microscopic elastic behavior governing the relative motion of crack faces, is necessary if one wants to correctly describe the characteristic sickle shape of the experimental dissipation loops.

In fig. II.7 the behavior of dissipation loops is depicted when increasing the value of the material parameter, $\tilde{k}_2$. It can be observed that the micro-stiffness parameter $\tilde{k}_2$ also can be related to microscopic elastic mechanisms, which makes the whole specimen more rigid when this parameter takes higher values. Nevertheless, the

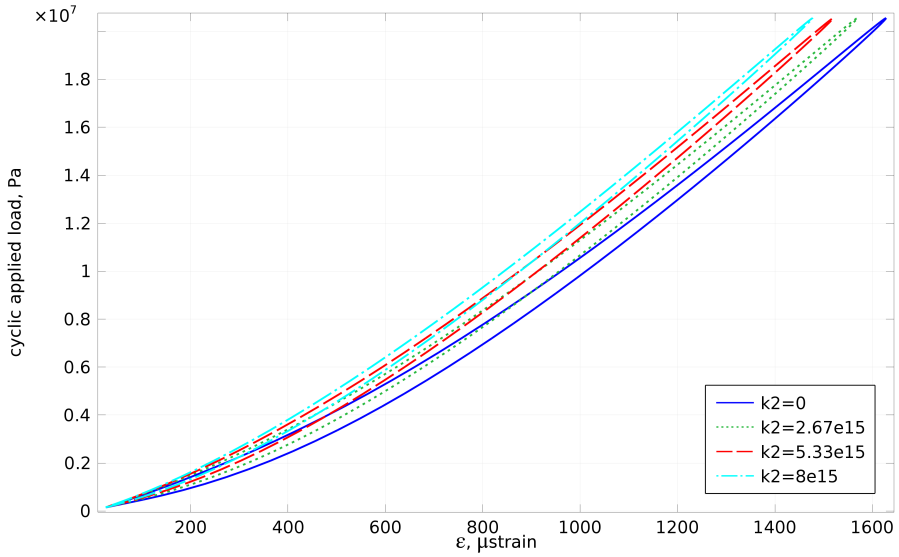

Figure II.7: Influence of the material parameter $\tilde{k}_2$ on energy dissipation loops for cement-based materials. $\tilde{k}_2 = [1 \times 10^{10},\ 2.67 \times 10^{15},\ 5.33 \times 10^{15},\ 8 \times 10^{15}]$.

influence of this parameter on dissipation loop shape and amplitude is less pronounced when compared with that due to $\tilde{k}_3$. This is sensible since the microscopic non-linearities associated with the parameter $\tilde{k}_3$ are of higher order than those associated with $\tilde{k}_2$. Numerical simulations show that values of $\tilde{k}_2$ which span in the range $[0, 10^{15}]$ do not substantially affect the dissipation behavior of the system. On the other hand, for the values of $\tilde{k}_2$ shown in tab. II.2, a rigidifying effect of the material for higher values of $\tilde{k}_2$ can be observed.

Figure II.8 shows how the material parameter $\tilde{k}_1$ affects the stress-strain cycles. It is possible to notice that an increase of the parameter $\tilde{k}_1$ does not directly affect the amount of energy dissipation, but changes the stiffness of the material considered in a similar way as $\tilde{k}_2$.

II.7.2 Some typical plots showing the periodic variation in time of relevant quantities

It is well-known (see e.g. Volpato [1956]) that well-behaving ODEs when forcing terms are periodic show solutions which are periodic as well. The dissipation effects which we have introduced in the previous eqs. (II.28) have been regularized in order to be sure that the aforementioned well-behavior assumptions are verified. Therefore, when the simulation is performed for a time interval which is long enough, the calculated solution will become –within numerical error– periodic. By a judicious

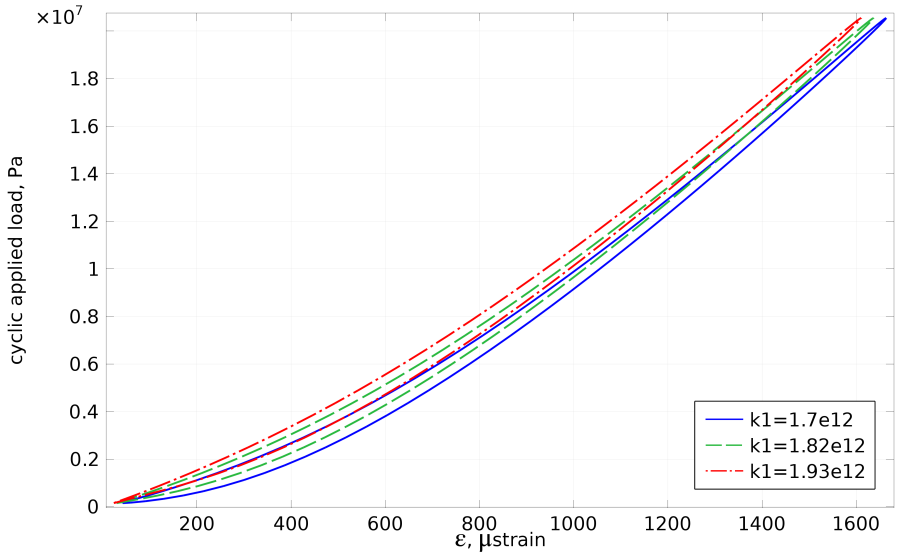

Figure II.8: Influence of the material parameter $\tilde{k}_1$ on energy dissipation loops for cement-based materials. $\tilde{k}_1 = [1.7\,10^{12},\ 1.8\,10^{12},\ 1.93\,10^{12}]$.

choice of initial conditions the convergence towards stationary solutions has been reduced.

We plot the following time dependent quantities

- friction term in the equation for φ;
- the crack faces relative displacement φ and its time derivative;
- the specimen elongation ε and its time derivative.

Figure II.9 shows the typical periodic evolution for Coulomb friction. The different stiffness properties due to the introduced non-linear term produces an asymmetric evolution of this friction term. As a consequence the relative dissipation loops will show a distance between the loading/unloading branches whose varying shape strongly depends on the non-linear behavior considered.

Figure II.10 shows the typical periodic evolution of the crack faces relative displacement. We notice a different behavior in the neighborhood of the maximum and minimum level of the cyclic external compressive load due to elastic non-linearities of the model considered. It is even worth noticing that near to the aforementioned levels, two different time delays with respect to the applied cyclic load can be detected. This circumstance is related to the assumed dissipation mechanism and to the introduced elastic non-linearities.

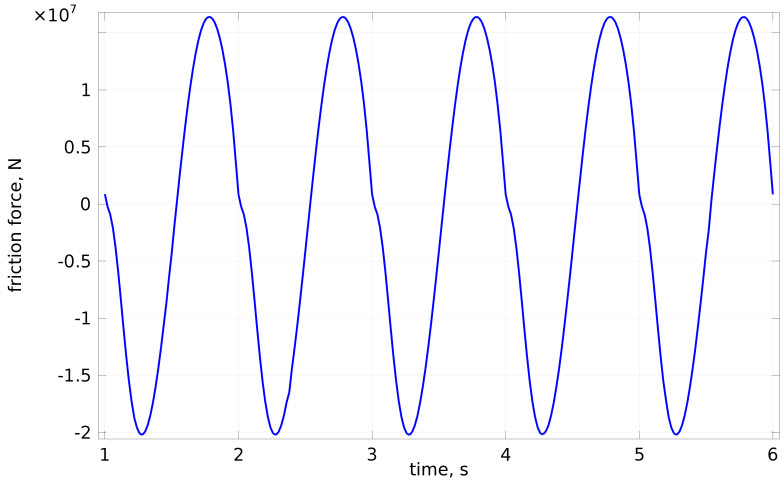

Figure II.9: Periodic evolution for Coulomb friction.

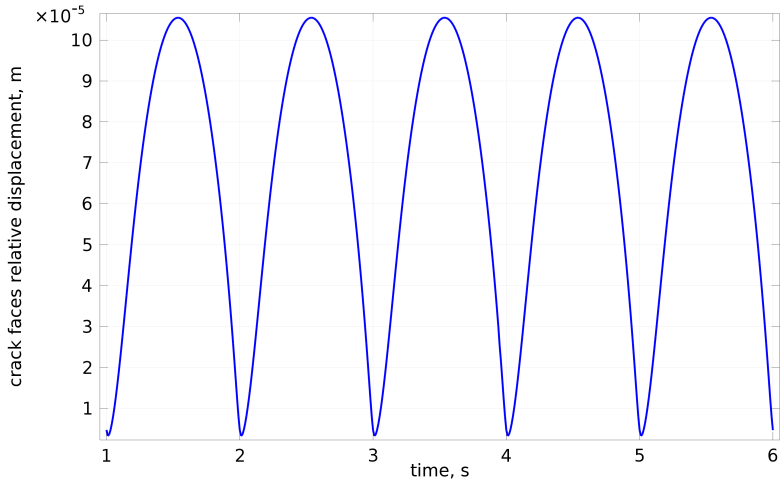

Figure II.10: Periodic evolution of the crack faces relative displacement.

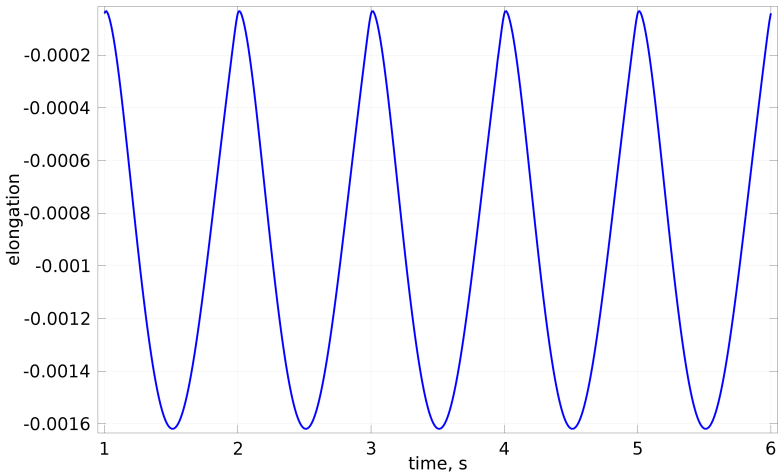

Figure II.11: Periodic evolution of the specimen elongation.

Figure II.11 shows the typical periodic evolution of the specimen elongation. Similar considerations as those raised for the variable φ can be made for the elongation, even if in this case the differences in the neighborhood of the maximum and minimum amplitude of the cyclic load are less emphasized.

Figure II.12 shows the typical periodic evolution of the relative velocity of crack faces. The time dependence of this velocity shows clearly the effect of the Coulomb dissipation effect introduced.

Figure II.13 shows the typical periodic evolution of the specimen elongation rate. It is possible, also in these time evolution plots, to clearly detect the different effect of Coulomb dissipation in the loading/unloading cycles due to the elastic non-linearity introduced.

II.8 Discussion

The modeling process presented in the present work proves that it is possible, by means of a simple non-linear system of ordinary differential equations, to carefully describe both quantitatively and qualitatively the available experimental evidence on compression of cylindrical modified concrete specimen. In particular, it is proven that, even if the applied compression force is related to elongation by a (nearly) linear relationship, some non-linearities in the dissipation loop may be ascribed to non-linear elastic phenomena involving the newly introduced microstructural parameter which describes internal micro-motions. More precisely, we want to interpret the physical meaning of this micro-structural parameter in terms of the overall relative

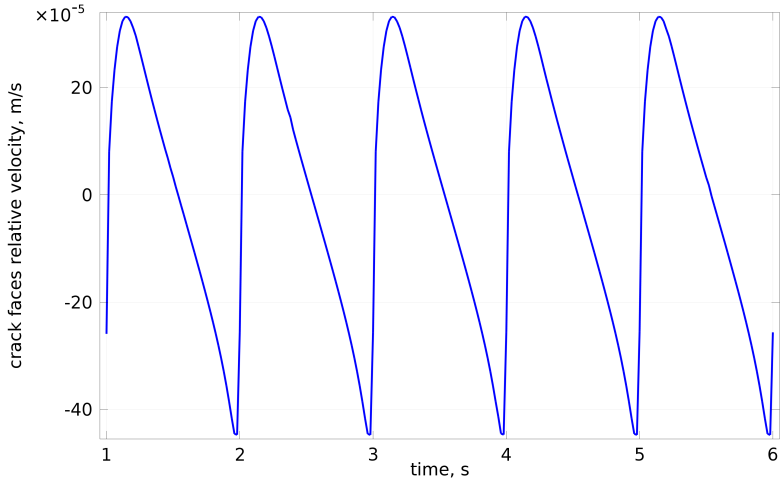

Figure II.12: Periodic evolution of crack faces relative velocity.

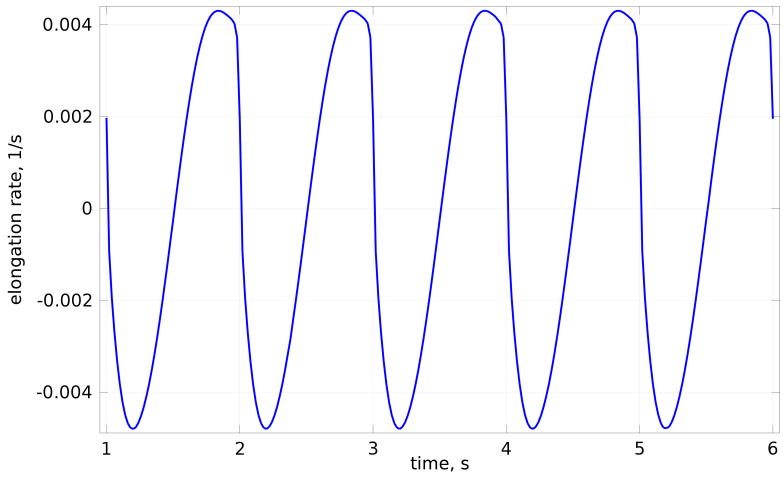

Figure II.13: Periodic evolution of the specimen elongation rate.

displacement of the faces of the cracks which characterize the microstructure of concrete-type specimens. The time rate of the same micro-structural parameter is the source of the only friction effect considered in this work, namely, the Coulomb friction force.

By means of a series of numerical simulations, we have proven that a physically reasonable set of ranges for introduced constitutive parameters can be found which describes the whole variety of dissipation loops measured in Madeo [2006]. The results presented justify the need for more complex models in order to describe: *(i)* bending and compression periodic deformation of considered cylindrical specimens, *(ii)* coupling between bending and shear with micro-deformation, *(iii)* more complex micro-motions in which relative displacement of crack faces may depend on the orientation and localization of cracks, and *(iv)* the longer range effects of micro-cracks-induced micro-deformation in the neighborhood of considered REV, i.e. those effects which can be modeled by allowing for the dependence of deformation energy on higher gradients of introduced kinematical fields.

Chapter III

Mechanical Testing

On the basis of the micro-macro theory previously presented, a set of concrete specimens with micro-additives has been prepared, resulting in the achievement of new concrete-like materials. In order to see how the presence of these additives can affect the friction coefficient between the two faces of each crack and the crack density inside the concrete matrix, a measurement campaign has been carried out. Specifically, all specimens were tested following two different procedures. As a first step, each specimen was tested under cyclic loading to determine the volume energy dissipated. Subsequently, a compression test was conducted for measurement of material strength. The experimental data have been used to perform a parameter identification and they seem to indicate that the proposed model is suitable to forecast the dissipation energy level.

III.1 Test Specimens and Materials

The specimen is a simple cylinder having a ratio of length to diameter, L/d, equal to 2. The choice of a specimen length represents a compromise. Buckling may occur if L/d ratio is relatively large. If this happens, the test result is not representative of the measure of the fundamental compressive behavior of the material. Buckling is affected by the unavoidable small imperfections in the geometry of the test specimen and its alignment with respect to the testing machine. In fact, the ends of the specimen can be almost parallel, but never perfectly so. Conversely, if L/d is small, the test result is affected by the details of the conditions at the end. In particular, as the specimen is compressed, the diameter increases due to the Poisson effect, but friction retards this motion at the ends, resulting in deformation into a barrel shape. This effect can be minimized by proper lubrication of the ends. Thus, the choice of a too small L/d ratio may result in a situation where the behavior of the

specimen is dominated by the end effects. Considering both the desirability of small L/d to avoid buckling and large L/d to avoid end effects, a reasonable compromise is $L/d = 2$ for brittle materials, in which end effects are small. The test specimen used have a circular cross section of diameter $d = 11.28$ cm and a length $L = 22$ cm; its ends are provided with caps to ensure that the test cylinder has smooth, parallel, uniform bearing surfaces perpendicular to the applied axial load during compressive test.

Concrete is a composite material that can be seen as a porous matrix in which pores of two different sizes can be located. In particular, families of pores of almost 10^{-3} microns and of 1-100 microns can be detected. The second ones can be efficaciously modeled as families of mesocracks inside an undamaged matrix. These mesocracks have a great influence on the macroscopic mechanical properties of the concrete since they are expected to determine a decay in the average strength of the material. In fact, it is easy to understand that an undamaged matrix would have a better resistance to an external load than a porous matrix. On the basis of this consideration, together with the micro-macro theory previously presented, a set of concrete specimens with micro-additives has been prepared. Some additives with a size comparable to that of the mesocracks have been added to the cement paste resulting in the creation of new concrete-like materials. These additives are called 'fillers' for their ability of 'filling' the mesocracks of the matrix. In order to see how the presence of these additives can affect the friction coefficient between the two faces of each crack, together with the crack density inside the concrete matrix, a series of experimental tests has been prepared. A testing procedure on these new materials has been set up and possible correlations between friction and mechanical properties of concrete are searched. It is clear that the friction coefficient depends on the physical properties of the additives, such as the shape and size of the grains and the roughness of the grain surfaces. For example, some of the grains can present a smooth film on their surface and thus a lower friction coefficient.

In particular, the type of additive chosen is GS 4; it has an appropriate size to properly interact with mesocracks and physical properties that improve the dynamic behavior of concrete. The main characteristics of this additive are shown in tab. III.1:

All fillers are obtained from carbonate rocks (such as inert limestone) so that the principal constituent (almost 99%) is Calcium Carbonate ($CaCO_3$). It has been shown, up to now, that the different fillers are expected to change, in some way, the friction coefficient on the basis of their physical properties. Another parameter that can affect the friction coefficient is the quantity of filler added to the cement powder. In fact, it can be understood that if the quantity of filler is irrelevant, the friction coefficient remains almost unvaried. On the other hand, if the quantity of

Table III.1: Physical and chemical characteristics of GS 4.

Characteristics	Value	Unit
Specific Weight	2.71	kg/dm^3
Apparent Density	600	g/l
Particles Shape	Rhombohedrical	-
White Index	80.50	-
Yellow Index	3.80	-
Coating Power	260	μ
D.O.P. Absorption	25.50±1	%
Oil Absorption	15.50±1	%
H_2O Absorption	18.50±1	%

filler added is higher, a certain amount of free additive remains in the cement paste, affecting the ordinary chemical reactions and resulting in a variation of the overall mechanical properties of concrete. It is for this reason that an 'optimal' quantity of additive must be found. In our case, this amount of filler was fixed on basis of the research performed in the Virginia Tech Polytechnic Institute (see Madeo [2006]), in which it was shown that, by using the filler GS4, it was enough to replace 3% of powder weight concrete, to optimize the required properties of the concrete.

III.1.1 Specimen preparation

The preparation of samples is one of the most important and sensitive points of our research and it must be conducted carefully.

At the beginning of the test campaign we analyzed the sand granulometry in order to compute the size distribution of sand grains available at the Laboratory LGCIE of INSA de Lyon. In detail, we performed two granulometric analyzes on two samples of dry sand, 1000 g weight each, using standard sieve whose meshes were defined by the standard (see EN 206 -1, 2005). This test allowed us to estimate the rate of each fraction of the sand and to draw the particle size curve. Then these results are compared with the size distribution of sand grains used in the previous research before mentioned that we considered as our reference curve (see fig. III.1).

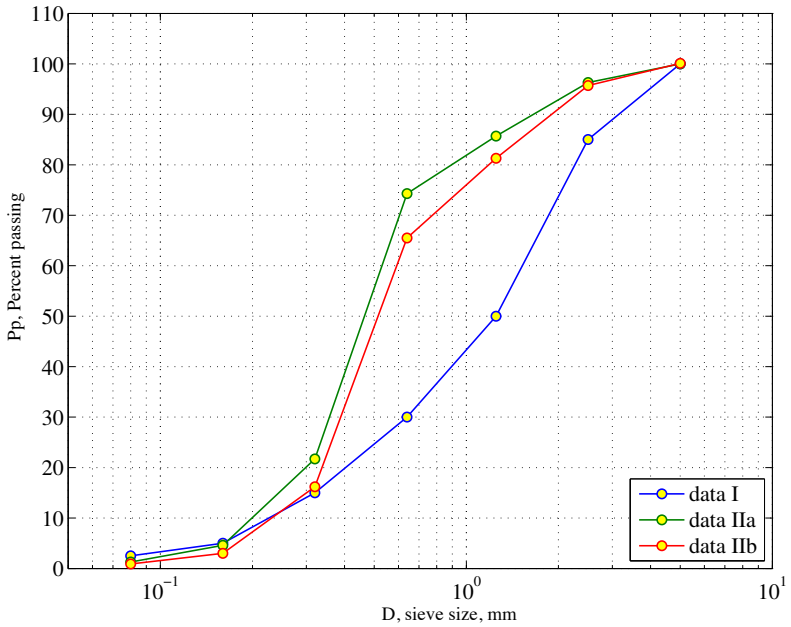

Figure III.1: Granulometric curve of the sand available at the Laboratory LGCIE (IIa, IIb) and the reference curve (I)

The fig. III.1 shows the granulometric curve of the sand used in Virginia Tech tests (I) and two curves related to the sand available at Laboratory LGCIE for two different sievings (IIa and IIb). We can note that the fraction of the finest particles (the remainders with grain size lesser than 80 μm) in the case (I) is significantly higher than the other cases (IIa, IIb), about two times. On the other hand, for the size of retained grains in the range of 160-640 μm the curves IIa and IIb are higher than the curve I. As regards the coarsest part of sand, grains greater than 1.25 mm, the percent retained is again higher in the first case rather than in the other two cases. Thus we can observe the different nature of the two sands. Moreover we note that the curves IIa and IIb relative to the two sievings performed are slightly different due to the non-perfect mixture of sand. These analyses on the grain size of sand available in the laboratory LGCIE showed that the differences between the sands were important enough, so we conducted tests on concrete made with both sands. It was expected that the composition of the sand must be the same as the previous work in order to ensure that the optimal replacement of filler of 3% in weight was still valid. Therefore, it was worthwhile to reproduce the same sand as in the preceding Virginia Tech tests. Knowing the curve of the desired particle size for the sand, we performed several sieving stages to separate and to stock the different fractions of sand. We repeated this action until the volume of each part was sufficient to recreate the sand required (see fig. III.2). After completing the sieving

Table III.2: Sieve analysis results on sand I.

Sieve size	Percent retained	Cumulative retained %	Percent passing
2.50 mm	15	15	85
1.25 mm	35	50	50
640 μm	20	70	30
320 μm	15	85	15
160 μm	10	95	5
80 μm	2.5	97.5	2.5

Table III.3: Sieve analysis results on sand IIa.

Sieve size	Percent retained	Cumulative retained %	Percent passing
2.50 mm	3.7	3.7	96.3
1.25 mm	10.6	14.3	85.7
640 μm	11.4	25.7	74.3
320 μm	52.6	78.3	21.7
160 μm	17.1	95.4	4.6
80 μm	3.3	98.7	1.3

process of the sand, we examined the particle size curve of the new sand to be sure that it corresponds to the desired curve. In order to make that, we carried out two sieving stages with the same procedure, considering two cases: dry and wet sample. It was noted that the shapes of the granulometric curves, as well as the rate of each fraction, were very close to each other. It was, therefore, concluded that the sand has been recreated with the specifications required by our research. The results of these analyzes are summarized in tabs. III.2, III.3 and III.4.

As regards the gravel available to the laboratory LGCIE, a granulometric analysis was performed to obtain data on particle size. Two sievings with the same procedure used in the case of sand (2 samples of dry gravel, whose weight was 1000 g each) were carried out. The size of the particles of gravel could assume less importance

Table III.4: Sieve analysis results on sand IIb.

Sieve size	Percent retained	Cumulative retained %	Percent passing
2.50 mm	4.4	4.4	95.6
1.25 mm	14.4	18.8	81.2
640 μm	15.8	34.6	65.4
320 μm	49.3	83.9	16.1
160 μm	13.2	97.1	2.9
80 μm	2.1	99.2	0.8

Figure III.2: A sand vibrating sieve machine and some sieve frames.

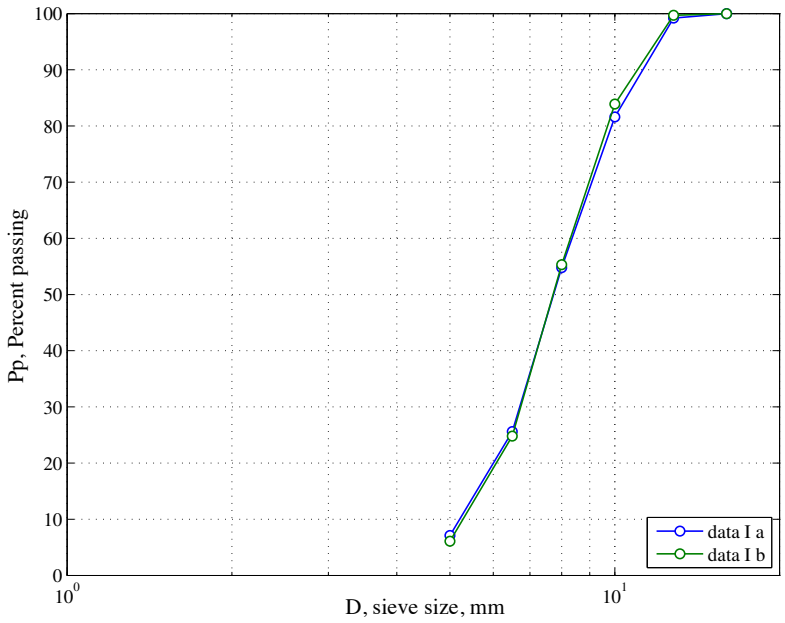

Figure III.3: Granulometric curve of the gravel available at the Laboratory LGCIE (Ia, Ib)

than that of sand; the particles of gravel have dimensions much greater than those of sand and as well as to those of the filling material. It could be therefore accepted that the gravel does not affect the efficacy of filler. Sieving test performed on the gravel at laboratory LGCIE were intended to verify the homogeneity of the particle size distribution in order to produce samples with the same physical and mechanical characteristics. The results of the particle size of the gravel are shown in fig. III.3, for two sieving stages (Ia and Ib). The two granulometric curves are almost similar, therefore the grain size of the gravel was uniformly distributed, see tabs. III.5 and III.6. To properly assess the amount of water to be used in the concrete mix, the quantity by weight of water contained in the pores of the granular materials used in the mixture was taken into account.

To estimate the amount of water present in the sand and gravel, we followed the procedure described below. We measured a volume of components using a accurate balance. This material was been placed on a plate well heated and we waited a couple of minutes to evaporate the excess water. After that, we again measured the weight of these samples in order to estimate the water content. The results of this analysis are presented in the following two tables. At the end of this procedure, the final volume of gravel and sand present in the mixture was increased in order to compensate for the weight of the water filling the voids, and therefore the amount

Table III.5: Sieve analysis results on gravel Ia.

Sieve size	Percent retained	Cumulative retained %	Percent passing
16.0 mm	0.0	0.0	100
12.8 mm	0.8	0.8	99.2
10.0 mm	17.6	18.4	81.6
8.0 mm	26.8	45.2	54.8
6.5 mm	29.2	74.4	25.6
5.0 mm	18.5	92.9	7.1

Table III.6: Sieve analysis results on gravel Ib.

Sieve size	Percent retained	Cumulative retained %	Percent passing
16.0 mm	0.0	0.0	100
12.8 mm	0.3	0.3	99.7
10.0 mm	15.8	16.1	83.9
8.0 mm	28.6	44.7	55.3
6.5 mm	30.5	75.2	24.8
5.0 mm	18.7	93.9	6.1

Table III.7: Mix I: Standard concrete with sand granulometric curve (I), w_c=0.487.

Composition	Weight ratio, kg	Ratio %
Sand	12.5	35.1
Gravel	16.57	46.2
Cement	4.52	12.6
Water	2.39	6.14
Total	35.98	100

of water added during the preparation of concrete was reduced. All this is necessary due to the importance of water content that significantly affects the mechanical strength of the concrete.

Seven concrete mixtures are used. All mixtures use Portland cement to produce a 28-day compressive strength of 32 MPa or 52 MPa, a crushed limestones coarse aggregate as shown in fig. III.3, and sand fine aggregate with granulometric curve (I) and (II) of fig. III.2. Mixtures are characterized by a water-to-cement ratio w_c in the range 0.49-0.69[1].

A concrete mix without addition of micro-particles was prepared as a reference material for the sake of comparison; moreover mixtures with 3 % and 3.5 % of filler are prepared. In details, we can summarize all the compositions used to make the testing samples, see tables from III.7 to III.11. In tabs. III.7, III.8 and III.9 concrete mixtures are characterized by a compressive strength of 52 MPa, i.e. a grade of concrete M52.

The mixture relative to tabs. III.10 and III.11 are molded with a cement to obtain a grade of concrete of M32 and M52. In this case, the two strength levels are obtained by using cement powders having different chemical properties, which, when used in the recipe, and in the same quantity, they produce concretes with different nominal strengths.

The procedure for the specimen preparation was carried out with caution, taking into account the determination of all components. Sand and gravel were inserted in a cement mixer. A part of the quantity of water required was then gradually poured into the mixture thus obtained. After the mixture became sufficiently uniform, the

[1]The w_c ratio (mass ratio of water to cement) is the key factor that determines the strength of concrete. A lower w_c ratio will yield a concrete which is stronger and more durable, while a higher w_c ratio yields a concrete with a larger slump, so it may be placed more easily.

Table III.8: Mix II: Modified Concrete with sand granulometric curve (I) and a use of filler of 3%, w_c=0.503.

Composition	Weight ratio, kg	Ratio %
Sand	12.5	35.1
Gravel	16.57	46.2
Cement	4.38	12.2
Water	2.39	6.14
Filler	0.13	0.377
Total	35.98	100

Table III.9: Mix III: Modified Concrete with sand granulometric curve (I) and a use of filler of 3.5%, w_c=0.507.

Composition	Weight ratio, kg	Ratio %
Sand	12.5	35.1
Gravel	16.57	46.2
Cement	4.36	12.1
Water	2.39	6.14
Filler	0.16	0.439
Total	35.98	100

Table III.10: Mix IV with M32, Mix V with M52: Standard concrete with sand granulometric curve (II), w_c=0.67.

Composition	Weight ratio, kg	Ratio %
Sand	21.25	35.1
Gravel	27.05	46.2
Cement	7.15	12.6
Water	4.8	6.14
Total	35.98	100

Table III.11: Mix VI with M32, Mix VII with M52: Modified Concrete with sand granulometric curve (II) and a use of filler of 3 %, w_c=0.69.

Composition	Weight ratio, kg	Ratio %
Sand	21.25	35.1
Gravel	27.05	46.2
Cement	6.94	11.51
Water	4.8	6.14
Filler	0.2145	0.356
Total	60.25	100

remaining amount of water and the filler, with different percentages depending on the recipe used, were introduced. The filler was added gradually to the mixture, to avoid that the particles being attached to each other. The pouring is continued until achieving of a compound as homogeneous as possible. Regarding the casting of concrete, firstly, it was filled to one half of the mold. To facilitate the compaction of the mixture and to expel the air, the mold was placed on a vibrating plate. Finally, we repeated the same procedure until the complete filling of the mold. The specimens thus obtained were subjected to the process of curing in an environment at controlled temperature and humidity for a period of 28 days.

III.2 Experimental Results

III.2.1 Cyclic tests

Experimental investigations on the dynamic behavior —dissipated energy— of modified plain concrete are performed under cyclic uniaxial compressive load. The test machine was controlled to impose a sinusoidal stress with a fixed frequency of $f = 1$ Hz for all the tests. This low frequency is chosen for avoiding inertial effects. More particularly, the considered load is

$$\sigma\left(t\right) = \left(\frac{\sigma_{\min} + \sigma_{\max}}{2}\right) + \left(\frac{\sigma_{\min} - \sigma_{\max}}{2}\right) \cos\left(2\pi f\, t\right)$$

where the values $\sigma_{\min}$, $\sigma_{\max}$ are related to the minimum and maximum forces applied. In detail, we conduct some tests with a force ranging from 19.62 to 176.58 kN and others with a bigger force between 19.62 and 392.4 kN. The peak load was chosen to avoid reaching an unsafe level of stress too close to the compressive strength of concrete material. On the other hand, the minimum level of compressive stress is small enough to ensure interactions of opposite porous surfaces inside the concrete matrix, hence, to enhance the friction of internal contact, on which the dissipated energy depends. Assuming that the stress range applied to the specimen is enough far from the failure stress, it can be predicted that an evolution of damage under these conditions due to fatigue phenomenon happens around a million of cycles. For this reason a limited number of cycles is considered in all test performed, specifically, a number of 100 cycles was chosen for each test. Since the cycling was limited to 100 cycles, it can be assumed that the cycling process did not significantly affect the mechanical properties of the specimens. The strain due to the applied load usually changes as the test progresses. This phenomenon is rapid at first, but the change from one cycle to the next decreases with increasing numbers of cycles. After a

small amount of cycles the behavior becomes approximately stable in that further changes are negligible. The cycles chosen for data analysis are placed after the middle of the experiment —usually the fiftieth cycle— because it is representative of a stable behavior of the material. Opel, Hulsbos [1966] reported that, repeated or cyclic loading has an adverse effect on concrete strength at stress levels greater than 50% of the compressive strength. For instance, in 5000 cycles of repeated loading, concrete failed at 70% of the ultimate monotonic loading strength. Progressive microcracking in the interfacial transition zone and the matrix are responsible for this phenomenon.

To be sure that the measured dissipation was not due to friction connected with the testing machine, a cyclic test on an aluminum specimen was run. A circular hollow section specimen of external diameter $D = 11.28$ cm, inner diameter $d = 9.5$ cm, and a length $L = 22$ cm, of precipitation hardened aluminum alloy (see fig. III.4), was tested under the same load range used for the concrete specimens. The aluminum tube has been designed so that the axial strain in concrete specimens is the same as in the aluminum sample, with the load being equal. In formulae:

$$\epsilon_z = \frac{P}{A_{Al}E_{Al}} = \frac{P}{A_cE_c} \Longrightarrow \frac{E_{Al}}{E_c} = \frac{A_c}{A_{Al}}$$

where E_{Al} and E_c are respectively the elastic modulus of aluminum and concrete, and A_{Al} , A_c are the areas respectively of the aluminum and concrete specimens.

Assuming the external diameter D to be equal to the concrete specimen diameter, we have

$$\frac{d}{D} = \sqrt{1 - \frac{E_c}{E_{Al}}}$$

The peak stress induced by this load is approximately equal to 35 MPa which is so far below the yield stress of the aluminum (for failure stresses of various aluminum alloys, see Dowling [2012]), so that essentially linear-elastic behavior of the specimen is expected in the absence of internal hysteresis of the machine. A linear elastic behavior was actually measured during the experiments (see fig. III.4), so it can be assumed that the energy dissipation measured from the concrete cyclic test is totally due to friction phenomena inside the specimen. As can be seen from fig. III.4, no significant hysteretic behavior can be detected; therefore, friction internal to the machine or between specimen and grips can be neglected. Since this dissipation is small compared to those measured from concrete specimens, it will be assumed that it is equal to zero. In other words, the energy dissipation measured from concrete specimens will be totally attributed to real material behavior, rather than to some effects due to the test apparatus.

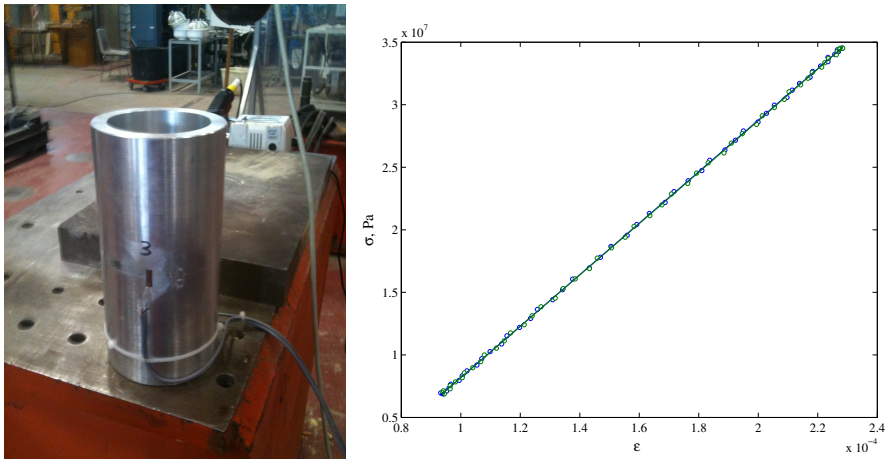

Figure III.4: Measured dissipation loop in aluminum sample.

In earlier tests, we detected the presence of an undesired degree of bending of the concrete specimens due to small misalignment or lack of complete lateral stability of the actuator, where the latter is due to motion within the restraints of its oil seals. The small lateral instability makes the position of the actuator not precisely defined, so that alignment is not definitive in the application of the compressive load. We examined various methods to reduce the bending, including raising the specimen support by about a meter, improving the alignment, using larger specimens, and finding an off-center location where the bending is minimized.

Finally, to address this issue, we decided to follow the procedure sketched below to find an off-center location on the basis of the Saint-Venant problem. Noting the cylindrical shape of specimens and the axial application of the loads, we can apply the Saint-Venant problem solution to evaluate quantitatively the degree of bending. We adopted a coordinate system with z-axis along the longitudinal axis of the cylinder and the origin on the lower base.

In the case of compressive and bending stress, we are in a state of uniaxial stress, and the solution of the Saint Venant problem is

$$\begin{cases} \sigma_x = \sigma_y = \sigma_{xy} = \sigma_{yz} = 0 \\ \sigma_z = ax + by + c \end{cases}$$

The related small strain tensor components are

$$\begin{cases} \epsilon_x = \epsilon_y = -\frac{\nu}{E}\sigma_z, \qquad \epsilon_z = \frac{\sigma_z}{E} = \frac{1}{E}(ax + by + c) \\ \epsilon_{xy} = \epsilon_{zx} = \epsilon_{zy} = 0 \end{cases} \tag{III.1}$$

where E and ν are the Young modulus and the Poisson ratio, respectively. By integrating the eqs. (III.1) we obtain the components of the displacement field:

Figure III.5: Set up for cyclic test.

$$\begin{cases} u_x = -\frac{a}{2E}z^2 - \frac{\nu}{E}\left[\frac{a}{2}(x^2-y^2) + bxy + cx\right] \\ u_y = -\frac{b}{2E}z^2 - \frac{\nu}{E}\left[axy + \frac{b}{2}(y^2-x^2) + cy\right] \\ u_z = \frac{1}{E}(ax+by+c)z \end{cases}$$

Each specimen was equipped with three strain gauges glued in the middle on the lateral surface at an angular distance of 120 degrees from each other (see fig. III.5). Considering that the x-axis points toward the first strain gauge, the gauges coordinates are:

$$g_i = \frac{d}{2}(\cos\varphi_i, \sin\varphi_i)$$

with $i = 1, 2, 3$, and the angles are $\varphi_1 = 0, \varphi_2 = \frac{2}{3}\pi$ and $\varphi_3 = \frac{4}{3}\pi$.

The measures of deformation, $\epsilon_z^{(i)}$ can be used to write an algebraic system of three equations in three unknowns a, b, c

$$\epsilon_z^{(i)} = \frac{1}{E}(a\frac{d}{2}\cos\varphi_i + b\frac{d}{2}\sin\varphi_i + c)$$

By solving this system, we can calculate the distribution of stress field σ_z in the specimens and we can distinguish one term of pure bending σ_{zb} and the other one of pure compression σ_{zc}:

$$\sigma_z = \sigma_{zb} + \sigma_{zc}, \quad \sigma_{zb} = (ax + by), \quad \sigma_{zc} = c \tag{III.2}$$

It is clear that from the eq. (III.2), if the coefficients a and b are zero, the pure bending term disappears, therefore these two coefficients can be used to quantify the effect of the bending. In order to avoid this problem, we performed an appropriate centering of the specimen relative to the axis of the test machine, moving the sample by small amounts in different directions and iterating this procedure until the coefficients a and b, evaluated each time, can be negligible.

In future acquisitions the next step should be to introduce a die set fixture. This consists of a base plate with three or four vertical posts rigidly and precisely mounted. Then these posts pass through bearings in an upper plate, so that vertical motion is allowed, while preventing lateral motion. Such devices are needed in industry for metal stamping operations where positioning must be precise.

III.2.2 Ramp failure tests

As briefly explained before, each specimen tested under uniaxial cyclic load was finally tested with a ramp test in order to measure its final resistance. The cylinders are tested on the two planar faces. The compression machine exerts a constant progressing force on the specimens till they fail, the rate of loading is 0.6 ± 0.2 MPa/s ($N/mm^2/s$). The reading at failure is the maximum compressive strength of the concrete. Table III.12 lists the ultimate strength for some representative concrete mixtures. The expected values and the related errors are evaluated from a set of six specimens for each mixture.

As shown in tab. III.12, a lower water to cement ratio w_c corresponds to a higher level of strength.

III.3 Data Analysis

III.3.1 Dissipation Energy Identification

After performing the cyclic tests, stress-strain graphics can be drawn on the basis of the measurements of the force applied to the specimen and deformation acquired by the strain gauges. As known, the area between the upper and the lower curve of a cycle represents the measured energy dissipation of the sample. This energy for each specimen has been measured by means of a precise procedure which will be discussed in the following and the obtained average value (calculated on 6 specimens)

Figure III.6: A ramp test to measure compressive strength.

Table III.12: Nominal and measured strength for the concrete mixtures examined.

Mix	Type	w_c	Grade of Concrete	Ultimate Strength
I	Standard	0.487	M52	51.0 ± 5.1 MPa
II	GS4 3%	0.503	M52	51.3 ± 5.2 MPa
III	GS4 3.5%	0.507	M52	59.0 ± 5.8 MPa
IV	Standard	0.67	M32	24.8 ± 2.5 MPa
V	Standard	0.67	M52	40.0 ± 4.0 MPa
VI	GS4 3%	0.69	M32	20.3 ± 2.0 MPa
VII	GS4 3%	0.69	M52	30.9 ± 3.1 MPa

is shown in tab. III.13. The procedure used to measure the energy dissipation can be summarized as follows

1. The mean of the three strain gauge measures $\hat{\epsilon}^{(j)}(t_i)$ with $j = 1, ..., 3$ is performed in order to make negligible a little bending effect remaining (see sec. III.2.1); the stress curve $\hat{\sigma}(t_i)$ is evaluated by dividing the acquired force by the nominal area of the sample.

2. Considering the signals referred to in the preceding item of n cycles, the expected value and the variance are estimated splitting the signal in n portions and regarding as each cycle as a determination of the corresponding variable. The initial point of the signal is chosen starting from the middle of the experiment –usually the 50^{th} cycle– because from this instant we can assume a stable behavior for the material.

3. The two branches of the loading and unloading curve have been fitted with second order polynomials.

4. The energy dissipation is determined computing the areas under each branches –loading and unloading curve– by mean of a simple definite integration and subtracting the two relative areas.

In order to perform the above mentioned procedure, the applied forces and the strain related to the strain gauges are collected as vectors depending on the time. We denote the measured applied external force per unit area by $\hat{\sigma}(t_i)$ at each time t_i

of the measure and the deformation acquired by the three strain gauges with $\hat{\epsilon}^{(j)}(t_i)$ $(j = 1, ..., 3)$.

Let the set of points $(t_i,\ y_i)$ be the result from a certain number, n, of determinations of the variable Y as function of the variable time, t, in correspondence of predetermined values of the time t_i. It is assumed that the errors in the values of t_i are negligible compared to those for the values y_i of the variable Y, so we can assume that each t_i is reproduced in repeated measures, while, for each t_i, the y_i fluctuate according to the law of the normal distribution. Under these conditions, for each t_i, it is easy to estimate the parameters of the probability distribution that characterizes a certain data-set $(y_{i1}, \dots y_{in})$: expected value, μ_i, and variance, $\mathtt{s}_i^2$. For the expected value an effective estimator is the arithmetic mean

$$\overline{Y}_i = \frac{1}{n}\sum_{j=1}^{n} y_{ij} \tag{III.3}$$

which also has a normal distribution with expected value and variance $\mathtt{s}_i^2/n$. An appropriate estimator for the variance of the sample, however, is given by

$$S_i^2 = \frac{1}{n-1}\sum_{j=1}^{n}\left(y_{ij} - \overline{Y}_i\right)^2 \tag{III.4}$$

In order to consider the confidence interval for the expected value μ_i it is appropriate to introduce a random variable $t_{\mu i}$ $(y_{i1}, y_{i2}, \dots y_{in})$

$$t_{\mu i} = \frac{\bar{Y}_i - \mu_i}{S_i/\sqrt{n}} \tag{III.5}$$

function of the n sample values $(y_{i1}, y_{i2}, \dots y_{in})$, to which it is possible to associate the Student's t-distribution, $f(t_{\mu i})$ with $n-1$ degrees of freedom. The knowledge of the statistics of this aleatory variable allows the detection of the probability with which the "true" value of the parameter μ_i is within a certain range. It is possible to determine, in fact, two parameters $t_{1-\alpha/2}$ and $t_{\alpha/2}$ such that the integral

$$\int_{t_{\alpha/2}}^{t_{1-\alpha/2}} f(t_{\mu i})\mathrm{d}t_{\mu i} = P\left(t_{1-\alpha/2} < t_{\mu i} < t_{\alpha/2}\right) \tag{III.6}$$

which represents the probability that the variable $t_{\mu i}$ is within the interval $\left(t_{1-\alpha/2},\ t_{\alpha/2}\right)$ is equal to a certain value $1-\alpha$, where α is called this level of significance, and is between zero and one. Since the Student's t-distribution is symmetric with respect to zero from (III.6) occurs with probability $1-\alpha$

$$-t_{\alpha/2} < \frac{\bar{Y}_i - \mu_i}{S_i/\sqrt{n}} < t_{\alpha/2} \tag{III.7}$$

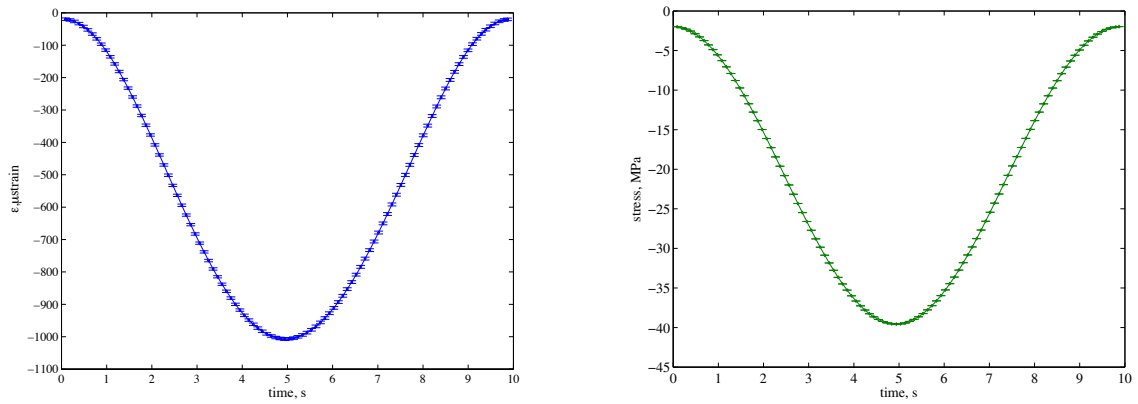

Figure III.7: Expected value of the strain ϵ and the stress σ for a representative cycle with an indication of 99.5 % confidence bounds.

The condition for $t_{\mu i}$ results for the parameter μ_i in the relationship

$$\bar{Y}_i - t_{\alpha/2}\frac{S_i}{\sqrt{n}} < \mu_i < \bar{Y}_i + t_{\alpha/2}\frac{S_i}{\sqrt{n}} \tag{III.8}$$

which allows determining, with probability $1-\alpha$, also called coefficient of confidence, the endpoints of the interval in which falls, within the "true" value of the parameter μ_i, which by definition is equal to its expected value and is related to the estimation of its average by the relation

$$E\left[Y\right] = \bar{Y}_i \pm t_{\alpha/2}\frac{S_i}{\sqrt{n}} \tag{III.9}$$

Therefore the resulting upper confidence limit E[Y] of the mean can be calculated with 99.5% confidence interval and $n = 24$ degrees of freedom using the following equation

$$E\left[Y\right] = \bar{Y}_i \pm 2.797\frac{S_i}{\sqrt{n}} \tag{III.10}$$

The 99.5% interval indicates that there is a chance of 99.5% that a new observation will fall within the bounds.

Figures III.7 and III.8 show, for a representative cycle, the results relative to the items 1 and 2 of the procedure above mentioned, i.e. expected values of the strain ϵ and the stress σ and an indication of 99.5 % confidence bounds. It is worth noting that the measurement system has a precision[2], related to reproducibility and repeatability, which is very high. Moreover we can see the error estimate for the stress has a very low level because the cyclic load is driven by a feedback loop that

[2]the degree to which repeated measurements under unchanged conditions show the same results.

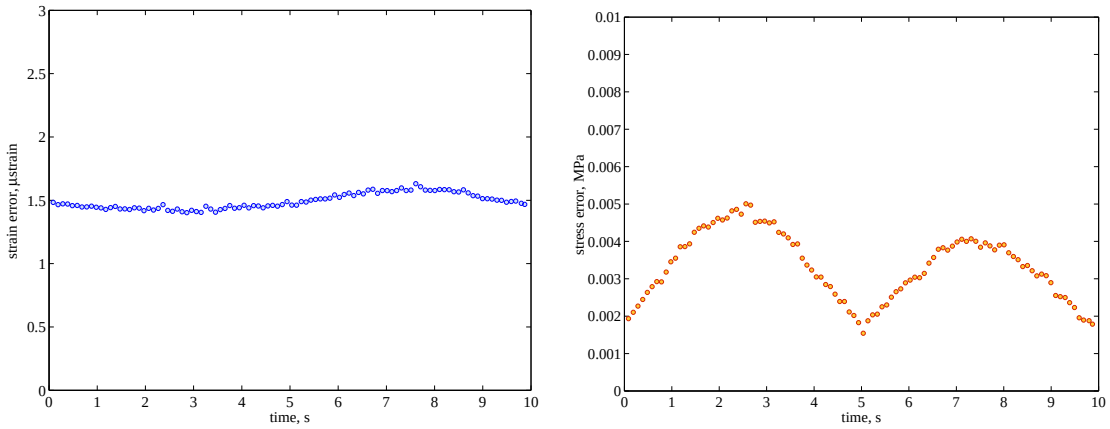

Figure III.8: Error estimates of the strain ϵ and the stress σ.

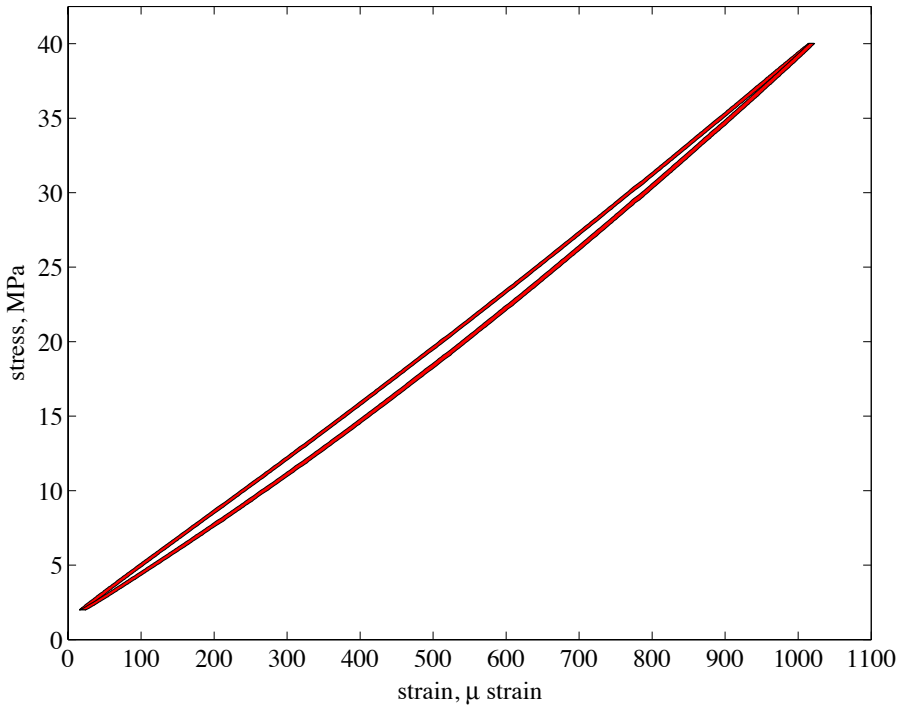

Figure III.9: Dissipation loop with confidence bounds.

enhances the precision of the test apparatus. Thus, in what follows we neglect the errors on the stress.

Figure III.9 exhibits the dissipation energy loop with 99.5 % confidence bounds for a typical concrete specimen.

The energy dissipation, that is the area between the loading and unloading curves of a cycle, is extracted from the actual measured data by performing polynomial curve fits. Polynomial models for loading and unloading curves are given by

$$\sigma = \sum_{k=1}^{n+1} a_k \epsilon^{n+1-k} \tag{III.11}$$

where n is the degree of the polynomial. The main advantages of polynomial fits include reasonable flexibility for data that is not too complicated, and they are linear, which means the fitting process is simple. The main disadvantage is that high-degree fits can become unstable. Additionally, polynomials of any degree can provide a good fit within the data range, but can diverge wildly outside that range. Therefore, caution is needed when extrapolating with polynomials.

To obtain the polynomial coefficient estimates, a least-squares method is employed to minimize the summed square of residuals. The residual for the ith data point r_i is defined as the difference between the observed response value $\hat{\sigma}\left(t_i\right)$ and the fitted response value σ given by eq. (III.11), and is identified as the error associated with the data

$$r_i = \hat{\sigma}\left(\langle\hat{\epsilon}_i\rangle\right) - \sigma\left(\langle\hat{\epsilon}_i\rangle\right)$$

in which the angle brackets stand for the average of the three strain gauge signals. The summed square of residuals is given by

$$S = \sum_{i=1}^{N} \left[\hat{\sigma}\left(\langle\hat{\epsilon}_i\rangle\right) - \sigma\left(\langle\hat{\epsilon}_i\rangle\right)\right]^2$$

where N is the number of data points included in the fit and S is the sum of squares error estimate. The curve fit process has to determine the values of the unknown polynomial coefficients such that the error S is minimized. After performing the curve fits, to evaluate the goodness of fit the R^2 indicator has been utilized. Indeed, R^2 can take on any value less than or equal to one, with a value closer to one indicating a better fit. In particular, the R^2 is adjusted based on the residual degrees of freedom, V, defined as the number of data values N minus the number of fitted coefficients $n+1$. Therefore, the degrees of freedom adjusted R^2 is defined as

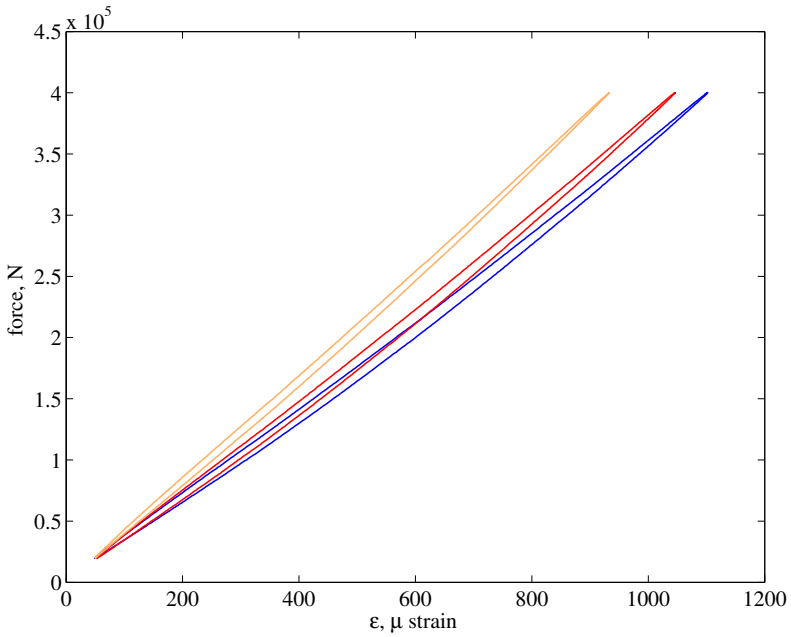

Figure III.10: The dissipation loops for the first three mixtures considered. From right to left: mix I (standard concrete), mix II (modified concrete with 3% of micro-filler) and mix III (modified concrete with 3.5% of micro-filler).

$$R^2 = 1 - \frac{SSE \cdot (N-1)}{SST \cdot V}$$

in which SSE is the sum of squares due to error and represents the total deviation from the fit to the response values whilst SST is also called the sum of squares about the mean and represents the total deviation from the mean to the response values. In particular, for the fits performed the resulting R^2 values are very close to one.

The damping performance of concrete can be improved by adding to the mixture different kinds of micro-particles which change the porosity of the matrix and thus the contact interaction between internal surfaces of voids.

Figure III.10 shows dissipation loops for each of mix I, II and III with M52 grade of concrete and a content of filler increasing: 0%, 3%, 3.5%. It is noted that a greater quantity of micro-particles, in this case, produces a higher level of stiffness. Thus, if the quantity of these particles is too high, then the effect is to reduce the porosity of the concrete and decrease the capability of a relative displacement between the opposite pore faces, which in turn implies smaller dissipation. Figures III.11 to III.14 exhibit the results of cyclic tests carried out on the specimens, prepared as described above, with mixes IV,V, VI and VII, respectively. In particular, for the

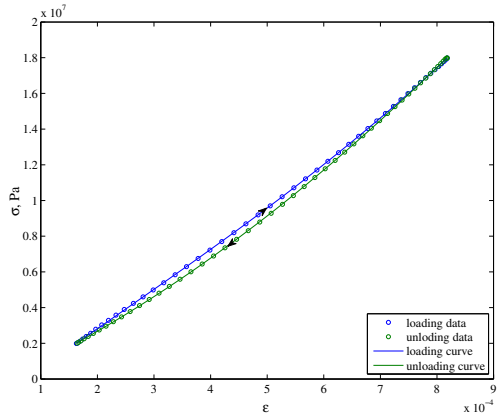

Figure III.11: Mix IV: dissipation loop for a M32 grade of standard concrete.

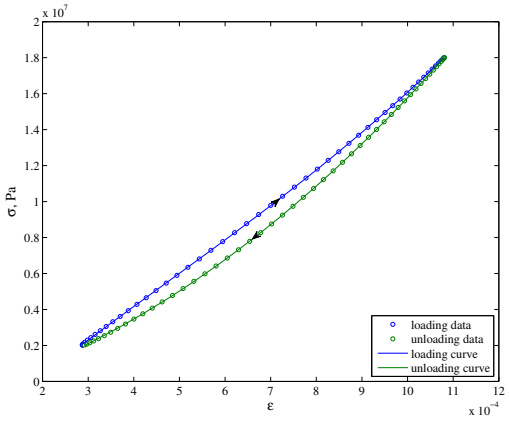

Figure III.12: Mix VI: dissipation loop for a M32 grade of modified concrete.

sake of comparison, the dissipation loops for a representative cycle are shown in a stress-strain diagram for a standard concrete as a reference material (see fig. III.11) and for a modified concrete with the addition of 3% of micro-filler (fig. III.12),both for a concrete of strength 32 MPa. Figures III.13 and III.14 provide a similar comparison for concrete with the strength of 52 MPa. It was determined that the energy dissipation of the concrete increases with increasing content of micro-particles. On the other hand, an increasing percentage of micro-particle additions can degrade the mechanical strength of material (see thesis Madeo [2006]). Thus, there is a reasonable compromise in incorporating these micro-particles to obtain higher damping without weakening the mechanical properties.

It is worth noting that the mixtures with strength of 32 MPa exhibit a more significant dissipative effect than the mixtures with strength of 52 MPa. In fact, the latter types of samples are more rigid, and, the micro-relative displacements of pore's faces inside the concrete matrix are smaller. Comparing the two pictures of fig. III.11 and III.12 for a M32 grade of concrete, it is possible to note an increase of a cycle deformation magnitude from about 650 μstrain to 800 μstrain passing from the mix IV, i.e. a standard concrete, to the mix VI, that is a modified concrete with a 3% of filler. Analogously, the figs. III.13 and III.14 for a M52 grade of concrete, it is possible to note an increase of a cycle deformation magnitude from about 530 μstrain to 630 μstrain passing from the mix V, i.e. a standard concrete, to the mix VII, that is a modified concrete with a 3% of filler.

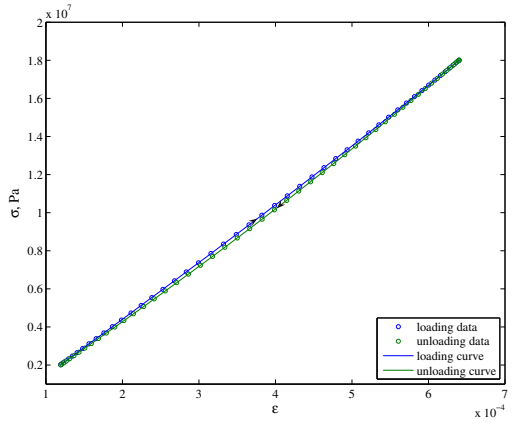

Figure III.13: Mix V: dissipation loop for a M52 grade of standard concrete.

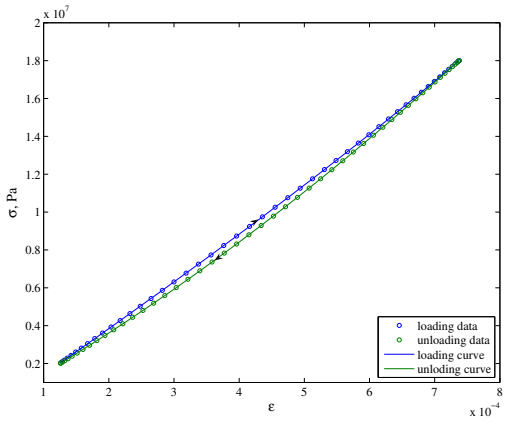

Figure III.14: Mix VII: dissipation loop for a M52 grade of modified concrete.

Table III.13: Dissipated energy for the concrete mixtures examined.

Mix	Type	Grade of Concrete	dissipated energy per cycle
I	Standard	M52	0.824 ± 0.061 J
II	GS4 3%	M52	0.729 ± 0.056 J
III	GS4 3.5%	M52	0.364 ± 0.028 J
IV	Standard	M32	0.891 ± 0.067 J
V	Standard	M52	0.167 ± 0.014 J
VI	GS4 3%	M32	1.31 ± 0.098 J
VII	GS4 3%	M52	0.368 ± 0.027 J

Table III.14: Mix I: Dissipated Energies per cycle for a standard concrete.

Frequency (Hz)	0.8	0.5	0.3	0.1
Dissipated Energy (J/c)	0.88	1.22	1.58	1.98

In tab. III.13, the dissipation energy measured for the seven concrete mixtures are listed. The expected values and the related errors are evaluated from a set of six specimens for each mixture with a cyclic load at a frequency of 1 Hz. The mixtures II and III display a decrease of dissipated energy of 11.5% and 55.8%, respectively, relative to mixture I, i.e. the standard concrete with the same grade. On the other hand, the concrete with M32 grade manifests an increase of dissipated energy, comparing mix IV and mix VI, of 47%. Furthermore the concrete with M52 grade, comparing mixV and mix VII, presents an increment of 120%.

III.3.2 Test analysis with varying frequency cycle

Since frictional forces arise as a results of a relative velocity of porous surfaces in a concrete matrix, we performed experimental tests in order to account for this issue. Specifically, we considered cyclic tests with varying frequency of load ranging from 0.1 Hz to 0.8 Hz, i.e. relative micro-velocity, and with a load included between 19.62 and 392.4 kN, i.e. about 72% of the ultimate compressive strength. Following the procedure described in sec. III.3.1, the dissipated energy for different kinds of specimen is estimated.

Figures III.15, III.16, III.17 and III.18 show the measured strains by the 3 strain gauges and the related dissipative loops for frequencies 0.8, 0.5, 0.3 and 0.1 Hz for Mix I, i.e. a standard concrete. In these figures the strains are related to the last cycles because they are representative of stable behavior. Furthermore, the tab. III.14 summarizes the dissipated energy for the different frequencies tested. It is possible to note an increase in the dissipated energy for reducing the cycle frequency. Assuming the test with a load cycle frequency of 0.8 Hz as a reference, tab. III.14 reveals a relative increase of 38.6%, 79.5% and 125% for the frequencies 0.5, 0.3 and 0.1 Hz, respectively.

Figures III.19, III.20, III.21 and III.22 show the measured strains by the 3 strain gauges and the related dissipative loops for the frequencies 0.8, 0.5, 0.3 and 0.1 Hz for the Mix II, i.e. a modified concrete with 3% of filler. Furthermore, tab. III.15 summarizes the dissipated energy for the different frequencies tested. In the same way, a tab. III.15 shows a relative increase of 75%, 133% and 206% for the frequencies

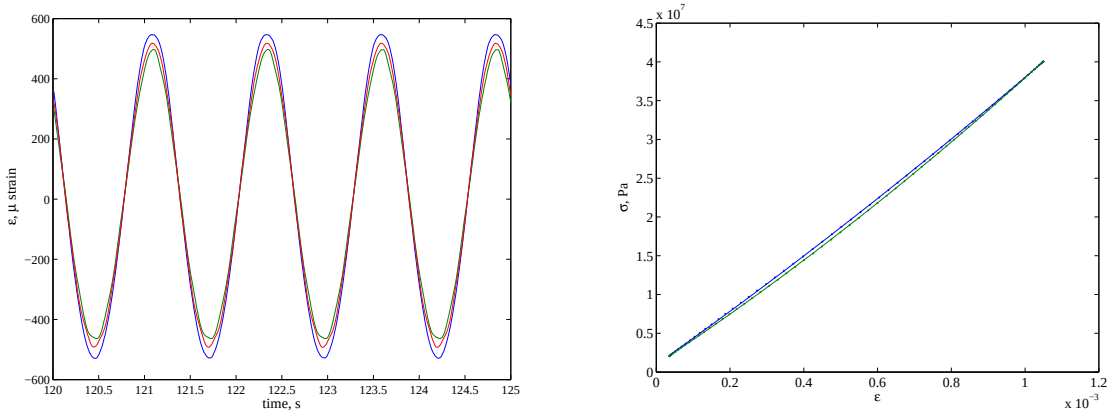

Figure III.15: The measured strains by the 3 strain gauges and the related dissipative loop for the mix I and frequency 0.8 Hz.

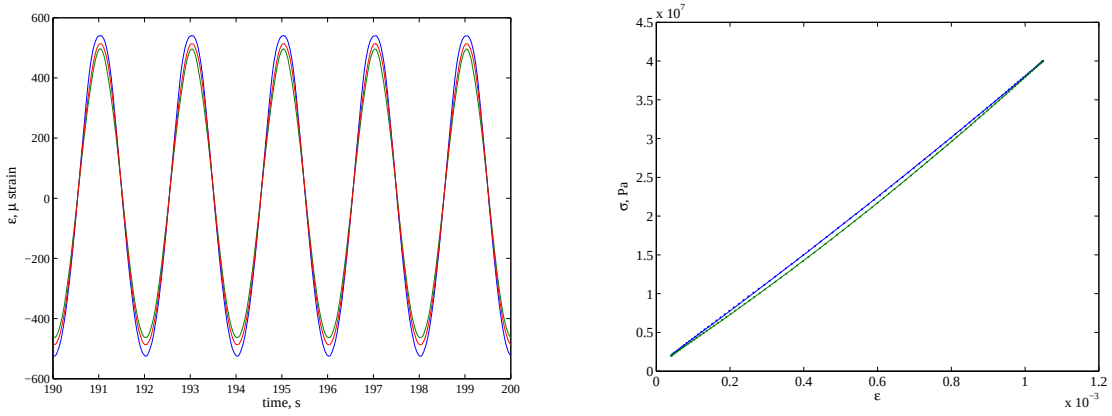

Figure III.16: The measured strains by the 3 strain gauges and the related dissipative loop for the mix I and frequency 0.5 Hz.

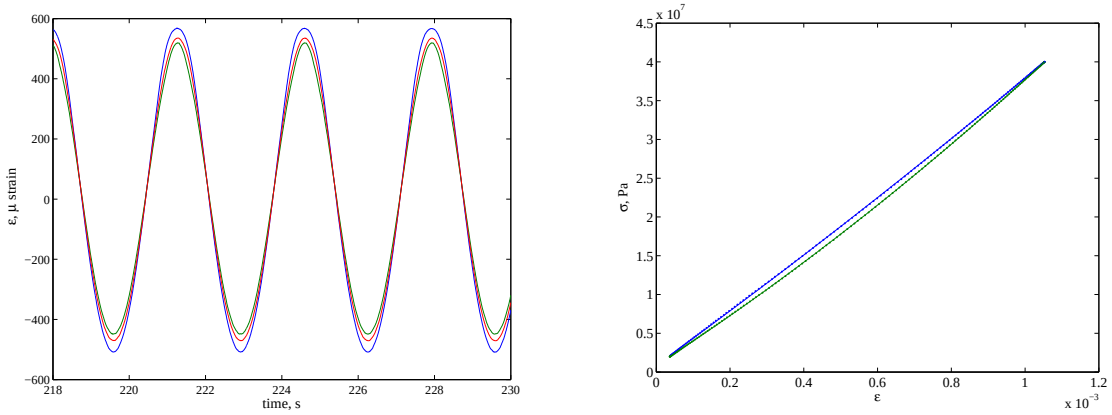

Figure III.17: The measured strains by the 3 strain gauges and the related dissipative loop for the mix I and frequency 0.3 Hz.

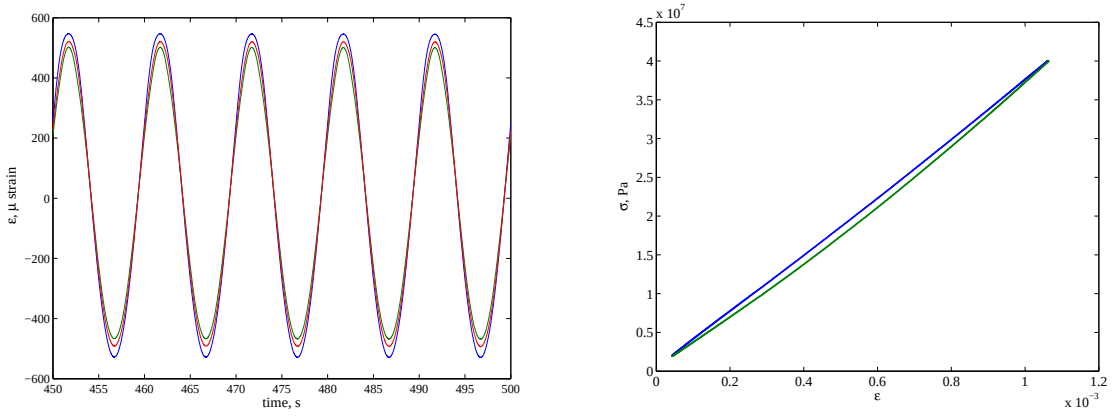

Figure III.18: The measured strains by the 3 strain gauges and the related dissipative loop for the mix I and frequency 0.1 Hz.

Table III.15: Mix II: Dissipated Energy per cycle for a modified concrete with 3% of filler.

Frequency (Hz)	0.8	0.5	0.3	0.1
Dissipated Energy (J/c)	0.52	0.91	1.21	1.59

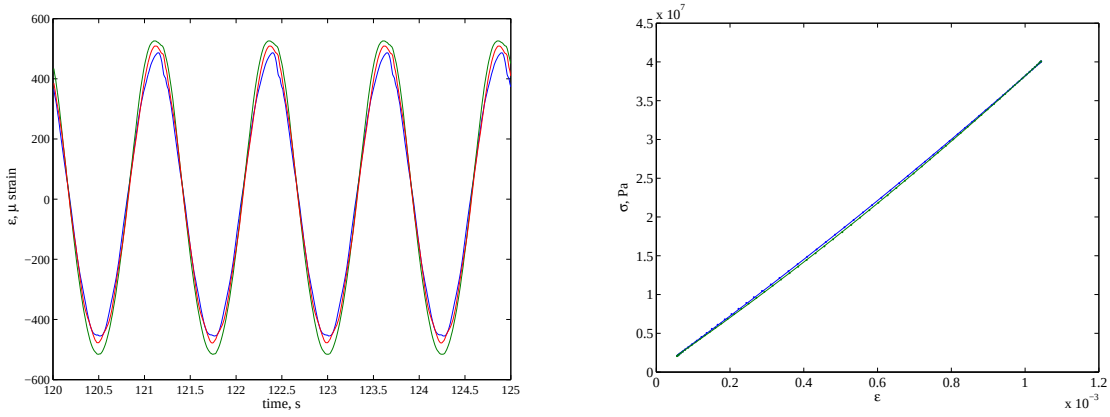

Figure III.19: The measured strains by the 3 strain gauges and the related dissipative loop for the mix II and frequency 0.8 Hz.

0.5, 0.3 and 0.1 Hz, respectively.

Figures III.23, III.24, III.25 and III.26 show the measured strains by the 3 strain gauges and the related dissipative loops for frequencies 0.8, 0.5, 0.3 and 0.1 Hz for the Mix III, i.e. a modified concrete with 3.5% of filler. Furthermore, tab. III.16 summarizes the dissipated energy for the different frequencies tested. Finally, tab. III.16 exhibits a relative increase of 92%, 162% and 240% for the frequencies 0.5, 0.3 and 0.1 Hz respectively.

This analysis, thus, shows in all cases that the dissipated energy increases with decreasing frequency and the more rigid the mixture, the greater the effect on the dissipated energy of the variation of the frequency. This means that the friction in tested concrete presents a sort of 'Stribeck effect', i.e. a friction phenomenon

Table III.16: Mix III: Dissipated Energy per cycle for a modified concrete with 3.5% of filler.

Frequency (Hz)	0.8	0.5	0.3	0.1
Dissipated Energy (J/c)	0.37	0.71	0.97	1.26

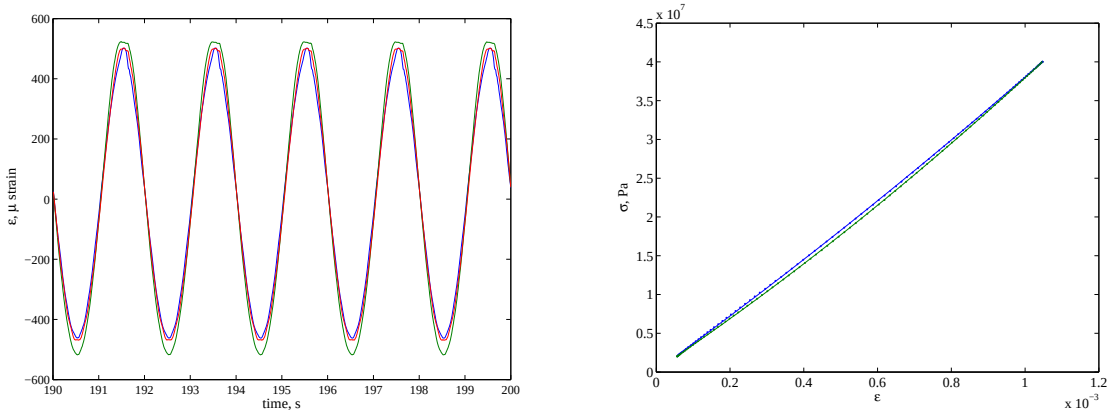

Figure III.20: The measured strains by the 3 strain gauges and the related dissipative loop for the mix II and frequency 0.5 Hz.

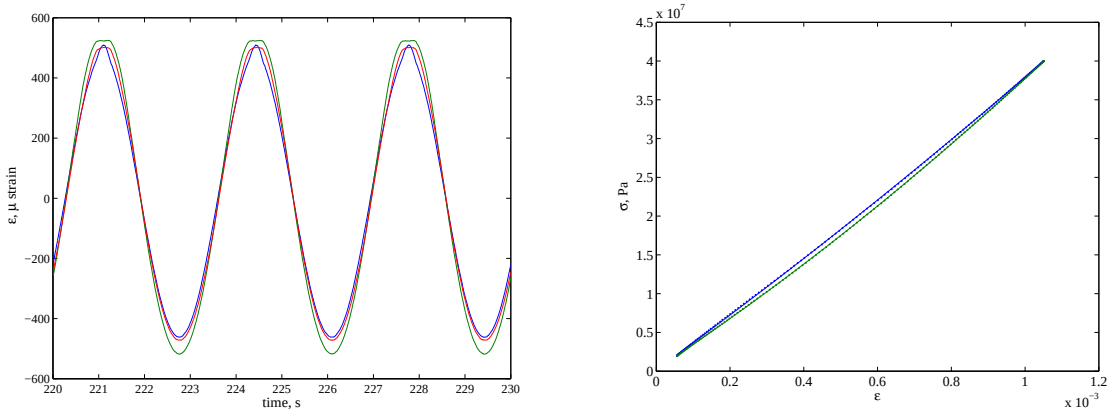

Figure III.21: The measured strains by the 3 strain gauges and the related dissipative loop for the mix II and frequency 0.3 Hz.

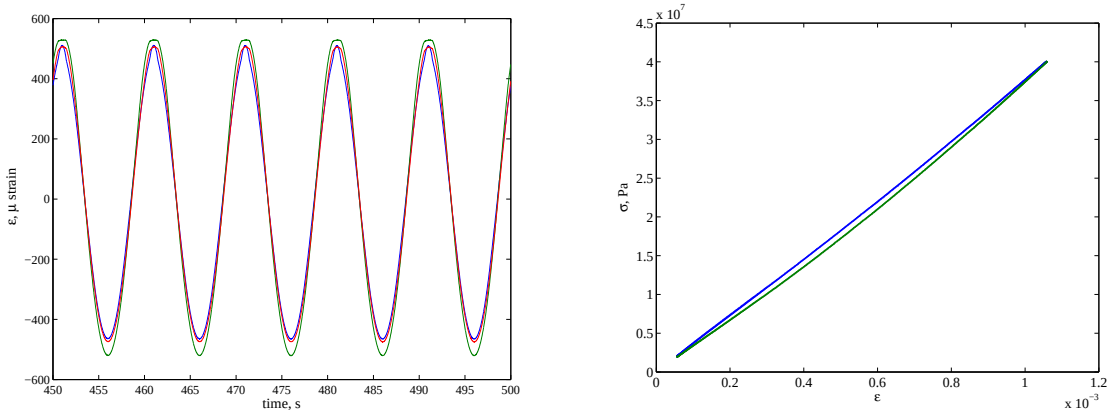

Figure III.22: The measured strains by the 3 strain gauges and the related dissipative loop for the mix II and frequency 0.1 Hz.

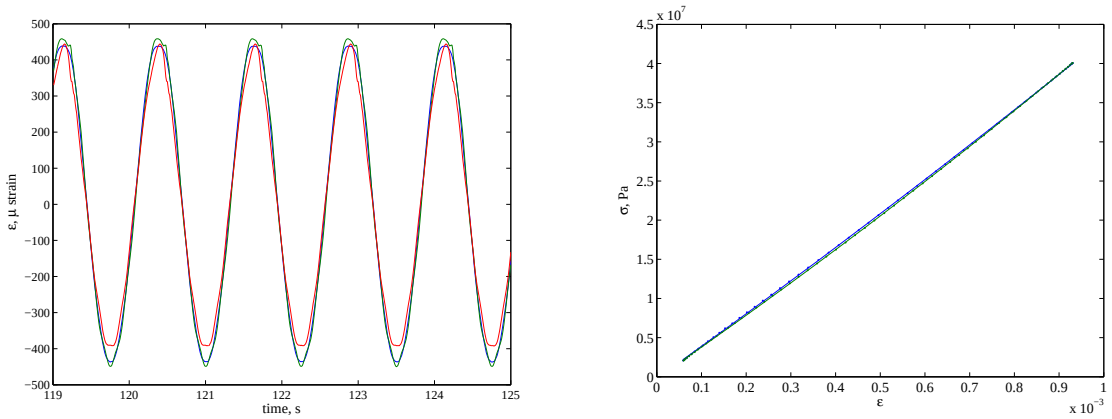

Figure III.23: The measured strains by the 3 strain gauges and the related dissipative loop for the mix III and frequency 0.8 Hz.

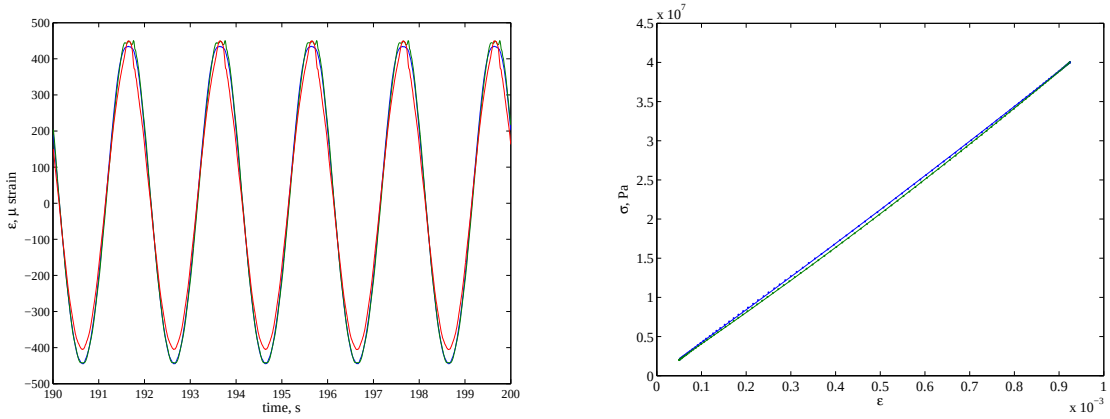

Figure III.24: The measured strains by the 3 strain gauges and the related dissipative loop for the mix III and frequency 0.5 Hz.

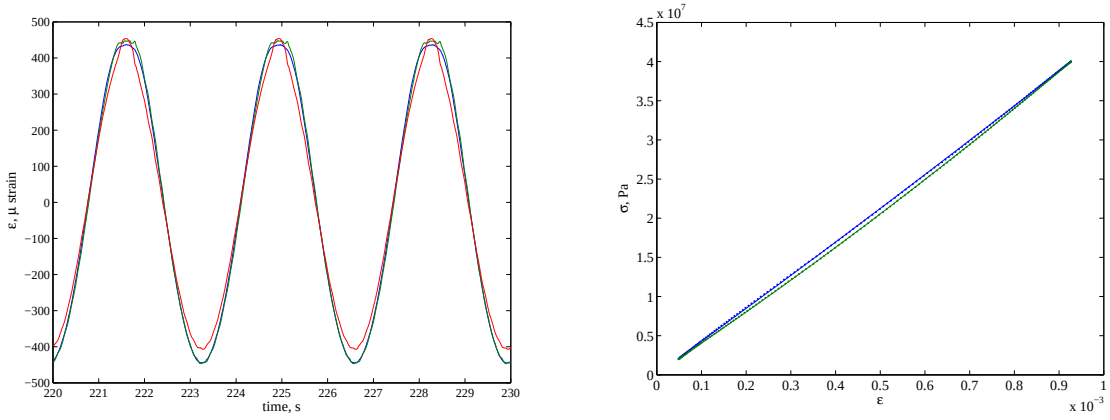

Figure III.25: The measured strains by the 3 strain gauges and the related dissipative loop for the mix III and frequency 0.3 Hz.

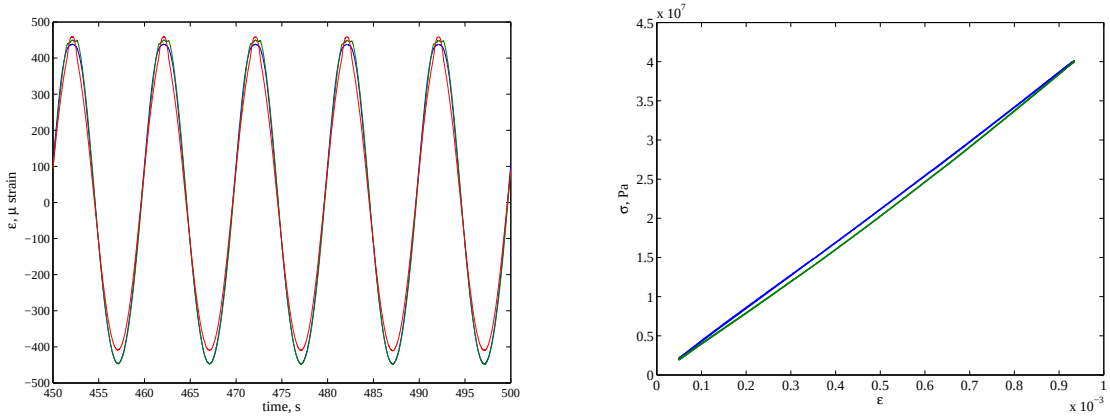

Figure III.26: The measured strains by the 3 strain gauges and the related dissipative loop for the mix III and frequency 0.1 Hz.

that gives rise at low velocity to decreasing friction with increasing velocity. The proposed model is characterized by both Coulomb and viscous effects, therefore, at low velocity range, the dissipation increases with velocity, and at high velocity range, friction is rate-independent. To overcome this problem, it is possible to address this issue taking into account models that include the effect of Stribeck. An example of such a formulation is the LuGre model proposed by De Wit [1995] or the Leuven model proposed by Swevers et al. [2000].

III.4 Parameter identification

In this section, we turn our attention to the problem of finding the best material parameters for the model that describes the functional relationship existing between the strain variable ϵ, and the stress variable σ, in order to interpolate the set of N points $(\sigma_i,\ \epsilon_i)$ resulting from a certain number, n, of measures of these quantities. In this regard, for the regression, we consider the model described above in sec. II.6. For the sake of simplicity, we assume that the errors on the values of stress σ_i are much smaller than the errors which affect the values of the strain ϵ_i, so that it is possible to think that each σ_i attains close results in repeating measurements under unchanged conditions, while for each σ_i, the ϵ fluctuates according to the normal distribution. For each arbitrary value of σ_i the measure of strain ϵ is represented by the random variable ϵ_i normally distributed with expected value $f(\sigma_i;\ a_1, \dots a_\nu)$ and variance $\mathtt{s}_i^2$. In particular, the material parameters that we want to estimate are the macro-stiffness K, the micro-stiffnesses k_1, k_2, k_3, the coupling coefficient α and dissipation coefficients ζ, η.

Denote the model of the eq. II.6 with the relationship $\epsilon_i = f(\sigma_i\ ;\ a_1,\ a_2, ..a_\nu)$, where a_j, with j ranging from one to $\nu = 7$, are the parameters to be found. If we assume the independence of the measures in addition to the assumptions already made, the probability density that $\epsilon_i = f(\sigma_i\ ,\ a_1,\ a_2, ..a_\nu)$ is the expected value of the strain for any one observation and is given by

$$P\left(\sigma_i\right) = \frac{1}{\mathtt{s}_i\sqrt{2\pi}}\exp\left(-\frac{\left[\epsilon_i - f(\sigma_i;\ a_1,\ a_2, ..a_\nu)\right]^2}{2\mathtt{s}_i^2}\right)$$

The total probability of obtaining a set of N measurements, $(\sigma_i,\ \epsilon_i)$, is equal to the product of the probabilities for each data point:

$$P_{tot} = \prod_{i=1}^{N}\frac{1}{\mathtt{s}_i\sqrt{2\pi}}\exp\left(-\frac{\left[\epsilon_i - f(\sigma_i;\ a_1,\ a_2, ..a_\nu)\right]^2}{2\mathtt{s}_i^2}\right) \approx$$

$$\approx \exp\left(-\sum_{i=1}^{N}\frac{\left[\epsilon_i - f(\sigma_i;\ a_1,\ a_2, ..a_\nu)\right]^2}{2\mathtt{s}_i^2}\right) \quad \text{(III.12)}$$

The best estimates for the parameters a_j are those for which eq. (III.12) attains its maximum value. Maximizing the probability is equivalent to minimizing the sum in the exponential term of P_{tot}, i.e. to calculating the minimum of the sum of squared residuals respect to the expected value $f(\sigma_i\ ;\ a_1,\ a_2, ..a_\nu)$ weighted by the reciprocal of the variance. This approach clearly leads to an extension of the least squares method with variances as weights. However, for the assumptions made, the exponent of the last term of the relation (III.12) appears to be a random variable of χ^2 with $N-\nu$ degrees of freedom. Therefore, it follows that its statistical properties and the goodness of fit can be judged by the chi-square test (see Appendix B). According to sec. II.6 the function $f(\sigma_i\ ;\ a_1,\ a_2, ..a_\nu)$ is computed by means of a Simulink model that solves the ODE system (II.28) to obtain the strain ϵ in a representative cycle load. In figs. III.27-III.29 the schematic diagrams of this system are shown. In particular, the block diagram of the governing equation for the macro-scale is exhibited in fig. III.28 while the block scheme of the equation related to the micro-scale is depicted in fig. III.29. We observe in the block diagram III.28 the possibility to take into account a viscous damping by means of a manual switch that toggles between two modes, with and without damping.

To avoid further undesirable uncertainties, the input forcing term used in the simulations is the acquired measure of the load in the experimental tests.

In tab. III.17, material parameters estimated by curve fitting are listed for the mix I (the label 'St M52' standing for a M52 grade of standard concrete), the mix

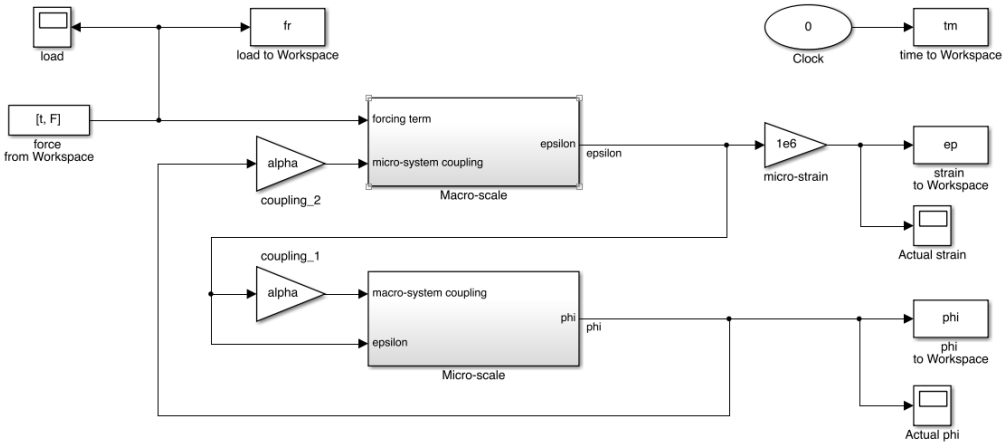

Figure III.27: Block diagram to simulate concrete with micro-structure.

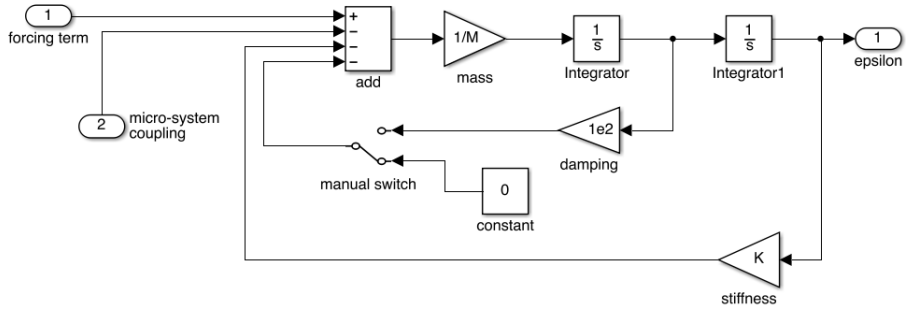

Figure III.28: Block diagram of the macro-system.

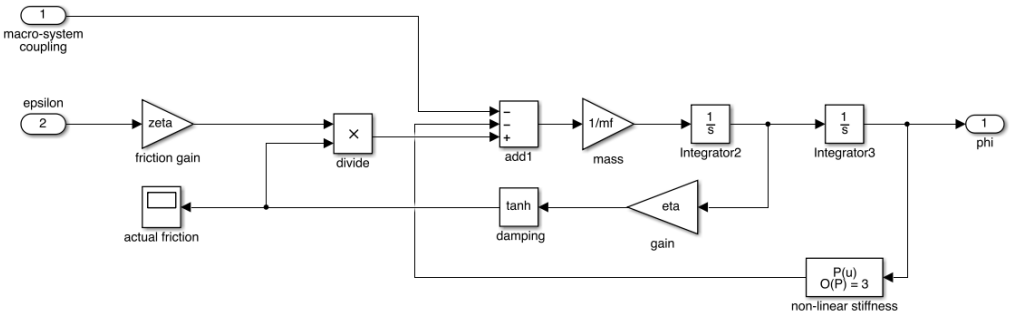

Figure III.29: Block diagram of the micro-system.

Table III.17: Material parameters of mix I, II and III.

Parameters	Fit I (St M52)	Fit II ($GS4_3$ M52)	Fit III ($GS4_{3.5}$ M52)	Unit
K	1.06×10^8	1.28×10^8	1.20×10^8	Nm
$\tilde{k}_1$	4.24×10^9	2.12×10^9	2.12×10^9	N/m
$\tilde{k}_2$	1.76×10^5	2.64×10^5	2.64×10^5	N/m^2
$\tilde{k}_3$	2.37×10^{17}	1.71×10^{16}	5.98×10^{16}	N/m^3
$\tilde{\alpha}$	3.96×10^8	3.30×10^8	2.59×10^8	N
$\tilde{\zeta}$	1.63×10^8	5.34×10^7	1.17×10^8	N
η	9.85×10^3	7.88×10^3	7.88×10^3	s/m

II (the label '$GS4_3$ M52' standing for a M52 grade of modified concrete with 3% replacement of micro-filler), and the mix III (the label '$GS4_{3.5}$ M52' standing for a M52 grade of modified concrete with 3.5% replacement of micro-filler).

In fig. III.30 the measured data and the regression curve for a representative cycle related to the mix I are depicted. The reduced chi-square is 1.54; thus the parameter values obtained can be accepted as representative of the concrete considered.

In figure III.31 the measured data and the regression curve for a cycle related to the mix II with 3% replacement of micro-filler are depicted. The reduced chi-square is 1.33; thus, the parameter values obtained can be accepted as representative of the concrete considered.

In figure III.32 the measured data and the regression curve for a cycle related to the mix III with 3.5% replacement of micro-filler are depicted. The reduced chi-

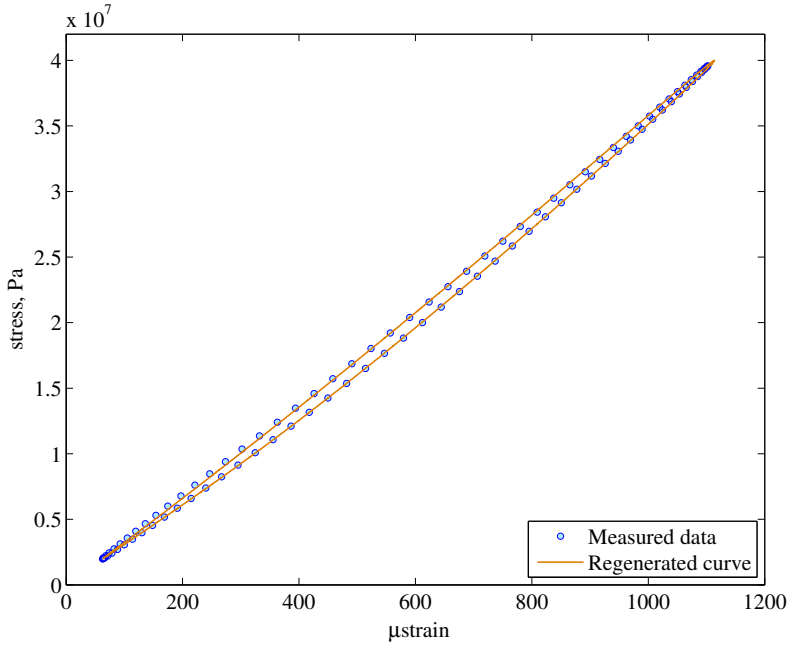

Figure III.30: Measured data and regenerated curve for mix I (St M52).

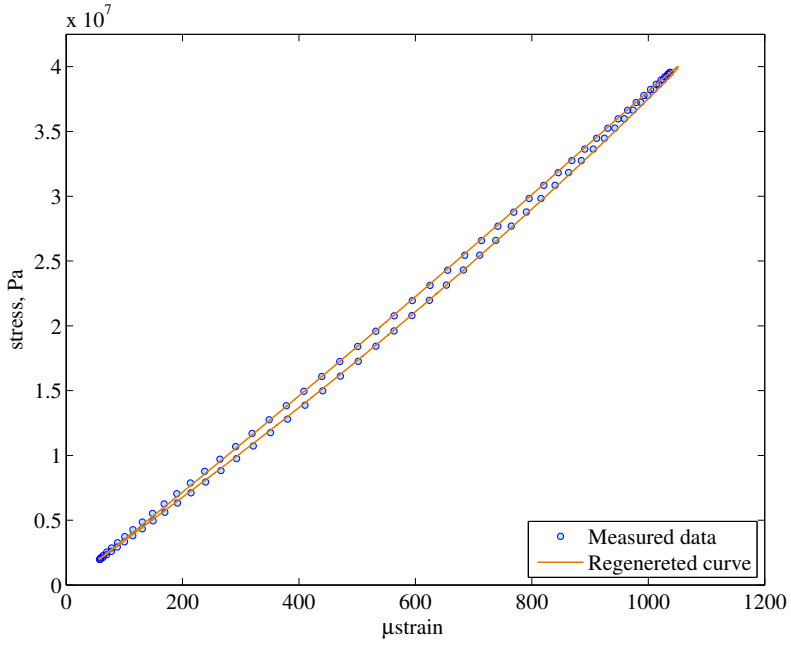

Figure III.31: Measured data and regenerated curve for mix II ($GS4_3$ M52).

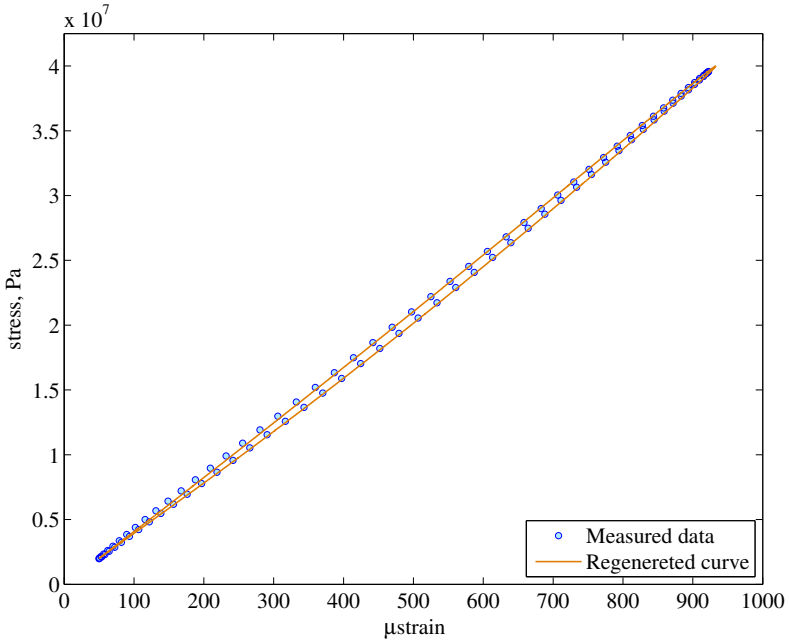

Figure III.32: Measured data and regenerated curve for mix III ($GS4_{3.5}$ M52).

square is 4.31, thus, its estimated sample value is greater than 1.5. We may conclude that either *(i)* the model represented by the $\epsilon_i = f(\sigma_i\ ,\ a_1,\ a_2, ..a_\nu)$ is a valid one but that a statistically improbable excursion of χ^2 has occurred, or *(ii)* that our model is so poorly chosen that an unacceptably large value of χ^2 has resulted.

In tab. III.18, material parameters estimated by curve fitting are listed for the mix IV (the label 'St M32' standing for a M32 grade of standard concrete) and the mix VI (the label '$GS4_3$ M32' standing for a M32 grade of modified concrete with 3% replacement of micro-filler).

In fig. III.33 the measured data and the regression curve for a cycle related to the mix IV (St M32) are depicted. The reduced chi-square is 2.41; thus, its estimated sample value is greater than 1.5. In fig. III.34 the measured data and the regression curve for a cycle related to the mix VI ($GS4_3$ M32) are depicted. The reduced chi-square is 1.36; thus, the parameter values obtained can be accepted as representative of the concrete considered.

In tab. III.19, material parameters estimated by curve fitting are listed for the mix V (the label 'St M52' standing for a M52 grade of standard concrete) and the mix VII (the label '$GS4_3$ M52' standing for a M52 grade of modified concrete with 3% replacement of micro-filler).

In fig. III.35 the measured data and the regression curve for a cycle related to the mix V (St M52) are depicted. The reduced chi-square is 1.99; thus, its estimated

Table III.18: Material parameters of mix IV and VI.

Parameters	Fit IV (St M32)	Fit VI ($GS4_3$ M32)	Unit
K	8.93×10^7	8.40×10^7	Nm
$\tilde{k}_1$	4.09×10^9	4.09×10^9	N/m
$\tilde{k}_2$	2.07×10^{11}	2.07×10^{11}	N/m^2
$\tilde{k}_3$	2.68×10^{17}	1.98×10^{17}	N/m^3
$\tilde{\alpha}$	4.40×10^8	4.38×10^8	N
$\tilde{\zeta}$	7.26×10^8	5.50×10^8	N
η	2.00×10^2	2.00×10^2	s/m

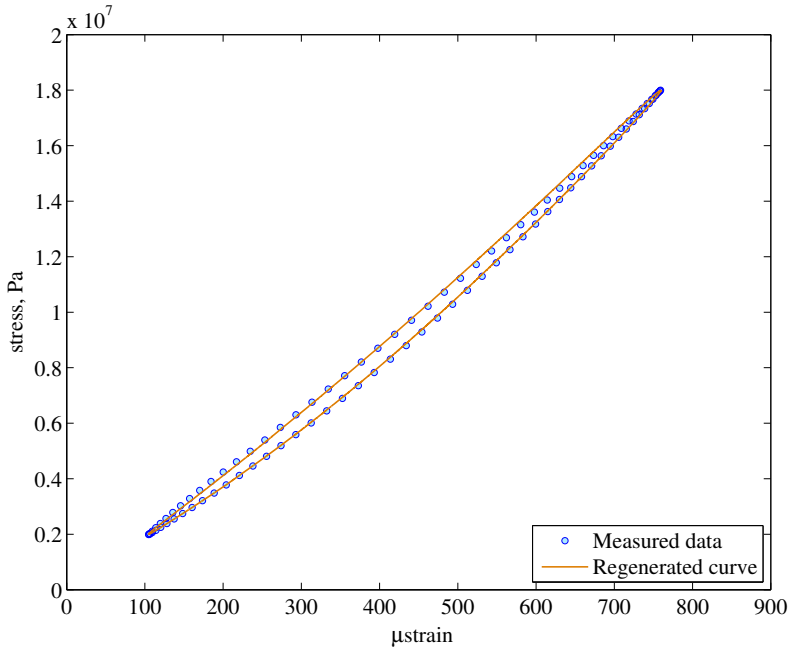

Figure III.33: Measured data and regenerated curve for mix IV (St M32).

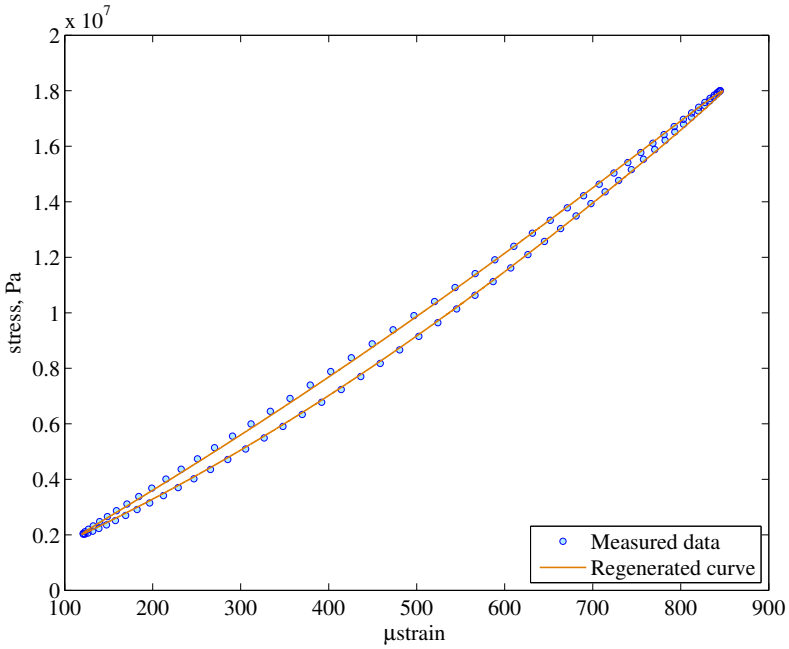

Figure III.34: Measured data and regenerated curve for mix VI ($GS4_3$ M32).

Table III.19: Material parameters of mix V and VII.

Parameters	Fit V (St M52)	Fit VII ($GS4_3$ M52)	Unit
K	1.04×10^8	9.10×10^7	Nm
$\tilde{k}_1$	4.62×10^9	4.62×10^9	N/m
$\tilde{k}_2$	2.07×10^{11}	2.64×10^{11}	N/m^2
$\tilde{k}_3$	2.20×10^{17}	3.08×10^{17}	N/m^3
$\tilde{\alpha}$	4.40×10^8	4.40×10^8	N
$\tilde{\zeta}$	1.76×10^8	4.62×10^8	N
η	2.00×10^2	2.00×10^2	s/m

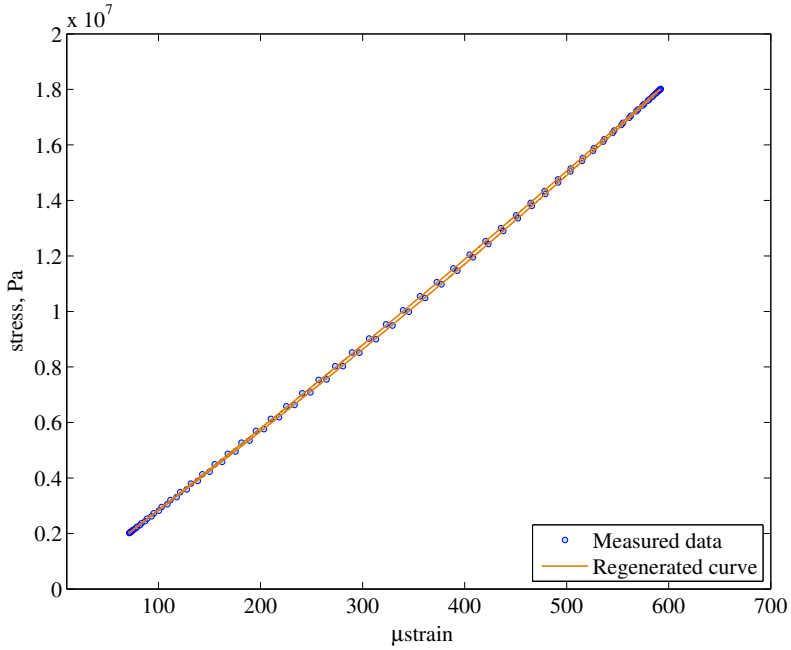

Figure III.35: Measured data and regenerated curve for mix V (St M52).

sample value is greater than 1.5. In fig. III.36 the measured data and the regression curve for a cycle related to the mix VII ($GS4_3$ M52) are depicted; the reduced chi-square is 0.38.

III.5 Discussions

Parameter estimation plays a critical role in accurately describing system behavior through mathematical models such as the proposed one. Thus, a figure of merit is required to understand how good is the identification made. Herein, the parameter identification performed by the method presented in sec. III.4, based on the principle of Maximum Likelihood, has been validated by the chi-square test to assess the goodness of fit.

This analysis shows that, in the cases examined, there are concrete mixtures for which the proposed model is acceptable directly, and there are cases in which the value of the reduced chi-square is higher than the minimum threshold chosen for the test. The mixtures of concrete with a high reduced chi-square are:

- Mix III with 3.5% replacement of micro-filler and a compressive strength of 52 MPa;
- Mix IV with standard concrete and a compressive strength of 32 MPa;

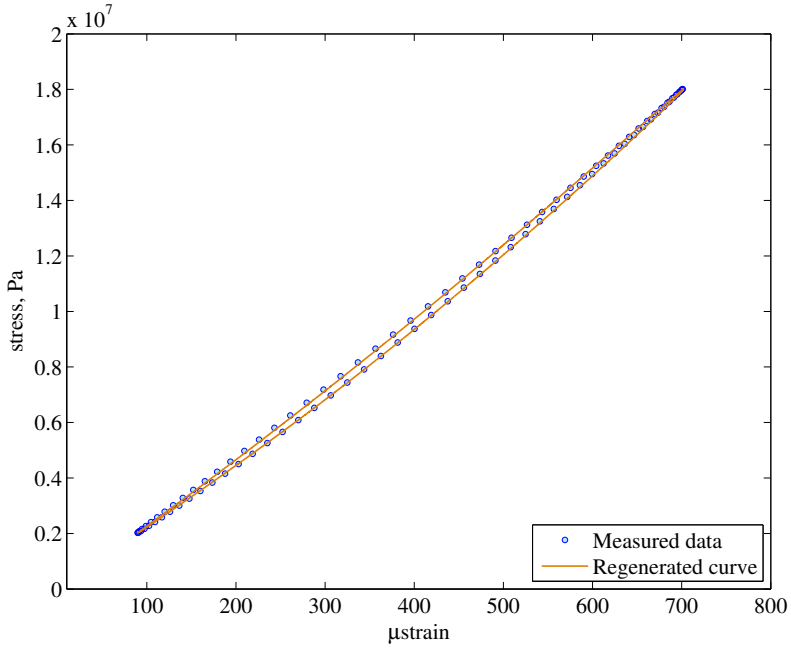

Figure III.36: Measured data and regenerated curve for mix VII ($GS4_3$ M52).

- Mix V with standard concrete and a compressive strength of 52 MPa.

Comparing the squared deviations between the strain measurement $\epsilon_i^{(m)}$, in μstrain, and the simulation $\epsilon_i^{(c)}$, in μstrain, with the variances obtained from the strain measures S_i^2 (see eq. (III.4)), it is possible to understand why the chi-square test fails, and then to evaluate what are the critical issues for the proposed model to improve it. In the case of mix III, the variance measured, which has a uniform distribution on the whole cycle, indicates a good precision in the measurement system and, thus the high value of reduced chi-square requires an improvement of the model (see fig. III.37). Similar considerations can be done for the mix IV (see fig. III.38). In the other case, the distribution of the variance on the cycle is evidence of a low accuracy of the measures and, thus such measurements need a more in-depth analysis (see fig. III.39).

However, it is evident from figs. III.30–III.36 that for all mixtures the dissipation energy level, i.e. the loop areas, forecast by the model presented agrees reasonably well with experimental data. In the above mentioned cases, the analysis performed indicates some critical issues and, thus, future efforts will be dedicated to enhance these problems.

The performed identifications allow us to characterize the effect of each material parameter introduced by the proposed model. From tab. III.17 concerning mix I, II and III, it is possible to note that the coupling coefficient $\tilde{\alpha}$ decreases with

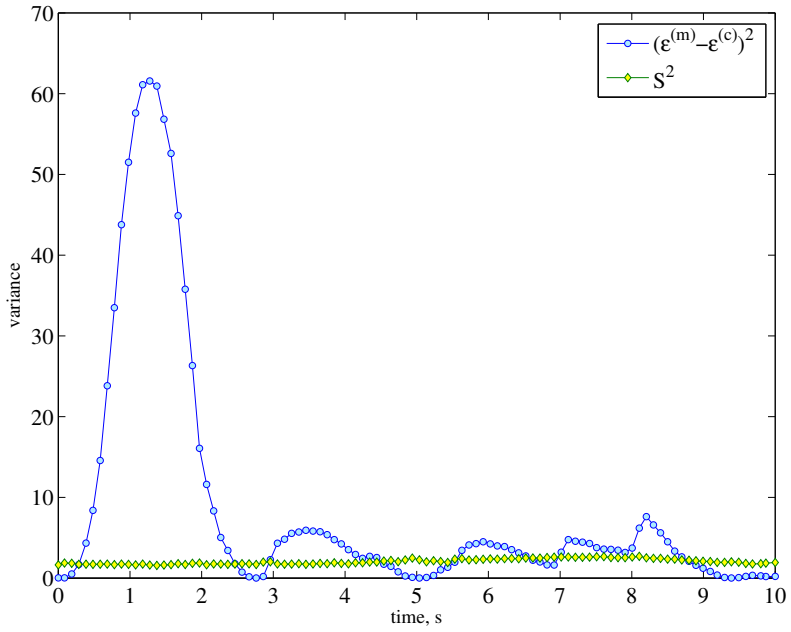

Figure III.37: Mix III: squared deviations between the measurement and the model $\left(\epsilon_i^{(m)} - \epsilon_i^{(c)}\right)^2$, measured variances S_i^2 expressed in micro-strain.

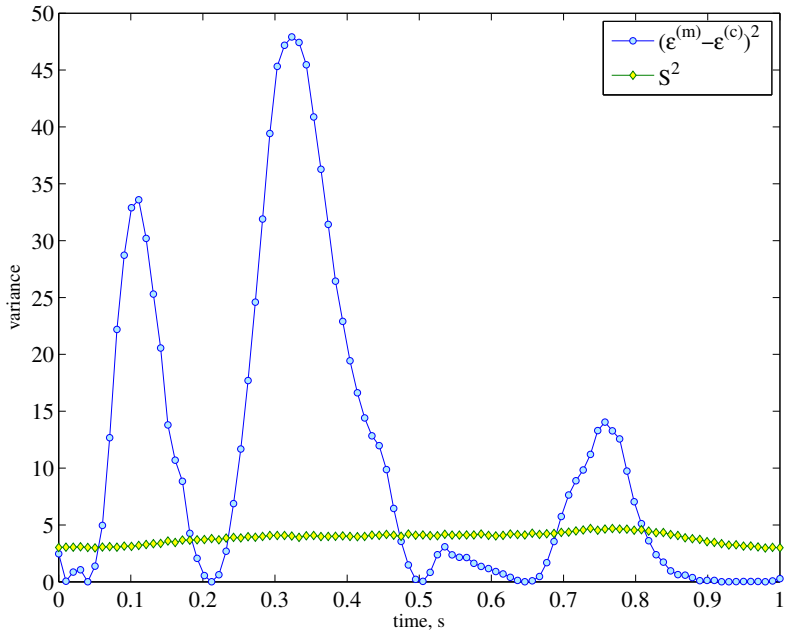

Figure III.38: Mix IV: squared deviations between the measurement and the model $\left(\epsilon_i^{(m)} - \epsilon_i^{(c)}\right)^2$, measured variances S_i^2 expressed in micro-strain.

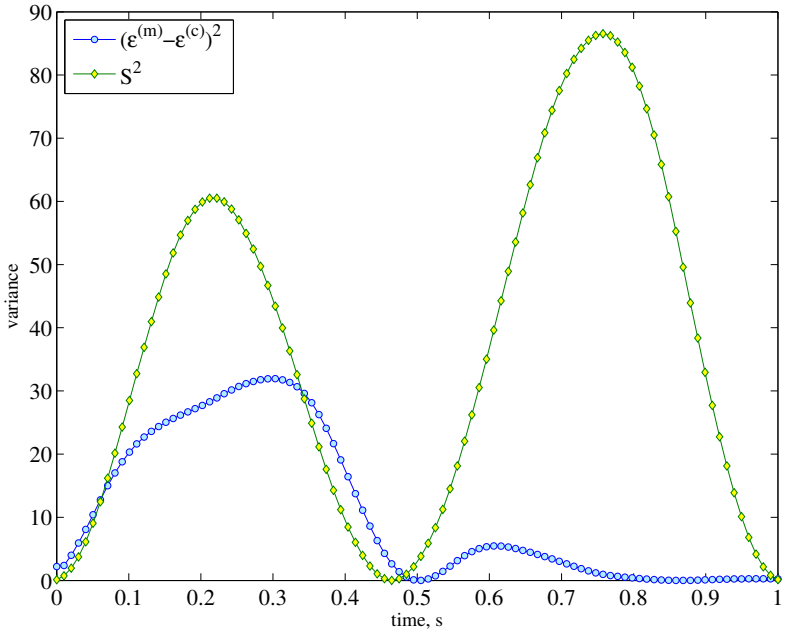

Figure III.39: Mix V: squared deviations between the measurement and the model $\left(\epsilon_i^{(m)} - \epsilon_i^{(c)}\right)^2$, measured variances S_i^2 expressed in micro-strain.

increasing content of filler, i.e. the effect of the micro-slip is decreased by adding more filler for mixtures that have a low water-to-cement ratio w_c ($w_c \simeq 0.5$). On the contrary, when the water-to-cement ratio is higher ($w_c \simeq 0.7$), as for mix IV, V, VI and VII, the coupling coefficient $\tilde{\alpha}$ seems not to be affected by the micro-particle content (see tabs. III.18 and III.19). In the cases of mix I, II and III, the friction coefficient $\tilde{\zeta}$ appears to be related to the non-linearity of the micro-structure; in fact, considering the micro-stiffness ratios $\tilde{k}_3/\tilde{k}_1$, which is a measure of nonlinearity, it is possible to note that the greater the ratio, the higher is the friction coefficient $\tilde{\zeta}$. In fact, for mix I, II and III the ratio $\tilde{k}_3/\tilde{k}_1$ is equal to 5.59×10^7, 8.06×10^6 and 2.82×10^7, respectively and the coefficient $\tilde{\zeta}$ equals 1.63×10^8 N, 5.34×10^7 N and 1.17×10^8 N. The same relationship can be found in mix IV, V, VI and VII also taking into account the ratio $\tilde{k}_2/\tilde{k}_1$, less relevant in the previous cases because the very low values of $\tilde{k}_2$. For mix IV, V, VI and VII, the ratio $\tilde{k}_3/\tilde{k}_1$ is respectively equal to 6.56×10^7, 4.76×10^7, 4.84×10^7 and 6.67×10^7, in the same way the ratio $\tilde{k}_2/\tilde{k}_1$ is 50.5, 44.8, 50.5 and 57.1 and the coefficient $\tilde{\zeta}$ equals 7.26×10^8 N, 1.76×10^8 N, 5.50×10^8 N, and 4.62×10^8 N. Furthermore, including the proposed model Coulomb and viscous effects such that the viscous dissipation is dominant in the low micro-slip velocity range while Coulomb friction is significant beyond a given micro-velocity level, the dissipation slope η plays a crucial role to define the

extension of the ranges corresponding to these different behaviors. For mix I, II and III, when the water-to-cement ratio is low ($w_c \simeq 0.5$), the dissipation slope η is an order of magnitude greater than that of the other mixtures which are characterize by a greater w_c; hence, the first three mixtures show a more considerable Coulomb effect.

Chapter IV

Conclusions

The modeling process presented in this work proves that it is possible, by means of a simple non-linear system of ordinary differential equations, to carefully describe both quantitatively and qualitatively the available experimental evidence on compression of cylindrical modified concrete specimen. In particular, it is proven that, even if the applied compression force is related to elongation by a (nearly) linear relationship, some non-linearities in the dissipation loop may be ascribed to non-linear elastic phenomena involving the newly introduced microstructural parameter which describes internal micro-motions. More precisely, the physical meaning of this micro-structural parameter can be interpreted in terms of the overall relative displacement of crack faces which characterize the microstructure of concrete-type specimens. The time rate of the same micro-structural parameter is the source of the only friction effect considered in this work: the one related to Coulomb friction force. By means of a series of numerical simulations, we have proved that a physically reasonable set of ranges for introduced constitutive parameters can be found which describes the whole variety of dissipation loops measured in Madeo [2006] and in several laboratory tests. The presented results justify the need for more complex models in order to describe *(i)* bending and compression periodic deformation of considered cylindrical specimens, *(ii)* coupling between bending and shear with micro-deformation, *(iii)* more complex micro-motions in which relative displacement of crack faces may depend on the orientation and localization of cracks, *(iv)* the longer range effects of micro-cracks-induced micro-deformation in the neighborhood of considered REV, i.e. those effects which can be modeled by allowing for the dependence of deformation energy on higher gradients of introduced kinematical fields, *(v)* a load frequency dependence of the dissipation energy. Furthermore, the effect of micro-particles additives such as calcium carbonate on internal dissipation of concrete was experimentally investigated for seven kinds of concrete mixture. All

specimens were tested under cyclic loading in order to evaluate energy dissipation from the area of dissipated loop detected in stress-strain diagram relative to a representative cycle. The experimental determination of the energy dissipated shows a significant increase in the damping capability of the cement-based materials with micro-filler compared to the standard concrete, in some cases in which the water-to-cement ratio is enough high. In all tests, the friction coefficient $\tilde{\zeta}$ appears related to the non-linearity of the micro-structure; indeed, it is possible to note that when non-linearities are more significant, the friction coefficient is higher.

Appendix A

Student's t-distribution

Student's t-distribution, or simply the t-distribution, is a family of continuous probability distributions that arise when estimating the mean of a normally distributed population in situations where the sample size is small and population standard deviation is unknown. The t-distribution is symmetric and bell-shaped, like the normal distribution, but has heavier tails, meaning that it is more prone to producing values that fall far from its mean. This makes it useful for understanding the statistical behavior of certain types of ratios of random quantities, in which variation in the denominator is amplified and may produce outlying values when the denominator of the ratio falls close to zero.

Student's t-distribution has the probability density function given by

$$f(t;\nu) = \frac{\Gamma\left(\frac{\nu+1}{2}\right)}{\sqrt{\nu\pi}\Gamma\left(\frac{\nu}{2}\right)}\left(1+\frac{t^2}{\nu}\right)^{-\frac{\nu+1}{2}} \tag{A.1}$$

where ν is the number of degrees of freedom and Γ is the gamma function. The probability density function is symmetric, and its overall shape resembles the bell shape of a normally distributed variable with mean 0 and variance 1, except that it is a bit lower and wider. As the number of degrees of freedom grows, the t-distribution approaches the normal distribution with mean 0 and variance 1. If $\nu = 1$ this distribution come close to the Cauchy distribution, $f(t) = 1/\left[\pi\left(1+t^2\right)\right]$, whose mean and variance are undefined.

Student's t-distribution with ν degrees of freedom can be defined as the distribution of the random variable T

$$T = Z\sqrt{\frac{\nu}{V}} \tag{A.2}$$

where Z is a random variable normally distributed with expected value 0 and variance 1, and the random variable V has a chi-squared distribution with ν degrees of freedom, being Z and V independent.

Suppose $X_1, \ldots, X_n$ are independent realizations of the normally-distributed, random variable X, which has an expected value μ and variance $\mathtt{s}^2$. Standard estimators of μ and $\mathtt{s}^2$ are: $\bar{X}_n$ the sample arithmetic mean and S_n^2 the standard variance from the sample. It can be shown that the random variable

$$Z = \frac{\bar{X} - \mu}{\sqrt{\mathtt{s}^2/n}} \tag{A.3}$$

is normally distributed with mean 0 and variance 1, while the random variable

$$V = \frac{(n-1)\, S_n^2}{\mathtt{s}^2} \tag{A.4}$$

has a chi-squared distribution with $\nu = n - 1$ degrees of freedom. The two random variable are independent according to Cochran's theorem. Without knowing the variance $\mathtt{s}^2$ it is not possible compare the estimators $\bar{X}$ and S_n^2 with Z and V which have probability distribution known. Nevertheless the random variable

$$T = \frac{\bar{X} - \mu}{\sqrt{S_n^2/n}} = \frac{\bar{X} - \mu}{\sqrt{\frac{\mathtt{s}^2}{n}\frac{(n-1)S_n^2}{(n-1)\mathtt{s}^2}}} = \frac{Z}{\sqrt{V/(n-1)}} \tag{A.5}$$

has a Student's t-distribution as defined above. Thus for inference purposes T is a useful *'pivotal quantity'*; it depends on ν, but not μ or $\mathtt{s}$; the lack of dependence on μ and $\mathtt{s}$ is what makes the t-distribution important in both theory and practice.

Appendix B

Chi-Square: Testing for Goodness of Fit

In a previous section we discussed briefly a procedure for fitting a hypothesized function to a set of experimental data points. Such a procedure involves minimizing a quantity we called Φ in order to determine best estimates for certain function parameters, such as, in our case, material parameters characterizing the model (II.28). Φ is proportional to a statistical measure called χ^2, or *chi-square*[1], a quantity commonly used to test whether any given data are well described by some hypothesized function. Such a determination is called a chi-square test for goodness of fit. In the following, we discuss concisely about χ^2 and its statistical distribution, and show how it can be used as a test for goodness of fit.

If ν independent variables x_i are normally distributed with expected value μ_i and variance $\mathtt{s}_i^2$, then the quantity known as *chi-square* is defined by

$$\chi^2 \equiv \sum_{i=1}^{\nu} \frac{(x_i - \mu_i)^2}{\mathtt{s}_i^2} \tag{B.1}$$

Note that ideally, given the random fluctuations of the values of x_i about their mean values μ_i, each term in the sum will be of order unity. Hence, if we have chosen the μ_i and the $\mathtt{s}_i$ correctly, we may expect that a calculated value of χ^2 will be approximately equal to ν. If it is, then we may conclude that the data are well described by the values we have chosen for the μ_i, that is, by the hypothesized function. If a calculated value of χ^2 turns out to be much larger than ν, and we have correctly estimated the values for the $\mathtt{s}_i$, we may possibly conclude that our data are not well-described by our hypothesized set of the μ_i. This is the general

[1]The notation of χ^2 is traditional and possibly misleading. It is a single statistical variable, and not the square of some quantity χ. It is therefore not *chi squared*, but *chi-square*.

idea of the χ^2 test. In what follows we spell out the details of the procedure.

The quantity χ^2 defined in eq. (B.1) has the probability distribution given by

$$f\left(\chi^2\right) = \frac{1}{2^{\nu/2}\Gamma\left(\nu/2\right)} e^{-\chi^2/2} \left(\chi^2\right)^{(\nu/2)-1} \tag{B.2}$$

This is known as the χ^2-*distribution* with ν degrees of freedom, being ν a positive integer. Sometimes we write it as $f(\chi^2_\nu)$ when we wish to specify the value of ν. The mean value of χ^2_ν is equal to ν, and its variance is equal to 2ν. The distribution is highly skewed for small values of ν, and becomes more symmetric as ν increases, approaching a Gaussian distribution for large ν, just as predicted by the Central Limit Theorem.

Considering a set of N experimentally measured quantities y_i, depending on as many values of x_i it is possible, in a curve fitting, to test whether the assumed relationship f between x and y characterized by r parameters a_r is well-described by the hypothesized predicted values $\mu_i = f\left(x_i; a_r\right)$ by means of the *chi-square* test. In other words, the chi-square statistic is used as a 'figure of merit' when fitting a function, f, to data, $\{x_i, y_i\}$ to evaluate the 'goodness of fit'. In details, a sum like that shown in eq. (B.1), with N terms, constitutes a sample value for χ^2. Computing the sum, estimates for the $\mathtt{s}_i$, that are independently obtained for each y_i, are used. Now imagine that we could repeat our experiment many times. Each time, we would obtain a data sample, and thus, a sample value for χ^2 . If our data were well-described by our hypothesis, we would expect our sample values of χ^2 to be distributed according to eq. (B.2). The expected distribution of our samples of χ^2 will not have N degrees of freedom because the interpolating function using for the fit as estimates of μ depends on r parameters. Therefore, the number of degrees of freedom becomes $\nu = N - r$, and the resulting χ^2 sample will be one having ν (rather than N) degrees of freedom.

This explains the origin of the rule of thumb for chi-square fitting that states that a 'good fit' is achieved when the *reduced chi-square*, χ^2/ν, equals one. Since errors can sometimes be non-Gaussian or not robust, a model is typically only rejected for very low values of P –probability that this value of chi-square, or a larger one, could arise by chance– such as 0.001. This means that for a number of degrees of freedom of about 100, the reduced chi-square must be less than 1.5.

Bibliography

L. Adelaide, B. Richard, F. Ragueneau, C. Cremona, Thermodynamical admissibility of a set of constitutive equations coupling elasticity, isotropic damage and internal sliding, C. R. Mecanique 338 (2010) 158–163.

S. Andrieux, Y. Bamberger, J.J. Marigo, Un modèle de matériau microfissuré pour les roches et les bétons, Journal de mécanique théorique et appliquée, 5(3) (1986) 471–513.

J.J. Alibert, P. Seppecher, F. dell'Isola, Truss modular beams with deformation energy depending on higher displacement gradients, Mathematics and Mechanics of Solids 8 (2003) 51–73.

H. Altenbach, V.A. Eremeyev, Analysis of the viscoelastic behavior of plates made of functionally graded materials, ZAMM Zeitschrift fur Angewandte Mathematik und Mechanik, 88(5) (2008) 332–341.

H. Altenbach, V.A. Eremeyev, On the bending of viscoelastic plates made of polymer foams, Acta Mechanica 204(3-4) (2009)a 137–154.

H. Altenbach, V.A. Eremeyev, On the linear theory of micropolar plates, ZAMM Zeitschrift fur Angewandte Mathematik und Mechanik 89(4) (2009)b 242–256.

H. Altenbach, V.A. Eremeyev, On the effective stiffness of plates made of hyperelastic materials with initial stresses, International Journal of Non-Linear Mechanics 45(10) (2010)a 976–981.

H. Altenbach, V.A. Eremeyev, L.P. Lebedev, L.A. Rendón, Acceleration waves and ellipticity in thermoelastic micropolar media, Archive of Applied Mechanics 80(3) (2010) 217–227.

H. Altenbach, V.A. Eremeyev, L.P. Lebedev, On the spectrum and stiffness of an elastic body with surface stresses, ZAMM Zeitschrift fur Angewandte Mathematik und Mechanik 91(9) (2011) 699–710.

H. Altenbach, V.A. Eremeyev, On the shell theory on the nanoscale with surface stresses, International Journal of Engineering Science 49(12) (2011) 1294–1301.

H. Altenbach, V.A. Eremeyev, N.F. Morozov, Surface viscoelasticity and effective properties of thin-walled structures at the nanoscale, International Journal of Engineering Science (2012) Article in Press.

U. Andreaus, F. dell'Isola, M. Porfiri, Piezoelectric passive distributed controllers for beam flexural vibrations, JVC/Journal of Vibration and Control 10(5) (2004) 625–659.

U. Andreaus, G.C. Ruta, A review of the problem of the shear centre(s) Continuum Mechanics and Thermodynamics 10 (1998).

U. Andreaus, P. Baragatti, Fatigue crack growth, free vibrations, and breathing crack detection of aluminium alloy and steel beams, Journal of Strain Analysis for Engineering Design 44 (2009).

N. Auffray, R. Bouchet, Y. Brechet, Derivation of anisotropic matrix for bi-dimensional strain-gradient elasticity behaviour, International Journal of Solids and Structures 46(2) (2009) 440–454.

N. Auffray, R. Bouchet, Y. Brechet, Strain gradient elastic homogenization of bidimensional cellular media, International Journal of Solids and Structures 47(13) (2010) 1698–1710.

J. Bastien, M. Schatzman, C.-H. Lamarque, Study of some rheological models with a finite number of degrees of freedom, European Journal of Mechanics A/Solids 19(2) (2000) 277–307.

R.C. Batra, F. dell'Isola, G.C. Ruta, Second-order solution of Saint-Venant's problem for an elastic bar predeformed in flexure, International Journal of Non-Linear Mechanics 40 (2-3) (2005) 411–422.

A.O. Belyakov, A.P. Seyranian, A. Luongo, Dynamics of the pendulum with periodically varying length, Physica D: Nonlinear Phenomena 238 (16) (2009) 1589–1597.

J. Beyrouthy, Reduction 3D-1D d'un modele viscoelastique en grandes deformations., C.R. Acad. Sci. Paris, Ser.I, Vol. 239-243 (2007) 115-130.

J. Beyrouthy and P. Neff, A viscoelastic thin rod model for large deformations: numerical examples. Math. Mech. Solids, 16(8) (2011), 887-896.

S.S. Bhattacharjee, P. Léger. Seismic cracking and energy dissipation in concrete gravity dams. Earthquake Engineering & Structural Dynamics 22 (11) (1993) 991–1007.

M. A. Biot, Generalized Theory of Acoustic Propagation in Porous Dissipative Media, The Journal of the Acoustical Society of America, 34 (1962) 1254–1264.

M. A. Biot, Mechanics of Deformation and Acoustic Propagation in Porous Media, J. Appl. Phys. 33 (1962)a 1482–1498.

M. A. Biot, Theory of Propagation of Elastic Waves in a Fluid-Saturated Porous Solid. II. Higher Frequency Range, The Journal of the Acoustical Society of America, 28 (1956) 179–191.

M. A. Biot, General Theory of Three-Dimensional Consolidation, Journal of Applied Physics, 12 (1941) 155–164.

M. Bîrsan, H. Altenbach, T. Sadowski, V.A. Eremeyev, D. Pietras, Deformation analysis of functionally graded beams by the direct approach, Composites Part B: Engineering 43 (3) (2012) 1315–1328.

M. Bongué Boma, M. Brocato. A continuum model of micro-cracks in concrete, Continuum Mechanics and Thermodynamics 22(2) (2010) 137–161.

Z. Boukria, A Limam, Experimental damage analysis of concrete structures using the vibration signature - Part II: Located damage (crack), International Journal of Mechanics 6 (1) (2012) 28–34.

B. Budiansky and J.R. O'Connel, Elastic moduli of a cracked solid. Int. J. Solids Structures 12 (1976) 81–97.

A. Cazzani and C. Lovadina, On some mixed finite element methods for plane membrane problems, Computational Mechanics 20(6) (1997), 560–572.

A. Cazzani and P. Ruge, Numerical aspects of coupling strongly frequency-dependent soil-foundation models with structural finite elements in the time-domain, Soil Dynamics and Earthquake Engineering, 37 (2012), 56–72.

A.G. Bowland, R.E. Weyers, F.A. Charney, N.E. Dowling, T.M. Murray, and A. Ramniceanu, Effect of Vibration Amplitude on Concrete with Damping Additives. ACI Materials Journal, 109(3) (2012) 371-378.

A. D. Brailsford, The role of internal stresses in internal friction, Phisics-Letter 8, 12(2) (1964).

P.M. Buechner, R.S. Lakes, Size effects in the elasticity and viscoelasticity of bone, Biomechan. Model. Mechanobiol. 1 (2003) 295–301.

A. Carcaterra, A. Akay, I.M. Koç, Near-irreversibility in a conservative linear structure with singularity points in its modal density, Journal of the Acoustical Society of America 119 (2006) 2141–2149.

A. Carcaterra, A. Akay, Theoretical foundations of apparent-damping phenomena and nearly irreversible energy exchange in linear conservative systems, Journal of the Acoustical Society of America 12 (2007) 1971–1982.

A. Carcaterra, A. Akay, Dissipation in a finite-size bath, Physical Review E 84 (2011).

A. Carpinteri, G. Lacidogna, N. Pugno, Scaling of energy dissipation in crushing and fragmentation: a fractal and statistical analysis based on particle size distribution, International Journal of Fracture 129 (2004) 131–139.

D. Ciancio, I. Carol, M. Cuomo, Crack opening conditions at 'corner nodes' in FE analysis with cracking along mesh lines, Engineering Fracture Mechanics 74 (13) (2007) 1963–1982.

D. Ciancio, I. Carol, M. Cuomo, On inter-element forces in the FEM-displacement formulation, and implications for stress recovery, International Journal for Numerical Methods in Engineering 66 (3) (2006) 502–528.

L. Contrafatto, M. Cuomo, A new thermodynamically consistent continuum model for hardening plasticity coupled with damage, International Journal of Solids and Structures 39 (2002) 6241–6271.

L. Contrafatto, M. Cuomo, A framework of elastic–plastic damaging model for concrete under multiaxial stress states, International Journal of Plasticity 22 (2006) 2272–2300.

L. Contrafatto, M. Cuomo, A globally convergent numerical algorithm for damaging elasto-plasticity based on the Multiplier method, International Journal for Numerical Methods in Engineering 63 (2005) 1089–1125.

R. Contro, C. Poggi and A. Cazzani, Numerical Analysis of Fire Effects on Beam Structures, Engineering Computations (Swansea, Wales), 5(1) (1988), 53–58.

Cowin, S.C. and Nunziato, J.W., Linear elastic materials with voids. Journal of Elasticity 13(2), 125–147 (1983).

A. Culla, A. Sestieri, A. Carcaterra, Energy flow uncertainties in vibrating systems: Definition of a statistical confidence factor, Mechanical Systems and Signal Processing 17 (2003) 635–663.

M. Cuomo, G. Ventura, Complementary Energy Approach to Contact Problems Based on Consistent Augmented Lagrangian regularization, Mathematical and Computer Modelling 28 (1998) 185–204.

M. Cuomo, L. Contrafatto, Stress rate formulation for elastoplastic models with internal variables based on augmented Lagrangian regularisation, International Journal of Solids and Structures, 37 (2000) 3935–3964.

F. Darve, S. Labanieh, Incremental constitutive law for sands and clays: simulations of monotonic and cyclic tests*, International Journal for Numerical and Analytical Methods in Geomechanics* 6(2) (1982) 243–275.

F. dell'Isola, G. Ruta, and R. Batra, Generalized Poynting effects in predeformed prismatic bars, Journal of Elasticity 50 (1998) 181–196.

F. dell'Isola, C. Woźniak, On phase transition layers in certain micro-damaged two-phase solids, International Journal of Fracture 83 (2) (1997)a 175–189.

F. dell'Isola, C. Woźniak, On continuum modelling the interphase layers in certain two-phase elastic solids, ZAMM Zeitschrift fur Angewandte Mathematik und Mechanik 77 (7) (1997)b 519–526.

F. dell'Isola, P. Seppecher, The relationship between edge contact forces, double force and interstitial working allowed by the principle of virtual power, Comptes rendus de l'Académie des Sciences Serie IIb 321 (1995) 303–308.

F. dell'Isola, L. Rosa, C. Woźniak, Dynamics of solids with micro periodic nonconnected fluid inclusions, Archive of Applied Mechanics 67 (4) (1997)c 215–228.

F. dell'Isola, L. Rosa, C. Woźniak, A micro-structured continuum modelling compacting fluid-saturated grounds: The effects of pore-size scale parameter, Acta Mechanica 127 (1-4) (1998) 165–182.

F. dell'Isola, K. Hutter, What are the dominant thermomechanical processes in the basal sediment layer of large ice sheets?, Proceedings of the Royal Society of London. Series A: Mathematical, Physical and Engineering Sciences 454 (1998) 1169–1195.

F. dell'Isola, S. Vidoli, Damping of bending waves in truss beams by electrical transmission lines with PZT actuators, Archive of Applied Mechanics 68 (9) (1998)a 626–636.

F. dell'Isola, S. Vidoli, Continuum modelling of piezoelectromechanical truss beams: An application to vibration damping, Archive of Applied Mechanics 68 (1) (1998)b 1–19.

F. dell'Isola, R. Batra, Saint-Venant's Problem for Porous Linear Elastics Materials, Journal of Elasticity 47 (1997) 73–81.

F. dell'Isola, M. Guarascio, K.A. Hutter, Variational approach for the deformation of a saturated porous solid. A second-gradient theory extending Terzaghi's effective stress principle, Archive of Applied Mechanics 70 (2000) 323–337.

F. dell'Isola, A. Madeo, P. Seppecher, Boundary conditions at fluid-permeable interfaces in porous media: A variational approach, International Journal of Solids and Structures vol. 46(17) (2009) 3150–3164.

A. De Simone , A. Luongo, Nonlinear viscoelastic analysis of a cylindrical balloon squeezed between two rigid moving plates, International Journal of Solids and Structures 50 (2013) 2213–2223.

C.C. De Wit, A new model for control of systems with friction, IEEE Transactions on Automatic Control, 40(3) (1995) 419–425.

A. Di Egidio, A. Luongo, A. Paolone, Linear and non-linear interactions between static and dynamic bifurcations of damped planar beams, International Journal of Non-Linear Mechanics 42 (1) (2007) 88–98.

N.E. Dowling, Mechanical behavior of materials, Pearson, (2012).

U.E. Shamy, C. Denissen, Microscale energy dissipation mechanisms in cyclically-loaded granular soils, Geotechnical and Geological Engineering 30(2) (2012) 343–361.

V.A. Eremeyev, A.B. Freidin, L.L., Sharipova, Nonuniqueness and Stability in Problems of Equilibrium of Elastic Two-Phase Bodies, Doklady Physics 48 (7) (2003) 359–363.

V.A. Eremeyev, W. Pietraszkiewicz, The nonlinear theory of elastic shells with phase transitions, Journal of Elasticity 74 (1) (2004) 67–86.

V.A. Eremeyev, Acceleration waves in micropolar elastic media, Doklady Physics 50 (4) (2005) 204–206.

V.A. Eremeyev, H. Altenbach, N.F. Morozov, The influence of surface tension on the effective stiffness of nanosize plates, Doklady Physics 54 (2) (2009) 98–100.

V.A. Eremeyev, W. Pietraszkiewicz, Thermomechanics of shells undergoing phase transition, Journal of the Mechanics and Physics of Solids 59 (2011) 1395–1412.

A.C. Eringen, Microcontinuum field theories, Springer-Verlag, New York, 2001.

A.C. Eringen, E.S. Suhubi, Nonlinear theory of simple microelastic solids: I, Int. J. Eng. Sci. 2 (1964)a 189–203.

A.C. Eringen, E.S. Suhubi, Nonlinear theory of simple microelastic solids: II, Int. J. Eng. Sci. 2 (1964)b 389–404.

A.C. Eringen, D.G.B. Edelen, On nonlocal Elasticity, Int. J. Eng. Sci. 10 (1972) 233–248.

A. C. Eringen, Microcontinuum Field Theories I. Foundations and Solids, Springer Verlag, 1999.

G. Fantozzi and I.G. Ritchie, Internal friction caused by the intrinsic properties of dislocations, J. Phys. Colloques 42, C5-3-C5-23 (1981).

G. Fantozzi, C. Esnouf, W. Benoit, I.G. Ritchie. Internal friction and microdeformation due to the intrinsic properties of dislocations: The Bordoni relaxation, Progress in Materials Science 27(3-4) (1982) 311–451.

S. Federico, W. Herzog, On the permeability of fibre-reinforced porous materials, International Journal of Solids and Structures 45 (7-8) (2008)a 2160–2172.

S. Federico, W. Herzog, Towards an analytical model of soft biological tissues, Journal of Biomechanics 41(16) (2008)b 3309–3313.

S. Federico, T.C. Gasser, Nonlinear elasticity of biological tissues with statistical fibre orientation, Journal of the Royal Society Interface 7 (47) (2010) 955–966.

M. Ferretti, A. Madeo, F. dell'Isola, P. Boisse, Modelling the onset of shear boundary layers in fibrous composite reinforcements by second gradient theory, ZAMP (2013) in press.

S. Forest, R. Sievert, Nonlinear microstrain theories, Int. J. Solids Struct. 43 (2006) 7224–7245.

S. Forest, Micromorphic Approach for Gradient Elasticity, Viscoplasticity, and Damage, Journal of Engineering Mechanics 135(3) (2009) 117–131.

S. Forest, N.M. Cordero, E.P. Busso, First vs. second gradient of strain theory for capillarity effects in an elastic fluid at small length scales, Computational Materials Science 50 (2011) 1299–1304.

H. Frohlich and R. Sack, Theory of the Rheological Properties of Dispersions, Proc. R. Soc. Lond. A 185 (1946) 415–430.

E. Garusi, A. Tralli and A. Cazzani, An unsymmetric stress formulation for reissner-mindlin plates: A simple and locking-free rectangular element, International Journal of Computational Engineering Science 5(3) (2004), 589–618.

Germain, P., 1972. Sur l'application de la méthode des puissances virtuelles en mécanique des milieux continus. Comptes Rendus De L'Academie Des Sciences 274, A1051–A1055.

Germain, P., 1973. The method of virtual powers in continuum mechanics. Part two: Microstructure. Journal of Applied Mathematics 25 (3), 556–575.

Ghiba I.D., Neff P., Madeo A., Placidi L., Rosi G., 2013. The relaxed linear micromorphic continuum: existence, uniqueness and continuous dependence in dynamics. Submitted to Mathematics and Mechanics of Solids, arXiv:1308.3762v1.

A.E. Green, R.S. Rivlin, Multipolar continuum mechanics, Archive for Rational Mechanics and Analysis 17(2) (1964)a 113–114.

A.E. Green, R.S. Rivlin, Simple force and stress multipoles, Archive for Rational Mechanics and Analysis 16, (1964)b 325–353.

A.E. Green, R.S. Rivlin, On Cauchy's equations of motion, Zeitschrift für Angewandte Mathematik und Physik (ZAMP) 15 (1964)c 290–292.

A.E. Green, R.S. Rivlin, Multipolar continuum mechanics: functional theory. I, Proceedings of the Royal Society of London. Series A: Mathematical, Physical and Engineering Sciences 284 (1965) 303–324.

F. Hernández-Olivares, G. Barluenga, M. Bollati, B. Witoszek, Static and dynamic behaviour of recycled tyre rubber-filled concrete, Cement and Concrete Research 32 (2002) 1587–1596.

A. Hillerborg, M. Modéer, P.-E. Petersson, Analysis of crack formation and crack growth in concrete by means of fracture mechanics and finite elements, Cement and Concrete Research 6(6) (1976) 773–781.

M. Kachanov. A microcrack model of rock inelasticity - Part I: frictional sliding on microcraks; Part II: propagation of microcraks, Mech. Mater. 1 (1982) 19–41.

M. Kachanov. Elastic solids with many cracks and related problems, Advances in applied mechanics 30 (1994) 259–445.

A. L. Kimball, D. E. Lovell, Internal Friction in Solids, Phys. Rev. 30 (1927) 948–959.

P. Kotronis, R. Chambon, J. Mazars and F. Collin, Local second gradient models and damage mechanics: application to concrete, Bifurcations, Instabilities, Degradation in Geomechanics (2005) 127–142.

D. Krajcinovic. Damage mechanics, North-Holland, Amsterdam, The Netherlands (1996).

M. Jamal, L. Lahlou, M. Midani, H. Zarouni, A. Limam, N. Damil, M. Potier-Ferry, A semi-analytical buckling analysis of imperfect cylindrical shells under axial compression, International Journal of Solids and Structures 40 (5) (2003) 1311–1327.

C.-H. Lamarque, F. Bernardin, J. Bastien, Study of a rheological model with a friction term and a cubic term : deterministic and stochastic cases, European Journal of Mechanics, A/Solids 24 (2005) 572–592.

L.P. Lebedev, M.J. Cloud, V.A. Eremeyev, Tensor Analysis with Applications in Mechanics, New Jersey: World Scientific (2010).

T. Lekszycki, F. dell'Isola, A mixture model with evolving mass densities for describing synthesis and resorption phenomena in bones reconstructed with bioresorbable materials, ZAMM – Journal of Applied Mathematics and Mechanics / Zeitschrift für Angewandte Mathematik und Mechanik (2012).

C. Lomniz, Linear Dissipation in Solids, Journal of Applied Physics 28 (1957) 201–205.

F. D'Annibale, A. Luongo, A damage constitutive model for sliding friction coupled to wear, Continuum Mechanics and Thermodynamics 25(2-4) (2013) 503–522.

A. Luongo, Mode localization in dynamics and buckling of linear imperfect continuous structures, Nonlinear Dynamics, 25 (1-3) (2001) 133–156.

A. Luongo, A. Di Egidio, Bifurcation equations through multiple-scales analysis for a continuous model of a planar beam, Nonlinear Dynamics 41 (2005) 171–190.

A. Luongo, F. Romeo, A Transfer-matrix-perturbation approach to the dynamics of chains of nonlinear sliding beams, Journal of Vibration and Acoustics 128 (2006) 190–196.

A. Luongo, D. Zulli, G. Piccardo, On the effect of twist angle on nonlinear galloping of suspended cables, Computers & Structures 87 (2009) 1003–1014.

A. Madeo, Effect of Micro-Particle Additions on Frictional Energy Dissipation and Strength of Concrete University Libraries, Virginia Polytechnic Institute and State University, 2006.

A. Madeo, T. Lekszycki, F. dell'Isola, A continuum model for the bio-mechanical interactions between living tissue and bio-resorbable graft after bone reconstructive surgery, Comptes Rendus - Mecanique 339 (10) (2011) 625–640.

A. Madeo, D. George, T. Lekszycki, M. Nierenberger, Y. Rémond, A second gradient continuum model accounting for some effects of micro-structure on reconstructed bone remodelling, Comptes Rendus Mécanique 340(8) (2012) 575–589.

A. Madeo, F. dell'Isola, F. Darve, A continuum model for deformable, second gradient porous media partially saturated with compressible fluids, Journal of the Mechanics and Physics of Solids 61 (2013) 2196–2211.

C. Maurini, F. dell'Isola, D. del Vescovo, Comparison of piezoelectronic networks acting as distributed vibration absorbers, Mechanical Systems and Signal Processing 18 (2004) 1243–1271.

C. Maurini, J. Pouget, F. dell'Isola, On a model of layered piezoelectric beams including transverse stress effect, International journal of solids and structures 41 (2004) 4473–4502.

C. Maurini, J. Pouget, F. dell'Isola, Extension of the Euler Bernoulli model of piezoelectric laminates to include 3D effects via a mixed approach, Computers and Structures 84 (2006) 1438–1458.

J. K. Mackenzie, The Elastic Constants of a Solid containing Spherical Holes, Proc. Phys. Soc. B 63 (1950) 2–11.

P. K. Mehta, Paulo J. M. Monteiro, Concrete: Microstructure, Properties, and Materials, McGraw-Hill, 2005.

G. Michel, A. Limam, J.F. Jullien, Buckling of cylindrical shells under static and dynamic shear loading, Engineering Structures 22 (5) (2000) 535–543.

R.D. Mindlin, Micro-structure in linear elasticity, Archive for Rational Mechanics and Analysis 16 (1964) 51–78.

R.D. Mindlin, Second gradient of strain and surface tension in linear elasticity, International Journal of Solids and Structures 1 (1965) 417-438.

R.D. Mindlin, N.N. Eshel, On first strain-gradient theories in linear elasticity, International Journal of Solids and Structures, 4 (1968) 109–124.

A. Misra, C.S. Chang, Effective Elastic Moduli of Heterogeneous Granular Solids, International Journal of Solids and Structures, 30 (1993) 2547–2566.

A. Misra, Y. Yang, Micromechanical model for cohesive materials based upon pseudo-granular structure, International Journal of Solids and Structures 47 (2010) 2970–2981.

A. Misra, V. Singh, Micromechanical model for viscoelastic-materials undergoing damage, Continuum Mechanics and Thermodynamics, 25 (2013) 1–16.

A. Misra, W.Y. Ching, Theoretical nonlinear response of complex single crystal under multi-axial tensile loading, Scientific Reports, 3 (2013).

P. K. Mehta, Paulo J. M. Monteiro, Concrete: Microstructure, Properties, and Materials, McGraw-Hill, (2005).

B. Nadler, P. Papadopoulos, D.J. Steigmann, Multiscale constitutive modeling and numerical simulation of fabric material, International Journal of Solids and Structures, 43 (2006) 206–221.

S. Nemat-Nasser and M. Hori. Micromechanics: overall properties of heterogeneous materials, North-Holland, Amsterdam, The Netherlands (1993).

Neff P., Ghiba I.D., Madeo A., Placidi L., Rosi G., 2013. A unifying perspective: the relaxed micromorphic continuum. Existence, uniqueness and continuous dependence in dynamics. Submitted to Continuum Mechanics and Thermodynamics, arXiv:1308.3219v1.

P. Neff, Finite multiplicative plasticity for small elastic strains with linear balance equations and grain boundary relaxation. Cont. Mech. Thermodynamics, 15(2) (2003) 161–195.

P. Neff, A finite-strain elastic-plastic Cosserat theory for polycrystals with grain rotations. Int. J. Eng. Sci., 44 (2006) 574–594.

P. Neff, Local existence and uniqueness for quasistatic finite plasticity with grain boundary relaxation. Quart. Appl. Math., 63 (2005)a 88–116.

P. Neff , A geometrically exact viscoplastic membrane-shell with viscoelastic transverse shear resistance avoiding degeneracy in the thin-shell limit. Part I: The viscoelastic membrane-plate. Zeitschrift Angewandte Mathematik Physik (ZAMP), 56(1) (2005)b 148–182.

P. Neff, Local existence and uniqueness for a geometrically exact membrane-plate with viscoelastic transverse shear resistance. Math. Meth. Appl. Sci., 28 (2005)c 1031–1060.

F. S. Opel, C. L. Hulsbos, Probable fatigue life of plain concrete with stress gradient, ACI Journal, Proceedings 63(1) (1966) 59–82.

V. Pensée, D. Kondo, L. Dormieux, Micromechanics of anisotropic damage in rocks and concrete: unilateral effects modeling and coupling with friction, 15th ASCE Eng. Mechanics Conf. 2002.

W. Pietraszkiewicz, V.A. Eremeyev, On vectorially parameterized natural strain measures of the non-linear Cosserat continuum, International Journal of Solids and Structures 46 (11-12) (2009) 2477–2480.

W. Pietraszkiewicz, V.A. Eremeyev, V. Konopinska, Extended non-linear relations of elastic shells undergoing phase transitions, Zeitschrift für Angewandte Mathematik und Mechanik (ZAMM) 87 (2007) 150–159.

J. Pohd, O.T. Bruhns, On a thermodynamical consistent constitutive law based on the concept of internal variables, Mechanics Research Communications 20(2) (1993) 99–105.

M. Porfiri, F. dell'Isola, E. Santini, Modeling and design of passive electric networks interconnecting piezoelectric transducers for distributed vibration control, International Journal of Applied Electromagnetics and Mechanics 21 (2) (2005) 69–87.

S. Quiligotti, G.A. Maugin, F. dell'Isola, An Eshelbian approach to the nonlinear mechanics of constrained solid-fluid mixtures, Acta Mechanica 160 (2003) 45–60.

S. Quiligotti, G. A. Maugin, F. dell'Isola, Wave motions in unbounded poroelastic solids infused with compressible fluids, Zeitschrift für angewandte Mathematik und Physik ZAMP 53(6) (2002) 1110–1138.

Yu. N. Rabotonov, Creep problem in structural members, North-Holland, (1969).

E. Reccia, A. Cazzani and A. Cecchi, FEM-DEM Modeling for Out-of-plane Loaded Masonry Panels: A Limit Analysis Approach, Open Civil Engineering Journal 6(1) (2012), 231–238.

A. Rinaldi, Y.C. Lai, Damage Theory Of 2D Disordered Lattices: Energetics And Physical Foundations Of Damage Parameter, Int. J. Plasticity 23 (2007)a 1796–1825.

A. Rinaldi, D. Krajcinovic, S. Mastilovic, Statistical Damage Mechanics and Extreme Value Theory, Int. J. Damage Mech, 16(1) (2007) 57–76.

A. Rinaldi, Y.C. Lai, Statistical damage theory of 2D lattices: Energetics and physical foundations of damage parameter, International Journal of Plasticity 23 (2007)b 1796–1825.

A. Rinaldi, D. Krajcinovic, P. Peralta, Y.C. Lai, Lattice models of polycrystalline microstructures: A quantitative approach. Mechanics of Materials 40 (2008) 17–36.

A. Rinaldi, A rational model for 2D Disordered Lattices Under Uniaxial Loading, Int. J. Damage Mech. 18 (2009) 233–57.

A. Rinaldi, Statistical model with two order parameters for ductile and soft fiber bundles in nanoscience and biomaterials, Phys Rev E 83(4-2) (2011).

A. Rinaldi, Bottom-up modeling of damage in heterogeneous quasi-brittle solids, Continuum Mechanics and Thermodynamics 25(2-4) (2013) 359–373.

J. C. Savage, J. D. Byerlee, and D. A. Lockner. Is internal friction friction?, Geophysical research letters 23(5) (1996) 487–490.

A. Signorini, Sopra alcune questioni di elastostatica, Atti della Società Italiana per il Progresso delle Scienze, (1933).

M. Shillor, M. Sofonea and J.J. Telega, Models and Analysis of Quasistatic Contact, Lecture Notes in Physics 655, Springer, Berlin, (2004).

C. J. Spears, P. Feltham, On the amplitude-independent internal friction in crystalline solids, Journal of Materials Science 7(8) (1972) 969–971.

G. Sciarra, F. dell'Isola, K. Hutter, A solid-fluid mixture model allowing for solid dilatation under external pressure, Continuum Mechanics and Thermodynamics 13(5) (2001) 287–306.

G. Sciarra, F. dell'Isola, O. Coussy, Second gradient poromechanics, Int. J. Solids Struct 44(20) (2007) 6607–6629.

L.I. Sedov, Models of continuous media with internal degrees of freedom, Journal of Applied Mathematics and Mechanics 32 (1972) 803–819.

J. Swevers, F. Al-Bender, C. G. Ganseman, and T. Prajogo, An Integrated Friction Model Structure with Improved Presliding Behavior for Accurate Friction Compensation, IEEE Transactions on Automatic Control 45(4) (2000) 675–686.

R.A. Toupin, Elastic Materials with couple-stresses, Archive for Rational Mechanics and Analysis 11 (1962) 385–414.

R.A. Toupin, Theories of elasticity with couple-stress, Archive for Rational Mechanics and Analysis 17 (1964) 85–112.

Y. Yang, A. Misra, Higher-order stress-strain theory for damage modeling implemented in an element-free Galerkin formulation, Computer Modeling in Engineering and Sciences 64 (2010) 1–36.

Y. Yang, A. Misra, Micromechanics based second gradient continuum theory for shear band modeling in cohesive granular materials following damage elasticity, International Journal of Solids and Structures 49 (2012) 2500–2514.

Y. Yang, W.Y. Ching, A. Misra, Higher-order continuum theory applied to fracture simulation of nano-scale intergranular glassy film, Journal of Nanomechanics and Micromechanics 1 (2011) 60–71.

C.-T. Yu, A.S. Kobayashi, N.M. Hawkins, Energy-dissipation Mechanisms Associated with Rapid Fracture of Concrete, Experimental Mechanics 33(3) (1993) 205–211.

V.A. Yeremeyev, A.B. Freidin, L.L. Sharipova, The stability of the equilibrium of two-phase elastic solids, Journal of Applied Mathematics and mechanics (PMM) 71 (2007) 61–84.

S. Vidoli, F. dell'Isola, Modal coupling in one-dimensional electromechanical structured continua, Acta Mechanica 141 (2000) 37–50.

S. Vidoli, F. dell'Isola, Vibration control in plates by uniformly distributed PZT actuators interconnected via electric networks, European Journal of Mechanics, A/Solids 20(3) (2001) 435–456.

M. Volpato, Sull'esistenza di soluzioni periodiche per equazioni differenziali ordinarie del secondo ordine. Rendiconti del Seminario Matematico della Università di Padova 25 (1956) 371–385.

C. Zener, Internal friction in solids, Proc. Phys. Soc. 52 (1940) 152–166.

R. L. Wegel, H. Walther, Internal dissipation in solids for small cyclic strains, Physics 6 (1935) 141–157.

K. Weinberg and P. Neff, A geometrically exact thin membrane model-investigation of large deformations and wrinkling. Int. J. Num. Meth. Engrg., 74(6) (2007) 871-893.